Order Number 8914774

Theory of aperiodic systems

Lu, Jian Ping, Ph.D.

City University of New York, 1988

U·M·I

300 N. Zeeb Rd.
Ann Arbor, MI 48106

Theory Of Aperiodic Systems

by

Jian Ping Lu

A dissertation submitted to the Graduate Faculty in Physics in partial fulfillment of the requirements for the degree of Doctor of Philosophy, The City University of New York.

1988

This manuscript has been read and accepted for the Graduate Faculty in Physics in satisfaction of the dissertation requirement for the degree of Doctor of Philosophy.

23 Sept 1988
Date

Joseph L. Birman
Chairman of the Examining Committee

Sept 28 1988
Date

Joel Gersten
Executive Officer, Physics Program

Dr. Per Bak, Brookhaven National Laboratory

Prof. Herman Z. Cummins, City College, CUNY

Prof. Melvin Lax, City College, CUNY

Prof. Oliver Martin, City College, CUNY

Prof. Fred H. Pollak, Brooklyn College, CUNY

Prof. Bunji Sakita, City College, CUNY

Supervisory Committee

ABSTRACT

THEORY OF APERIODIC SYSTEMS

by

Jian Ping Lu

Advisor: Professor Joseph L. Birman

A systematic analysis of structural properties and electronic properties of quasiperiodic systems is presented. The relations between quasiperiodic systems and other aperiodic systems, such as incommensurate, random, and fractal structures, are examined. The topics discussed include: the geometrical structure; X-ray and electron diffraction pattern; the electronic and phonon energy spectra and wavefunctions; dynamic wave propagation and critical phenomena in quasiperiodic systems.

DEDICATION

To my parents

ACKNOWLEDGEMENTS

I am deeply indebted to Professor Birman, for his encouragement, confidence, advice and collaboration. There are few people that I have stayed close to for more than five years, and each of them has influenced my life to a certain degree. I am sure for the all years to come that I will be benefited, grateful and influenced by the years I spent with him.

I thank all the faculty at City College for their education, advice and discussion, especially Profs. H. Cummins, B. Sakita, M. Lax, M. Sarachik, J. Gersten, T. Boyer, O. Martin, H. Falk, R. R. Alfano, N. P. Chang, C. Yuan and M. Kaku.

Many thanks to those who have been associated with our group. They come from all over the world and make the group truly international and such a wonderful experience. They include Prof. K. Arya, Prof. Z. Su, Prof. S. Goshen, Prof. R. Berenson, Prof. T. Odagaki, Dr. J. Malinsky, Prof. X. Lei, Dr. S. Deonarine, Mr. S. Branis, Mr. A. Tolpin and Mr. M. Artoni.

Without the cheerful companionship and lively, sometimes productive discussions with many fellow students in the Physics Department, the life here would have not been complete. Thanks to: Miss. R. Tzani, Dr. C. Wang, Dr. H. Chou, Dr. X. Lu, Mr. B. Yudanin, Mr. B. Chen, and Ms. R. Gallagher.

Last, but not the least, I thank my girl friend Helen Y. Liu for her patience, encouragement, love and the wonderful time we spent together.

Table of Contents

List of Tables

List of Figures

Both figure captions and figures are placed at the end of each chapter.

CHAPTER 1

INTRODUCTION

1.1 INTRODUCTION

The history of solid state physics has been mostly identified with the theory of crystalline systems. Opening any solid state textbook one finds that much of our knowledge about solids is based on our understanding of periodic structures. However most naturally occurring materials do not exhibit periodicity. The increasing importance of these aperiodic materials in modern science and technology imposes a challenge for better understanding of non-periodic systems.

Despite great efforts in the past two decades, studies on nonperiodic systems have been concentrated mostly on random systems such as amorphous materials and liquid crystals. The physical properties of these materials are dramatically different from those of crystals due to the essential difference in their geometrical structure. Studies of these materials also require very different techniques from what one uses for periodic systems. So there is a wide gap between a random system and a periodic ordered system. In the last decade studies on two other systems, incommensurate structures and fractal structures, have only partially filled this gap.

Since the invention of crystallography it has been known that three (two) dimensional periodicity is incompatible with icosahedral (pentagonal) symmetry. This fact can be trivially proven: Assume there is five fold symmetry in the lattice along the z direction. Let **a**=(0,0,0) and **b**=(a,0,z) be two nearest neighbor lattice points so that the distance between them $d=(a^2+z^2)^{1/2}$, is the minimum distance between any two lattice points. A symmetry operation of rotation $2\pi/5$ anti-clockwise in **a** along the z direction leads to the image $\mathbf{b}'=(a\cos(2\pi/5), a\sin(2\pi/5), z)$. Or a symmetry operation of rotation $2\pi/5$ clockwise in **a** along the z direction leads to the image $\mathbf{a}'=(a(1-\cos(2\pi/5)), a\sin(2\pi/5), z)$. Both images **a'** and **b'** should be the lattice point. The distance between

these two lattice points is $d'=2a\cos(2\pi/5)=a/\tau<a\leq d$, where $\tau = (1+\sqrt{5})/2$ is the golden number. This is in contradiction with the assumption that d is the minimum distance.

Therefore it was a surprise that a new state of matter, the icosahedral quasicrystal as it is now known, which possess both icosahedral symmetry and long range order was discovered in 1984[1]. The discovery leads to many new experiments and several new compounds were found to have similar properties including long range ordered structures with other non-crystallographic symmetries[2-14]. Fig.1.1 shows an electron diffraction pattern of the material ($Al_{84}Mn_{16}$)[1]. The long range order is clearly demonstrated by the sharp Bragg peaks which possess the icosahedral symmetries. A new type of lattice -- quasiperiodic lattice -- was quickly proposed to be the basic structure model for this new material[15]. Long range order of a quasilattice is enforced by quasiperiodicity rather than periodicity. This enables the lattice to have a global symmetry which is not compatible with periodicity. The diffraction pattern, namely the Fourier transform, of a quasilattice can be shown to produce sharp Bragg peaks which possess non-crystallographic symmetries, such as pentagonal symmetry in two dimensions and icosahedral symmetry in three dimensions[16,17,18,19].

The mere existence of long range ordered structures with icosahedral symmetry at finite temperature has been partially explained through the investigation of the stability of such structure in the framework of Landau theory[20,21,22,23,24]. Different models, such as the random icosahedral packing model, were also proposed as the possible basic structure of the new material[25,26,27]. Up to the time of writing this dissertation, the question of a structural atomic model for any icosahedral crystals still remains an open question[28]. This is partially due to the difficulty of obtaining larger icosahedral crystal samples such that experiments can discriminate between different

models, i.e the atomic locations in space.

However the quasilattice as a new type of new lattice structure which possesses perfect long range order but no periodicity has attracted considerable interest on its own. In fact, prior to the discovery of quasicrystals, the subject had been studied by mathematicians in the context of tiling[29,30,31] (known as Penrose tiling after the physicist/mathematician Roger Penrose), and by crystallographers[32,33]. There are still many open questions about quasilattices, for example it was shown only very recently that an infinite perfect 2D Penrose tiling can be grown by local matching rules, but it is still unknown whether this is possible in three dimensions[34]. There are several review articles and books on these fascinating subjects[35,36,37,38].

It was the goal of this dissertation research to develop a theory for the structure and properties of aperiodic systems. The main effort concentrated on quasiperiodic systems, but at the same time I also studied their relationship to other aperiodic systems such as incommensurate and fractal structures. This provides insight into the physics of aperiodic systems and ultimately permit an understanding of the mechanisms behind their properties. The approach is particularly fruitful as one finds that a quasiperiodic system is an intermediate structure between the random disordered system as one limit and the periodic ordered system as the other limit. It possesses characteristics of both systems.

Part of the work reported in this dissertation has been published, or submitted for publications[39,40,41,42,43,44,45,46]; their titles and journal indices are included at the end of the thesis as the supplement. The structure of the thesis is: beside the current introductory chapter and the last concluding chapter, the main text is divided into four chapters. Each chapter emphasizes one aspect of physical properties.

Chapter 2 is mostly concerned with the structural aspects of quasiperiodic

lattices. First, the formal definitions of periodic and quasiperiodic lattices are given, and different ways of constructing a quasiperiodic lattice are discussed. Then the structure is analyzed in Fourier space, and in particular it is shown explicitly how sharp Bragg peaks in a diffraction pattern arise from quasiperiodicity. A new type of defect for quasiperiodic lattices, namely the *mistake* which we discovered, is studied. The effects of mistakes on long range order and on the diffraction pattern are analyzed. We discuss the dramatic consequence of mistakes: the redistribution of diffraction intensity causes some Bragg peaks which were not observable in the perfect quasilattice to become observable if there are mistakes in the quasilattice, and vise verse as is expected. The long range order of a quasiperiodic system is analyzed in terms of correlation functions. It is shown that long range correlation persists in a quasilattice even if there are mistakes, and this is the basic reason that mistakes are fundamentally different from the normal type of defects. In the last section of Chapter 2 we discuss the symmetry properties of quasilattices, particularly the relation between the crystallographic rotational symmetries of a higher dimensional periodic lattice, the symmetries of a quasilattice and its quasiperiodicity in the projection space. We prove a theorem which relates quasiperiodicity to the decomposability of the symmetry group in higher dimensions.

Chapter 3 concentrates on the static electronic and vibrational properties of quasiperiodic systems. Starting with numerical simulations, we find that the energy spectrum of a quasiperiodic system is a complex structure. It consists of a hierarchical structure of gaps with different gap width. Both gap position and width follow a certain scaling rule which is related directly to the dilation invariance of quasilattices. A real space renormalization technique is developed to predict the spectrum structure. This is possible due to the selfsimilarity of the quasilattice. Then the same method is applied to

analyze the tight binding electronic spectrum. To understand the energy spectrum in general, and in particular its relation to quasiperiodicity, we prove a quasi-Bloch theorem which provides the basic understanding of the Schrodinger equation in a quasiperiodic potential. Just as the Bloch theorem is important to provide an analytic framework for understanding the energy spectrum and wavefunctions of a periodic system, the quasi-Bloch theorem is the fundamental theorem that governs the analytical properties of a quasiperiodic system. The hierarchical structure of the energy spectrum, including the gap positions and gap widths, are successfully predicted by the quasi-Bloch theorem.

In Chapter 4 the dynamical properties of quasilattices are analyzed. In particular we examine the time dependent acoustic wave propagation in quasilattices. The relation between the quasiperiodic, incommensurate, periodic and random systems is most clearly illustrated in this problem. We find that in the short wavelength limit there is a tendency to localization in a quasiperiodic system just as for a random system. On the other side in the long wavelength limit, the quasiperiodic system shows characteristics of an incommensurately modulated system with a modulation wavelength depending on the incident wavelength. Furthermore we found a new resonance phenomenon for both the incommensurately modulated system and the quasiperiodic system. The results of numerical simulations are successfully analyzed in terms of the two-mode-coupling theory. We predict that such resonance phenomena may be experimentally observable in real systems such as the modulated superlattice structures.

Critical phenomena and the question of applicability of universality to a quasiperiodic systems are discussed in Chapter 5. This type of problem is important because the concept of universality has never been tested on non-periodic lattices. We study both the percolation and the Ising model on quasilattices. We find that

quasilattices belong to the same universality class as periodic lattices of the same Euclidian dimension. This is expected if universality holds. In our results the same critical exponents were found. We used both real space renormalization techniques and Monto Carlo simulations. An interesting result is that the percolation threshold of the 2D Penrose lattice is smaller than that of the 2D periodic lattice with the same average coordination number. This is due to the fact that in the Penrose quasilattice there are local fluctuations of coordinate number, and in the percolating process those vertices with high coordination number are more easily connected.

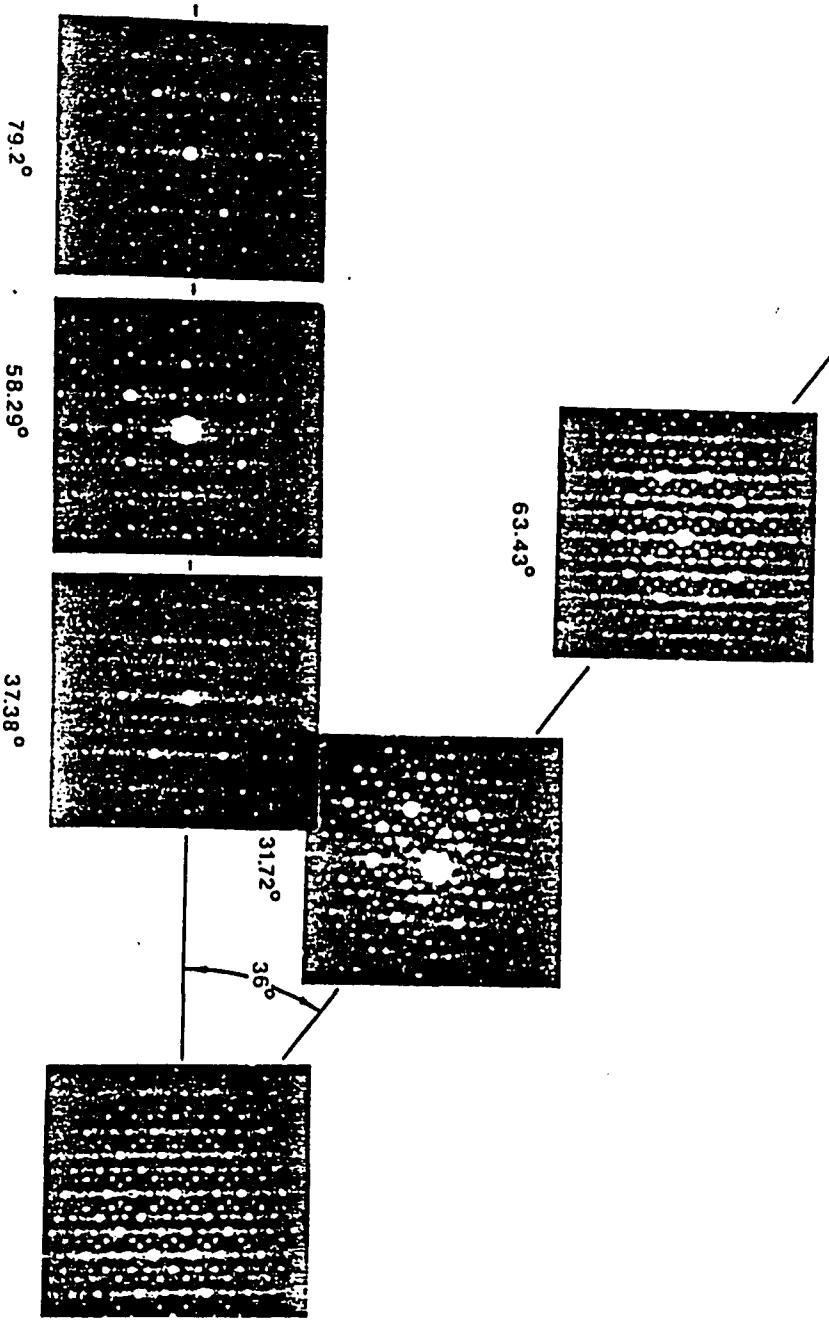

VOLUME 53, NUMBER 20 PHYSICAL REVIEW LETTERS 12 NOVEMBER 1984

Fig.1.1 Selected-area electron diffraction pattern of the first icosahedral crystal (copied from reference 1). The sharp Bragg peaks indicating the long range order of the sample, the orientation symmetry of the diffraction pattern matches the icosahedral group in three dimensions.

CHAPTER 2

GEOMETRICAL STRUCTURE AND DIFFRACTION EFFECTS

2.1 THE CONSTRUCTION OF QUASIPERIODIC LATTICES

Let us start with the definition of a periodic lattice. There are several ways to do it, each of which emphasizes one particular aspect of the geometrical structure. In one dimension one can use the following three definitions:

A) A one dimensional periodic lattice is a congruent set of points in one dimension. The coordinate of the nth point is defined by $x_n=na+x_0$, here a is the unit cell dimension, x_0 is an arbitrary constant that determines the coordinate.

B) A one dimensional periodic lattice is generated by repeated application of an inflation operation on unit cell A --> AA.

C) A one dimensional periodic lattice is a congruent array of all cells generated by translation operation x --> x+a of the basic unit cell A.

Definitions A and C can be easily generalized to higher dimension. For B it is not obvious. Each of the above definitions emphasizes one particular aspect of a periodic lattice, A for position order, B for selfsimilarity (inflation symmetry) and C for periodicity.

A general quasiperiodic lattice is a lattice built from a finite number of basic units and has infinite long range positional order, but no periodicity. In one dimension it can be defined in similar fashion as that of A and B, but not as in C because there is no periodicity. Let us start with simplest type of quasilattice

1) A quasilattice in one dimension is the congruent set of points whose coordinates are given by [46,47]

$$x(n) = n + \alpha + \frac{1}{\rho}\left[\frac{n+\beta}{\sigma}\right] \qquad 2.1.1$$

Here [z] stands for the integer part of z. σ is an irrational number (otherwise the lattice will be periodic). ρ is a real number which determines the length scale of two

different lattice spacings: 1 and (1+1/ρ). α and β are two arbitrary constants which determine the coordinate. The lattice spacing has been taken to be dimensionless. The most thoroughly studied example is the case $\rho = \sigma = \tau = (\sqrt{5}+1)/2$ (known as the golden number), which is known as the Fibonacci lattice. The distance between successive points can only take two value: either 1 or τ. If one uses B and A to represent them, then the sequence that determines the lattice is of the following form

A,AB,ABA,ABAAB,ABAABABA,ABAABABAABAAB,..... 2.1.2

As one can see from above, the sequence can be generated from the seed A by the induction rule

A ---> AB ; B ---> A 2.1.3

Generalizing this concept leads to the second definition of a quasilattice.

2) Let $\mathbf{a}=(a_1, a_2,..., a_g)$ be g basic units. Define this sequence as the zero stage. Then stage n+1 of the sequence is obtained from stage n by the substitution rule

a -----> M*a 2.1.4

The sequence determines the lattice. Here $\mathbf{M}=(m_{ij})$ is a $g \times g$ matrix with nonnegative integer entries. The matrix **M** and its interpretation fully determines the sequence.

In this paper our interpretation of the substitution rule Eq.2.1.4 is that: a_j is substituted by $m_{j1}\, a_1$ followed by $m_{j2}\, a_2$..., etc. Following are several examples:

(1) $\mathbf{M}=\begin{bmatrix}1 & 1\\ 1 & 0\end{bmatrix}$ *AB , ABA, ABAAB , ABAABABA , ...*

(2) $\mathbf{M}=\begin{bmatrix}1 & 2\\ 1 & 0\end{bmatrix}$ *AB, ABBA , ABBAAABB , ABBAAABBABBABBAA .....*

(3) $\mathbf{M}=\begin{bmatrix}1 & 1\\ 2 & 0\end{bmatrix}$ *AB* , *ABAA*, *ABAAABAB* , *ABAAABABABAAABAA* .....

(4) $\mathbf{M}=\begin{bmatrix}1 & 2\\ 1 & 1\end{bmatrix}$ *AB* , *ABBAB* , *ABBABABABBAB* 2.1.5

In the limit of such an induction procedure going to infinity the ratio between total number of elements of different type will converge to a limit. Let N_A^n, N_B^n be the number of A elements and B elements at stage n respectively: they satisfy the following recursion relations[39]

$$N_A^{n+1} = m_{11}N_A^n + m_{21}N_B^n$$

$$N_B^{n+1} = m_{12}N_A^n + m_{22}N_B^n \qquad 2.1.6$$

When n becomes infinite, if there is a limit

$$\eta = \lim_{n\to\infty} \frac{N_A^n}{N_B^n} \qquad 2.1.7$$

then

$$\eta = \frac{m_{11} - m_{22} + \sqrt{(m_{22} - m_{11})^2 + 4m_{12}m_{21}}}{2m_{12}} \qquad (m_{12} \neq 0) \qquad 2.1.8$$

For the examples given above, η has following values[39]

$$(1)\ \eta = \tau = \frac{1+\sqrt{5}}{2};\quad (2)\ \eta = 1;\quad (3)\ \eta = 2;\quad (4)\ \eta = \sqrt{2} \qquad 2.1.9$$

We see that it is not necessary to have an irrational number η to get a quasiperiodic lattice.

The simplest example of a quasiperiodic lattice is case (1), which is known as the Fibonacci lattice. The number τ is the golden number (golden mean). The sequence can

also be obtained by projecting a strip of a two dimensional square lattice onto one dimension[16,17,18,19]. This bring us to a third way of constructing a quasilattice

3) Let $\{L_{ij}=(i*a, j*b); i,j=\text{integer}\}$ be a rectangular lattice in two dimensions with lattice constants a and b. Draw a line with slope k (Fig.2.1). Take a unit cell which intersects with the line, slide it parallel along the line: one obtains a strip. Project all lattice points inside this strip perpendicularly onto the line: one gets a quasiperiodic lattice similar to that defined by Eq.2.1.1.

It is easy to see that the two basic units of the lattice are $A=a\cos\theta$, and $B=b\sin\theta$ ($\tan\theta=k$). Let N_A and N_B be number of A, B elements respectively, then $N_B=aN_A/bk$. From Eq.2.1.1 one finds that the two basic units are $A=1+1/\rho$ and $B=1$. The ratio between N_A and N_B obviously should be $N_A/N_B=(1/\sigma)/(1-1/\sigma)$. From these equations one immediately obtains the relation between the two sets of parameters[41]

$$\left(\frac{a}{b}\right)^2=\left(1+\frac{1}{\rho}\right)(\sigma-1);\qquad k^2=\frac{\left(1+\frac{1}{\rho}\right)}{\sigma-1} \tag{2.1.10}$$

Therefore there is an exact one-to-one correspondence between the two methods.

The projection method just described can be most easily generalized to a higher dimensional quasilattice. And most structural models for icosahedral crystals are based on such a construction, namely the 3D quasilattice obtained by projection from a six dimensional cubic lattice[16,19,28,48,49].

2.2 FOURIER ANALYSIS AND DIFFRACTION PATTERN

There are many ways to calculate the Fourier transform of a quasilattice just as there are several ways to construct them. I will describe two of them corresponding to the

construction (1) and (3).

Using z=[z]+{z}, where [z] and {z} represent the integer and the fractional part of z, one can rewrite Eq.2.1.1 as (for simplicity α and β are taken to be zero[41]):

$$x(n) = na + f(na) \qquad 2.2.1$$

here a=(1+1/ρσ) and f(z) is a periodic function of z with period σa

$$f(z) = -\frac{1}{\rho}\left\{\frac{z}{\sigma a}\right\} = \begin{cases} -\frac{1}{\rho}\left(1+\frac{z}{\sigma a}\right); & -\frac{\sigma a}{2} < z \le 0 \\ -\frac{z}{\sigma a \rho}; & 0 < z \le \frac{\sigma a}{2} \end{cases} \qquad 2.2.2$$

To calculate the diffraction pattern, one defines the density function

$$\rho(x) = \sum_{n=-\infty}^{\infty} \delta(x - x(n)) \qquad 2.2.3$$

The Fourier transform of the density function leads to the diffraction amplitude

$$F(q) = \frac{1}{N}\sum_{n} e^{iqx(n)} = \frac{1}{N}\sum e^{iqna + iqf(na)} \qquad 2.2.4$$

Since $e^{iqf(n)}$ is a periodic function of x with period σa, one can do the Fourier expansion

$$e^{iqf(\xi)} = \sum_{m} b_m e^{-im2\pi\frac{\xi}{\sigma a}}; \qquad b_m = i\frac{e^{-i\frac{q}{\rho}} - 1}{\frac{q}{\rho} - m2\pi} \qquad 2.2.5$$

Therefore

$$F(q) = \frac{1}{N}\sum_{n}\sum_{m} b_m e^{iq\frac{\pi}{2}} e^{i\left(q - m\frac{2\pi}{\sigma a}\right)na} \qquad 2.2.6$$

Now the summation over n can be carried out in the limit $N \to \infty$. According to the

Poisson sum formula this gives the Δ function, Δ(q)=0 for all q except Δ(0)=1. After some algebra one obtains

$$F(q) = \sum_{mn} \exp(-iz_{mn}) \frac{\sin \frac{z_{mn}}{2}}{\frac{z_{mn}}{2}} \Delta(qa - q_{mn}a) \qquad 2.2.7$$

where

$$q_{mn} = \frac{2\pi}{a}\left(n + \frac{m}{\sigma}\right); \quad z_{mn} = \frac{2\pi}{a}\left(\frac{n}{\rho} - m\right); \quad n, m = integer \qquad 2.2.8$$

If σ is an irrational number, q_{mn} will be dense everywhere in q space. Eq.2.2.7 has been obtained by several workers using different approaches[18,46,50]. The advantage of the present formalism is that the generalization to other type of quasiperiodic or almost periodic lattices, and also the calculation for lattices with mistakes is straightforward[41].

A second way to calculate the diffraction pattern is to use the projection method[18]. This is particularly convenient for higher dimensional quasilattices.As is shown in Fig.2.1, let x, y be the coordinates of a two-dimensional lattice along the lattice vector. Let ξ be the coordinate along the projection line, and η be in the perpendicular direction. As was described in the last section, the quasilattice points are obtained by projection of all 2D lattice points inside the strip onto the line. To calculate the Fourier transform one puts a delta function on each lattice point, so the density function of the quasilattice can be written as

$$\rho(\xi) = \int \rho(\xi, \eta) W(\eta) d\eta \qquad 2.2.9$$

where

$$\xi = x \cos\theta + y \sin\theta; \qquad \eta = -x \sin\theta + y \cos\theta \qquad 2.2.10$$

and W is the window function which defines the projection strip

$$W(\eta) = \begin{cases} 1 & if \ -a\sin\theta < \eta \le b\cos\theta \\ 0 & otherwise \end{cases} \qquad 2.2.11$$

and

$$\rho(\xi,\ \eta) = \sum_{ij} \delta(\mathbf{x} - \mathbf{X}_{ij}) \qquad 2.2.12$$

is the two dimensional lattice density. The Fourier transform of $\rho(\xi)$ is

$$\begin{aligned} F(q) &= \int \rho(\xi) e^{iq\xi} d\xi = \int \rho(\xi,\eta) W(\eta) e^{iq\xi} d\xi d\eta \\ &= \int \rho(\xi,\ \eta) \int \bar{w}(p) e^{ip\eta} dp\, e^{iq\xi} d\xi d\eta \\ &= \int S(k,\ p) \bar{w}(p)\ dp \end{aligned} \qquad 2.2.13$$

Where

$$S(k,\ p) = S(\mathbf{k}) = \sum_{mn} \Delta(\mathbf{k} - \mathbf{K}_{mn}) \qquad 2.2.14$$

is the structure factor of the 2D rectangular lattice, namely the Fourier transform of the two dimensional rectangular lattice density function. $\{\mathbf{M}_{mn}\}$ is the reciprocal lattice of $\{\mathbf{X}_{ij}\}$. W(p) is the Fourier transform of the window function which is easily calculated as

$$\bar{w}(p) = \frac{e^{ipd} - 1}{p} = e^{i\frac{pd}{2}} \frac{\sin\dfrac{pd}{2}}{\dfrac{pd}{2}} \qquad 2.2.15$$

here $d=a\sin\theta+b\cos\theta$ is the width of window function. Substituting this expression into Eq.2.2.13 one immediately gets the same results as Eq.2.2.7

2.3 MISTAKES -- DEFECTS IN A QUASILATTICE

2.3.1 One Dimensional Case

Real quasicrystals are obtained by highly non-equilibrium processes, so imperfection is inevitable. In this section I study the effect of one particular type of defect -- mistakes. Unexpected qualitative changes occur in diffraction intensities when mistakes are present.

Consider a perfect one dimensional quasilattice, namely the Fibonacci lattice defined Eq.2.2.1. As noted, the lattice spacing between two successive points can only be either $L=1+1/\tau$ or $S=1$* . Also one observed that in the perfect Fibonacci sequence the segments SS or LLL do no appear. One of the simplest type of defects in such a sequence is the transposition in sequential order of LS segments, namely from LS to SL. If we impose a restriction that the random occurrence of transpositions will not create the segment SS ot LLL which are prohibited in the perfect sequence, then it can be shown (see section 2.3.3) that the energy cost associated with such a defect is very small. Hence one expects that such a type of defect is generic[41]. Since it differs from the usual defect discussed in crystals and it is similar to mistakes in stacking sequence discussed by Wilson and others[51], we call it a *mistake*[40].

The simplest restriction requires that the three site configuration remains unchanged i.e. maintain the selection rules: no SS and no LLL. Careful examination of the Fibonacci lattice shows that possible mistakes consistent with these constraints have the form of a

---

* In this section and the rest of the thesis conventional notation L(long) S(short) will be used instead A and B as in section 2.1 and 2.2.

transposition in the five-site configuration: LLSLS->LSLLS (Fig.2.2).

Label the position of the nth lattice site in the imperfect Fibonacci lattice as x'(n). Suppose a mistake occurred at site n (Fig.2.2), namely

$$\begin{aligned} &x'(n-1) = x(n-1); \\ &x'(n) = x'(n-1) + S\ ; \qquad\qquad x(n) = x(n-1) + L \\ &x'(n+1) = x'(n) + L = x(n+1); \quad x(n+1) = x(n-1) + L + S \end{aligned} \tag{2.3.1}$$

This changes the Fourier transform from that of the perfect lattice F(q) to that of an imperfect lattice denoted F'(q): the term $e^{iqx(n)}$ is replaced by $e^{iqx'(n)}=e^{iqx(n)} - e^{iqx(n-1)}\Delta$, where $\Delta=e^{iqL} - e^{iqS}$.

For every LLSLS cluster in the perfect Fibonacci lattice, impose a probability p that it will flip into LSLLS. Label the position of these clusters by y(m)=x(n-1), where x(n-1) is the position of the atom which is between the first two long spacings of the cluster (Fig.2.1b). Note the set y(m) is only a subset of all x(n). The Fourier transform of the lattice with a given configuration of mistakes is

$$F'(q,\{\sigma\}) = \sum_{n=-\infty}^{\infty} e^{iqx'(n)} = \sum_{n} e^{iqx(n)} - \sum_{y(m)} e^{iqy(m)}\Delta(\sigma_m) \tag{2.3.2}$$

where

$$\Delta(\sigma_m) = e^{iqS\sigma_m} - e^{iqS}; \qquad \sigma_m = \begin{cases} \tau = \dfrac{L}{S}; & \text{with probability } p \\ 1; & \text{with probability } (1-p) \end{cases} \tag{2.3.3}$$

Assume mistakes occur independently with probability p at all possible sites y(m). To obtain the observed diffraction intensity I(q)=<FF*> one has to average over all possible configurations of {σ}. Defines D(q) by

$$\langle F'(q,\{\sigma\})F'^{*}(q,\{\sigma\})\rangle = |F'(q,\{\sigma\})|\langle F'^{*}(q,\{\sigma\})\rangle + D(q) \tag{2.3.4}$$

D(q) is the diffuse scattering. To calculate the first term, define

$$F'(q) = \langle F'(q,\{\sigma\})\rangle = F(q) - \langle f(\{\sigma\})\rangle \qquad 2.3.5$$

Here f({σ}) is the second term in Eq.2.3.2 and is a function of configuration {σ}:

$$\langle f(\{\sigma\})\rangle = \sum_{y(m)} e^{iqy(m)} \langle \Delta(\sigma_m)\rangle = p\Delta \sum_{y(m)} e^{iqy(m)} \qquad 2.3.6$$

with Δ=Δ(τ). Careful analysis of all possible sites reveals that the set y(m) itself forms a new Fibonacci lattice with basic lattice length S'=3L+2S=τ^4S (L=τS), and a possible shift of origin (Fig.2.1b). Therefore

$$F'(q) = F(q) - p\Delta F(\tau^4 q) \qquad 2.3.7$$

The diffraction function of the perfect Fibonacci lattice has been calculated in the last section. Substituting Eq.2.2.7 and Eq.2.3.3 into Eq.2.3.7, after some algebra one has

$$F'(q) = \sum_{mn} \frac{e^{i\frac{z_{mn}}{2}} \sin\left(\frac{z_{mn}}{2}\right) - p \sin\left(\frac{q_{mn}}{2\tau}\right) e^{i\varphi_{mn}} \sin\left(\frac{z_{mn}}{2\tau^4}\right)}{\frac{z_{mn}}{2}} \delta(qa - q_{mn}a) \qquad 2.3.8$$

where

$$\varphi_{mn} = \frac{z_{mn}}{2\tau^4} + \frac{q_{mn}}{2\tau} + \frac{\pi}{2} \qquad 2.3.9$$

The second term in Eq.2.3.4 can be calculated exactly[41]

$$D(q) = \frac{4p(1-p)\tau^{-4}}{N} \sin^2\left(\frac{q}{2\pi}\right) \qquad 2.3.10$$

where N is the linear dimension of the crystal in units of the average atomic spacing a. Experimentally, a typical diffraction peak line width Δq is about 10^{-2} in units of 1/a, so the

contribution of D(q) to the peak intensity is order of $p\Delta q/N\tau^4$. Presently available samples have $N=10^3$ in a single grain, so for p=0.2 the contribution is order of 10^{-6}. Therefore for all diffraction peaks whose intensity is larger then 10^{-6} of the maximum peak intensity, the diffuse background can be neglected. On the other hand those peaks whose intensity ratio to the maximum is of order 10^{-6} or smaller, will merge into the smooth background which is indistinguishable from other incoherent scattering. We are primarily interested in those peaks whose intensity is around a cut-off, which is taken to be much larger than the contribution from the diffuse term, so D(q) will be neglected in the following calculations.

From the above equations one sees that mistakes change the relative intensities of different Bragg peaks, depending on the value of p and q_{mn} . As expected some peaks decrease in intensity. **An unexpected result is that some peaks are enhanced.** Furthermore mistakes do not create linewidth for the diffraction peaks, this indicates that the long range correlation is not lost (see section 2.4). This effect is more pronounced in the three dimensional case, as we show below.

The restriction we have imposed on the imperfect quasilattice could be weakened, e.g. by allowing more general types of permutation, namely by permitting the variable σ_m in Eq.2.3.3 to have a continuous distribution. This will not change the overall calculation; however now the Δ will have a more complicated dependence on q. Another way of generalizing is to require that the n-site configuration be kept the same. Then instead of τ^4 in Eq.2.3.8 a different factor may appear.

2.3.2 Three Dimensional Case

Qualitatively one expects the same effects will occur in a three dimensional quasiperiodic structure, namely in the generalized Penrose tiling. Levine and Steinhardt[15,46] have shown that for the Ammann quasilattice, the Fourier transform is a

simple product of the Fourier transforms of three 1D Fibonacci lattice. Mathematically an Ammann lattice is a quasiperiodic hexagrid which is the simple direct product of six one dimensional quasiperiodic grids, each with grid direction along one of six five-fold symmetry axes (e_i, i=0,...,5) of an icosahedron. Since the skeleton of a three dimensional Penrose tiling is equivalent to an Ammann quasilattice, the qualitative result is also true for a general quasilattice. Because the hexagrid is non-singular (no more than three grids intersect at one point), the diffraction amplitude $F_3(\mathbf{k})$ of the vertices of the hexagrid can be written as[40]

$$F_3(\mathbf{q}) = \sum_{i>j>k} F(\mathbf{q}\bullet\mathbf{u}_{ijk})F(\mathbf{q}\bullet\mathbf{u}_{jki})F(\mathbf{q}\bullet\mathbf{u}_{kij}) \qquad 2.3.11$$

where F(x) is given by Eq.2.3.7 and

$$\mathbf{u}_{ijk} = \frac{\mathbf{e}_j \times \mathbf{e}_k}{\mathbf{e}_i \bullet (\mathbf{e}_j \times \mathbf{e}_k)} \qquad 2.3.12$$

Since the support of F(q) is the set $q=q_{mn}$, the argument of each factor in Eq.2.3.11 must be of the form q_{mn} in order that $F_3(\mathbf{q})$ be non-zero. This requires $\mathbf{q}$ to be of the form

$$\mathbf{q} = \frac{2\pi}{a}\left[\left(n_i + \frac{m_i}{\tau}\right)\mathbf{e}_i + \left(n_j + \frac{m_j}{\tau}\right)\mathbf{e}_j + \left(n_k + \frac{m_k}{\tau}\right)\mathbf{e}_k\right] \qquad 2.3.13$$

We now extend the class of mistakes to the three dimensional tiled lattice. Mistakes in tiling now correspond to a transposition of grid order. This kind of tiling is generated from the hexagrid by taking each grid sequence to follow the 1-D imperfect Fibonacci lattice. Therefore the diffraction amplitude $F'_3(\mathbf{q})$ of a quasilattice with mistakes will be expressed in terms of F'(q) of Eq.2.3.8 as

$$F'_3(\mathbf{q}) = \sum_{i>j>k} F'(\mathbf{q}\bullet\mathbf{u}_{ijk})\,F'(\mathbf{q}\bullet\mathbf{u}_{jki})\,F'(\mathbf{q}\bullet\mathbf{u}_{kij}) \qquad 2.3.14$$

This diffraction intensity is qualitatively different from that of Eq.2.3.11. As in the 1-D case: some quasi-Bragg peaks decrease in intensity as expected but **some peaks are enhanced**[40]. In Fig.2.3 we have plotted the results computed from Eq.2.3.11 (p=0) and Eq.2.3.14 taking p=0.2 in Eq.2.3.8. Only those Bragg peaks whose intensity is larger than some arbitrarily chosen cut off are shown.

Results are: some Bragg peaks in the diffraction pattern of the perfect quasilattice are extinguished, and some Bragg peaks previously absent now appear above threshold. A few examples of each are shown with arrows in Fig.2.3. This picture differs qualitatively from the diffraction pattern of a usual crystal with faults, where the effect of randomness always reduces the intensity of Bragg peaks[52]. These results are independent of the value chosen for the cut-off.

Fig.2.3 illustrates the symmetrical case. However this is not necessary, mistakes can be implemented so that five, two and three-fold rotational symmetry is lost, by choosing different parameters for different grid directions.

2.3.3 Energy Cost Associated With Mistakes

In this section we use a simple model to demonstrate the small energy required to produce a mistake. This implies that mistake is a generic disorder for a quasicrystal.

Assume the potential energy of the whole system is the sum of all pair-wise interactions

$$E = \sum_{x_n,\,x_m} V(|x_n - x_m|) \qquad 2.3.15$$

Suppose a mistake occurs at site y_m; as we pointed out in the last section, mistakes can

only occur in terms of a cluster transposition: LLSLS --> LSLLS. Owing to the constraint we impose (no LLL or SS), the cluster must have the form LSLLSLSL. It is clear from Fig.2.2 that a mistake only changes the position of the atom at y_m, not the neighboring sites in the cluster. Therefore the terms changed in Eq.2.3.15 are those associated with y_m. Up to the 4th nearest neighbor the contribution to the total potential energy from these terms are

$$V' = V(3L+S) + V(2L+S) + V(2L) + V(L) + V(S) + V(S+L) + V(2S+L) + V(2S+2L) \qquad 2.3.16$$

for the perfect lattice. And

$$V'' = V(S) + V(S+L) + V(2S+L) + V(2S+2L) + V(3L+S) + V(2L+S) + V(2L) + V(L) \qquad 2.3.17$$

for a lattice with a mistake. We see that V'=V". So if the interaction is a rapid decreasing function of distance, which physically is plausible, we can say that mistakes cost very little energy. On the other hand, by allowing mistakes, the system gains configuration entropy. Therefore the free energy of the whole system could be decreased. We believe this is one of reasons that mistakes could be often observed in quasicrystals. In fact several experiments on electron microscopy have clearly observed such type of defects[53,54,55].

The essential physics is contained in the imposed constraint on local order. This is unique for a quasilattice, since the cluster after the transposition: LSLLS, is allowed somewhere in the perfect lattice as a building block . Generally one can impose more than just nearest neighbor order. Then mistakes are still possible, but with rarer frequency (the scaling τ^4 in last section will be replaced by a different factor). Also the energy cost of mistakes will be even smaller, that is to say the equality V'=V" will be satisfied even when one considers more then the 4th nearest neighbor interactions. This result has no exact

counterpart in the normal crystal case. Consider for example stacking faults in the cubic closed packed layer structure[52]. The perfect sequence will be ···ABCABCABC··· or ···ACBACBACB···. Two types of fault could occur: ···ABC(B)ACB··· or ···ABC(B)CAB··· where the layer in the brackets is the layer at fault. One immediately sees that in both cases new clusters: BCB or CBC, are introduced. These new clusters are not allowed in the perfect sequences, therefore they must cost energy. Further there is no way one can impose local order constraints to avoid this, as we did for the case of a quasilattice.

In conclusion from many different view points mistakes are generic defects in quasicrystals.

2.4 LONG RANGE ORDER IN A QUASILATTICE

2.4.1 The Correlation Function

The lattice defined by Eq.2.1.1 has perfect long range correlation. To prove this we examine the pair correlation function. Assume at every lattice site there is an atom with identical mass and the total mass of system is normalized to 1. Then the mass density is

$$\rho(x) = \frac{1}{N}\sum_n \delta(x - x_n) \qquad 2.4.1$$

Here the summation is over all integers, and N-->∞ is understood. The two particle correlation function K and the pair correlation function G are defined as[56]

$$K(x_1, x_2) = \langle \rho(x_1)\rho(x_2) \rangle \qquad 2.4.2$$

$$G(x) = \int K(x', x' + x)dx' \qquad 2.4.3$$

For a perfect quasilattice one finds, from Eq.2.1.1

$$G_o(x) = \int \rho(x')\,\rho(x+x')dx'$$

$$= \frac{1}{N^2}\sum_{n,\,m}\delta(x'-x_n)\delta(x'+x-x_m)dx'$$

$$= \frac{1}{N^2}\sum_{n,\,m}\delta\left(x-(m-n)a+\frac{1}{\tau}\left(\left\{\frac{m}{\tau}\right\}-\left\{\frac{n}{\tau}\right\}\right)\right)$$

$$= \frac{1}{N^2}\sum_{n,\,l}\delta\left(x-la+\frac{1}{\tau}\left(\left\{\frac{n+l}{\tau}\right\}-\left\{\frac{n}{\tau}\right\}\right)\right) \qquad 2.4.4$$

$$= \frac{1}{N}\sum_{l}\left[\left(1-\left\{\frac{l}{\tau}\right\}\right)\delta\left(x-\left(l+\frac{1}{\tau}\left[\frac{l}{\tau}\right]\right)\right)\right.$$

$$\left.+\left(\left\{\frac{l}{\tau}\right\}\right)\delta\left(x-\left(l+\frac{1}{\tau}\left[\frac{l}{\tau}\right]\right)-\frac{1}{\tau}\right)\right]$$

Here $a=1+1/\tau^2$. In the last step we have used the property of the irrational number τ: $\left\{\frac{n}{\tau}\right\}$ is uniformly distributed in the interval (0,1) when n takes all integer values. So $G_0(x)$ is still a sum of δ functions. This is clear evidence that the positions of lattice points are infinitely correlated. From Eq.2.4.1 one also finds that the distance between two lattice points separated by l lattice sites can only take two values, namely either $l+1/\tau[l/\tau]$ or $l+1/\tau[l/\tau]+1/\tau$. From the point of view of "statistical symmetry" [56], this clearly shows that a quasicrystal belongs to the class of a crystal.

In a usual periodic system, when defects are introduced the long range correlation in the system are gradually weakened over a distance. An good example is the stacking faults. It was shown by Hendricks and Teller[52] that if there are faults in the stacking (such as those described in section 2.3.3) then the diffraction pattern will no longer be delta

function. Instead the peaks have finite width indicating finite correlation length.

So it is interesting to ask what effect will mistakes cause in quasiperiodic sequence on the long range order . Similarly to what I have shown above, the pair correlation function of the sequence in the presence of mistakes can be exactly calculated[41]:

$$G(x) = \bar{G}(x) + \hat{G}(x) \qquad 2.4.5$$

with

$$\bar{G}(x) = G_0(x) + \frac{p\tau^{-4}}{N}\sum_{x_n^0}\left[\delta\left(x - x_n^0 + \frac{1}{\tau}\right) - \delta\left(x - x_n^0 - \frac{1}{\tau}\right)\right]$$

$$+ \frac{p^2\tau^{-4}}{N}\sum_{y_m^0}\left[\left(3\left\{\frac{m}{\tau}\right\} - 1\right)\delta\left(x - y_m^0\right) + \left(2 - 3\left\{\frac{m}{\tau}\right\}\right)\delta\left(x - y_m^0 - \frac{1}{\tau}\right)\right.$$

$$\left. - \left(\left\{\frac{m}{\tau}\right\}\right)\delta\left(x - y_m^0 + \frac{1}{\tau}\right) - \left(1 - \left\{\frac{m}{\tau}\right\}\right)\delta\left(x - y_m^0 - \frac{2}{\tau}\right)\right] \qquad 2.4.6$$

and

$$\hat{G}(x) = \frac{p(1-p)}{N}\left[2\delta(x) - \delta\left(x - \frac{1}{\tau}\right) - \delta\left(x + \frac{1}{\tau}\right)\right] \qquad 2.4.7$$

Where $x_n^0 = n + \frac{1}{\tau}\left[\frac{n}{\tau}\right]$ is the Fibonacci lattice with $\alpha=\beta=0$, and y^0_m is the subset of x^0_n where the mistakes can occur (see section 2.3, Eq.2.3.1 and Eq.2.3.2).

From Eq.2.4.5-7, one sees that the pair correlation function is still a sum of δ functions even through we have introduced mistakes into the system. In other words the long range correlation of the quasilattice is preserved. This result is in agreement with the diffraction pattern we calculated in the last section.

2.4.2 The Configuration Number For Different Systems

A distinguish difference between a quasilattice, a periodic lattice and a random lattice is the configuration number C(n). It is defined as the total number of possible configurations for a randomly selected segment of length n cells. As it is well known C(n) is constant for a periodic lattice, and exponentially dependent on n for a random lattice. For the quasiperiodic lattice the upper bound for C(n) we found is linear in n. Take the Fibonacci lattice as example. For any integer n one can find an integer m such that $F_{m-2}<n<= F_{m-1}$, here F_m are Fibonacci numbers ($F_0=1$, $F_1=1$, $F_m=F_{m-1}+ F_{m-2}$). By the deflation procedure the whole lattice can be regarded as consisting of larger unit S' and L' only, which consists of F_{m-1} and F_m original cells respectively. Since the first F_{m-1} cells in L' are in the same order as S' (remember the deflation rules is LS-->L and L-->S), for any segment of length F_{m-1} the number of possible configurations is less then F_m which is certainly also an upper bound for C(n). Since F_m is in the same order of n, the upper bound of C(n) can not exceed linearity in n. So from this geopetrical aspect quasiperiodic systems are intermediate in between periodic ordered and random systems. Therefore it is not surprising that physical properties of quasicrystals possess characteristics of both crystals and amorphous materials (see also Chapter 4).

2.5 SYMMETRY AND QUASIPERIODICITY: WHEN IS A PROJECTED LATTICE A QUASIPERIODIC LATTICE ?

The group theoretical aspect of quasiperiodic lattices have been discussed by many people, in particular the higher dimensional embedding of quasilattice[57,58,59]. In ths section the relation between the crystallographic symmetry group of embedded higher dimension, the symmetry properties of quasilattice and the quasiperiodicity is discussed[42].

In general a lattice in N dimensions can be defined as an infinite set of points in N dimensions with a single condition: there is a nonzero lower bound for the distance between any pair of points. If the set can be integer-indexed by a finite number M of independent vectors, namely each point in the set can be written as integer combination of M fixed vectors, then the lattice is an ordered lattice and can be embedded in M dimensions. For the special case of M=N the lattice will be periodic, and a crystallographic group gives the full classification in terms of symmetry. On the other hand if M>N, the lattice will be non-periodic in N dimensions. In general it can be regarded as a projection of a sub-set of a periodic lattice in M dimensions onto N dimensions, and may not have any symmetry. However if the projection is properly chosen, as in the case of the Penrose lattice, the projected lattice carries the full or a sub- symmetry group of the periodic lattice in M dimensions. In this case the lattice will be nonperiodic.

A question immediately arises as one asks: In general what kind of projection will give rise to a non-periodic lattice? Furthermore what kind of projection will insure preservation of the symmetry operations of the starting periodic lattice? And is there a systematic way of finding the correct projection procedure? Some of these questions are answered in this section. We will show that: if the point group associated with the periodic lattice is R-decomposable and Q-irreducible (these terms will be defined shortly), then there is a natural projection scheme which will guarantee that the projected lattice is quasiperiodic; furthermore it carries point symmetries of the periodic lattice in higher dimension[42].

2.5.1 A Theorem

Let G be a crystallographic point group in M dimensions, let $E=(\mathbf{e}_1, \mathbf{e}_2, ...,\mathbf{e}_M)$ be the lattice basis vectors of the periodic lattice which has the point symmetry group G. Let

D(g) be the representation of group G with basis E, then D(g) is an M by M matrix with integer entries. Let F be one of the fields: Q-rational, R-real and Z-complex.

Definition: If there exists a matrix W with entries from the field F, such that

$$W^{-1}D(g)W = \begin{pmatrix} D_1(g) & 0 \\ 0 & D_2(g) \end{pmatrix} \qquad 2.5.1$$

then the group G is called F-decomposable in the basis E, otherwise it is called F-irreducible[60]. One can assume $D_1(g)$ is an irreducible representation of G without loss of generality.

If D(g) is R-decomposable, then W can be regarded as a transformation of basis from E to a new basis, $A=(\mathbf{a}_1, \mathbf{a}_2, ...,\mathbf{a}_M)$. A lattice vector **L** of the periodic lattice can be written in this case as:

$$\begin{aligned} \mathbf{L} &= n_1\mathbf{e}_1 + n_2\mathbf{e}_2 + \ldots + n_M\mathbf{e}_M = E \cdot \mathbf{n} \\ &= x_1\mathbf{a}_1 + x_2\mathbf{a}_2 + \ldots + x_M\mathbf{a}_M = A \cdot \mathbf{x} \end{aligned} \qquad 2.5.2$$

Here **n** is a column vector with integer entries, which indexes the lattice in E; and **x** indexes the lattice in the new basis A

$$A = (\mathbf{a}_1, \mathbf{a}_2, \ldots, \mathbf{a}_M) = E \cdot W = (\mathbf{e}_1, \mathbf{e}_2, \ldots, \mathbf{e}_M) \cdot W \qquad 2.5.3$$

and

$$\mathbf{x} = W^{-1}\mathbf{n} \qquad 2.5.4$$

In general the entries of **x** are from field F since the entries of W are from field F. The representation of the group in the new basis A is block diagonal, therefore the new basis naturally splits into two orthogonal sub-bases $A_1 \oplus A_2$.

Since $D_1(g)$ is an irreducible representation of G, it must be a faithful representation of a subgroup G_1 of G (G_1 can be G itself). So if one chooses the subspace spanned by A_1 as the projection space, the lattice L_1 obtained by projection from the periodic lattice L will have the full symmetry of group G_1. Therefore we have

Lemma 1: The lattice obtained by projection of the periodic lattice into the subspace spanned by A_1 will have symmetry group G or $G_1 \subset G$.

In general the projected lattice L_1 could be either periodic or non-periodic. The following lemma distinguishes the two cases.

Lemma 2: If D(g) is Q-decomposable, the projected lattice is periodic.

Proof: Since $x=W^{-1}n$ is in the field Q and the group G is finite, a subset of x will be in the ring of Z=integer. Therefore a sublattice of L_1 can be integer-indexed, and hence forms a periodic lattice. So L_1 is a periodic lattice.

Combining Lemma 1 and Lemma 2 we have following theorem:

Theorem: If D(g) R-decomposable but Q-irreducible, the projected lattice is quasiperiodic with symmetry group G_1.

Comment 1) The quasilattice can be integer-indexed by M independent vectors. This is obvious as the quasilattice is the result of a projection of an M dimensional periodic lattice, which is indexed by M independent lattice basis vectors. The projection of these lattice basis vectors into the subspace gives the basis vectors for indexing the quasilattice.

Comment 2) The quasilattice has symmetry group G_1 which is in general a subgroup of the symmetry group G of the M dimensional periodic lattice. If $D_1(g)$ is a faithful representation of G, then G_1 =G and the quasilattice has full point symmetry G. The examples we will give in the next section belong to this case.

Comment 3) To emphasize, it is the Q-irreducibility that makes the projected lattice a quasilattice, and it is the R-decomposability that guarantees the quasilattice has symmetry G.

Comment 4) The question remains in general how to construct the transformation matrix W. But if we know G_1 and its vector representation in N dimensions (the space spanned by the basis A_1), then there is a general scheme for construction of W. In the next section we we give examples for M=4, N=2.

The theorem provides a natural scheme to classify all quasilattices according to their symmetries. To identify a quasilattice, one needs: N -- the dimension of space in which the quasilattice exits; M -- the number of integer independent vectors needed to index the quasilattice; G -- the crystallographic group in M dimensions which is the symmetry group of the periodic lattice (the projection of this periodic lattice into the N dimension subspace gives the quasilattice); and G_1 -- the subgroup of G which is the symmetry group of the quasilattice. The set (N,M,G,G_1) is a complete and unique labelling of a quasilattice, and it should serve as rule to classify all quasilattices. In fact this classification scheme includes all the known classifications of periodic lattices, for which N=M and $G=G_1$.

In the following section we give examples for the case M=4, N=2.

2.5.2 From 4-D crystallographic point group to 2-D quasilattices

Four dimensional crystallographic point and space groups have been tabulated in the book *Crystallographic Groups Of Four-Dimensional Space* by H. Brown, et al[60]. In that book not only are the generators of all point groups given, but also the decomposability of all groups. Careful examination of the tables shows that there are 3 families containing 9 space groups which satisfy the condition of the theorem we presented in the last section, namely: they are R-decomposable and Q-irreducible into $2 \oplus 2$. At present, we concern

ourselves only with rotational symmetry so there are only 4 different symmetry types:

Family 18 --Octagonal, group 26/01/01, order of 8.

Family 19 --Decagonal, group 17/01/01, order of 5.

Family 19 --Decagonal, group 27/02/01, order of 10.

Family 20 --Dodecagonal, group 28/01/01, order of 12.

The notation for the groups is the same as in the book by Brown[60]. In Table.2.1 we have listed these four groups. The first row is the group notation. The second row is the order of group. The third is the matrix representation of the generator g of the group in the lattice basis. The 4th is the metric tensor in 4-D (the metric of a basis is a symmetric matrix whose entries are the inner products of basic vectors). Listed in the 5th row are: the transformation matrix W defined in Eq.2.5.3, which transforms the lattice basis to an orthogonal basis and breaks 4-D into $2 \oplus 2$. Furthermore the matrix representation of the group in the new basis is decomposed as shown in the 6th row, where the generator is given in terms of the new basis. (For the convenience of calculation, the generators used in the Table2.1 are the transpose of those generators given in the book by H. Brown et al.)

Notice that the representation of all generators in the new basis has the same form, namely block diagonalized into two $2 \oplus 2$ rotation matrices, each of which is exactly one of the only two possible faithful representations of the cyclic group of order n=5,8,10,12. Actually there are four faithful representations of the cyclic group of order n=5,8,10,12 if one counts the mirror image of each as a distinct representation. In fact these groups can only arise as symmetry groups of a periodic lattice in 4 or higher dimensions. The short hand notation (c,s,cc,ss) of row 6 is defined in row 7 where we give the four faithful representations in terms of a complex number $e^{i\phi}$. Finally in the last row we give a pictorial representation of the symmetry. The two vectors in each pattern are two vector faithful representations of the rotation groups.

In conclusion we observe that in general, an arbitrary projection of a high dimensional periodic lattice into low dimension will result in either a periodic or an aperiodic lattice. Furthermore if it is aperiodic, it may or may not posses any symmetry operations of the symmetry group of the high dimensional periodic lattice. We have partially answered these matters. In brief, we have shown that if the symmetry group of the periodic lattice is R-decomposable and Q-irreducible, then there is a natural scheme to pick up the projected subspace. The decomposition matrix transforms the lattice basis to a new basis which is split into at least two orthogonal subspaces. Projection of the periodic lattice into these subspaces will produce a quasilattice which will possess the partial or full symmetry group of the periodic lattice. Therefore the symmetry group of a quasilattice can be understood in terms of crystallographic groups of the periodic lattice in which the quasilattice is embedded. This provides a natural and simple scheme of classification of quasilattices in terms of their symmetries. We also demonstrated the theorem by working out a complete case of projection from all 4 dimensional periodic lattices onto 2 dimensions, and we obtained four quasilattices which are distinguishable from each other by their symmetries.

Table.1 4-D R-dec. and Q-irred. Groups and their decompositions

4-D Group	Family 18 26/01/01/	Family 19 27/01/01	Family 19 27/02/01	Family 20 28/01/01
Generator	$\begin{pmatrix} 0 & 0 & 0 & -1 \\ 1 & 0 & 0 & 0 \\ 0 & 1 & 0 & 0 \\ 0 & 0 & 1 & 0 \end{pmatrix}$	$\begin{pmatrix} 0 & 0 & 0 & 1 \\ -1 & -1 & -1 & -1 \\ 1 & 0 & 0 & 0 \\ 0 & 1 & 0 & 0 \end{pmatrix}$	$\begin{pmatrix} 1 & 1 & 1 & 1 \\ -1 & 0 & 0 & 0 \\ 0 & -1 & 0 & 0 \\ 0 & 0 & -1 & 0 \end{pmatrix}$	$\begin{pmatrix} 0 & 1 & 0 & 1 \\ -1 & 0 & -1 & 0 \\ 0 & -1 & 0 & 0 \\ 1 & 0 & 0 & 0 \end{pmatrix}$
Order n Angle ϕ	8 $2\pi/\ 8$	5 $2\pi/\ 5$	10 $2\pi/\ 10$	12 $2\pi/\ 12$
Metric matrix*	$\begin{pmatrix} a & b & 0 & -b \\ b & a & b & 0 \\ 0 & b & a & b \\ -b & 0 & a & a \end{pmatrix}$	$\begin{pmatrix} a & b & c & c \\ b & a & b & c \\ c & b & a & b \\ c & c & b & a \end{pmatrix}$	$\begin{pmatrix} a & b & c & c \\ b & a & b & c \\ c & b & a & b \\ c & c & b & a \end{pmatrix}$	$\begin{pmatrix} a & 0 & \frac{-a}{2} & b \\ 0 & a & -b & \frac{-a}{2} \\ \frac{-a}{2} & -b & a & 0 \\ b & \frac{-a}{2} & 0 & a \end{pmatrix}$
Transformation matrix W	$\begin{pmatrix} 1 & 0 & 1 & 0 \\ \frac{1}{\sqrt{2}} & \frac{1}{\sqrt{2}} & \frac{1}{\sqrt{2}} & \frac{1}{\sqrt{2}} \\ 0 & 1 & 0 & -1 \\ \frac{1}{\sqrt{2}} & \frac{1}{\sqrt{2}} & \frac{1}{\sqrt{2}} & \frac{1}{\sqrt{2}} \end{pmatrix}$	$\begin{pmatrix} 1 & 0 & 1 & 0 \\ cc & -ss & c & s \\ c & s & cc & ss \\ c & -s & cc & -ss \end{pmatrix}$	$\begin{pmatrix} 1 & 0 & 1 & 0 \\ -c & -s & cc & -ss \\ cc & ss & -c & -s \\ cc & -ss & -c & s \end{pmatrix}$	$\begin{pmatrix} 1 & 0 & 1 & 0 \\ 0 & -1 & 0 & -1 \\ \frac{1}{2} & \frac{\sqrt{3}}{2} & \frac{1}{2} & \frac{\sqrt{3}}{2} \\ \frac{\sqrt{3}}{2} & \frac{1}{2} & \frac{\sqrt{3}}{2} & \frac{1}{2} \end{pmatrix}$
New generator	$\begin{pmatrix} c & -s & 0 & 0 \\ s & c & 0 & 0 \\ 0 & 0 & cc & -ss \\ 0 & 0 & ss & cc \end{pmatrix}$	$\begin{pmatrix} c & -s & 0 & 0 \\ s & c & 0 & 0 \\ 0 & 0 & cc & -ss \\ 0 & 0 & ss & cc \end{pmatrix}$	$\begin{pmatrix} c & -s & 0 & 0 \\ s & c & 0 & 0 \\ 0 & 0 & cc & -ss \\ 0 & 0 & ss & cc \end{pmatrix}$	$\begin{pmatrix} c & -s & 0 & 0 \\ s & c & 0 & 0 \\ 0 & 0 & cc & -ss \\ 0 & 0 & ss & cc \end{pmatrix}$
Faithful rep. of cyclic group of order n	$c + is = e^{i\phi}$ $cc + iss = e^{i3\phi}$ $e^{-i\phi}$ $e^{-i3\phi}$	$c + is = e^{i\phi}$ $cc + iss = e^{i2\phi}$ $e^{-i\phi}$ $e^{-i2\phi}$	$c + is = e^{i\phi}$ $cc + iss = e^{i3\phi}$ $e^{-i\phi}$ $e^{-i3\phi}$	$c + is = e^{i\phi}$ $cc + iss = e^{i5\phi}$ $e^{-i\phi}$ $e^{-i5\phi}$
Symmetry pattern	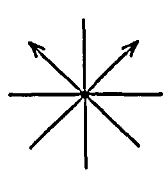	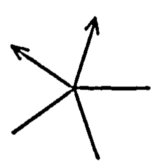	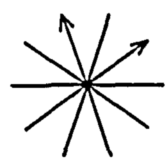	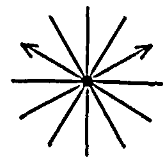

* a, b are two free parameters, and $c = -(a + b)/\ 2$.

Figure Captions

Fig.2.1 Construction of one dimensional quasilattice by projecting a strip of two dimensional rectangular lattice onto one dimension. (page 36)

Fig.2.2 a) Cluster LLSLS in the perfect Fibonacci lattice. b) A mistake occurred at site x(n): the cluster became LSLLS. c) A segment of a perfect Fibonacci lattice. All clusters of type LLSLS are underlined. The distance between these clusters is either $S'=3L+2S=\tau^4 S$ or $L'=5L+3S=\tau^4 L$ and follows the same Fibonacci sequence, hence form a Fibonacci lattice with basic length $S=\tau^4 S$. (page 37)

Fig.3.2 The diffraction pattern calculated from Eq.2.2.11 and Eq.2.2.14 with p=0.2 (the "concentration" of mistakes is $p\tau^{-4}=3\%$) in Eq.2.2.8. The radius of a spot corresponds to the intensity. Top row: perfect lattice; Bottom row: imperfect case. When mistakes occur, spots such as those shown by arrows in the top row are diminished below cut off, and spots such as those shown by arrows in the figures in the bottom row are enhanced above the cut off. Shown: diffraction on planes normal to: a) five-fold, b) two-fold, and c) three-fold axes. (page 38,39,40)

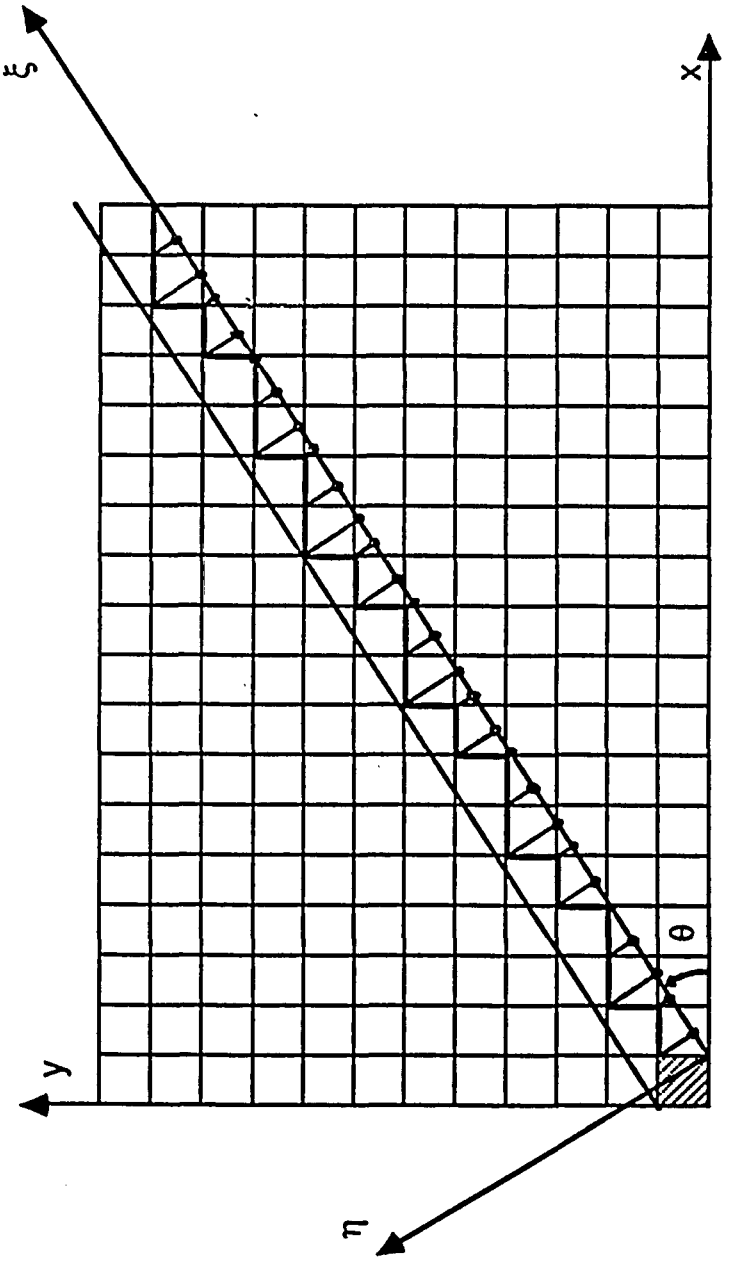

Fig.2.1

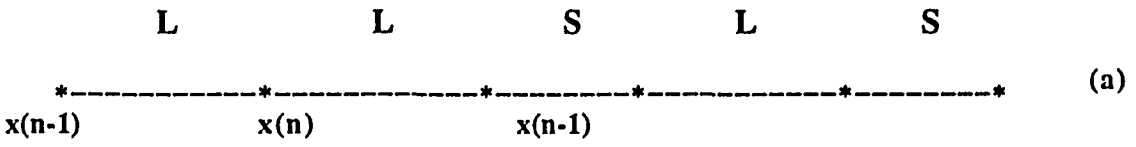

(a)

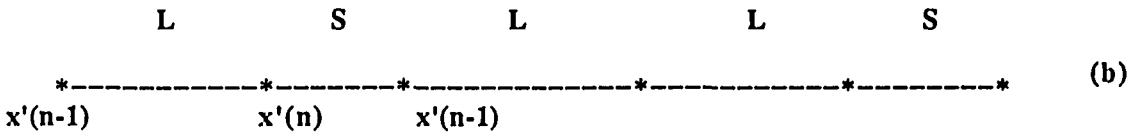

(b)

LS LLSLSLLS LLSLS LLSLSLLS LLSLSLLS LLSLS LLSLSLLS

L' S' L' L' S' L'

(c)

Fig.2.2

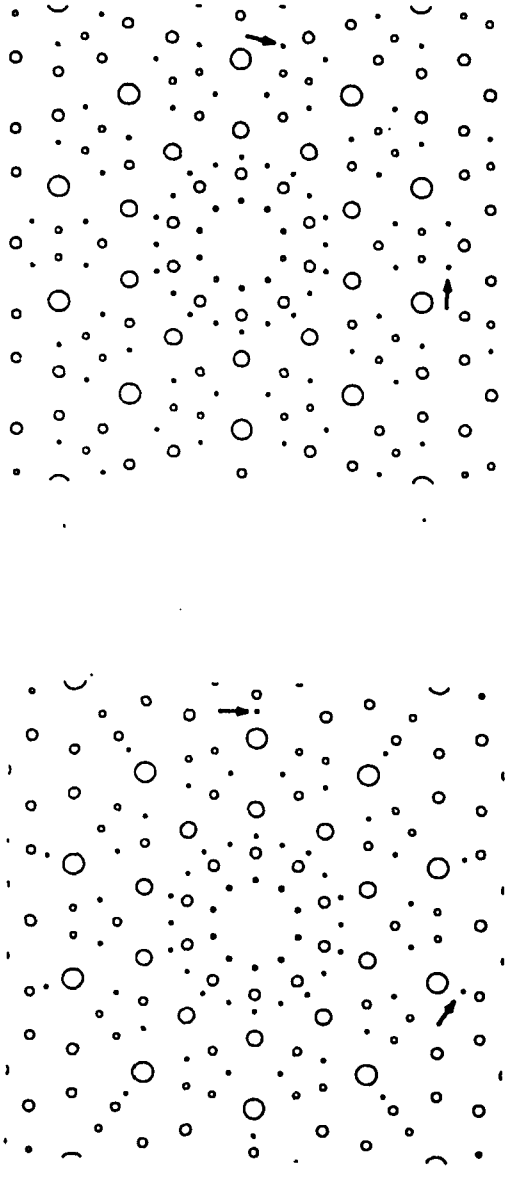

Fig.2.3a

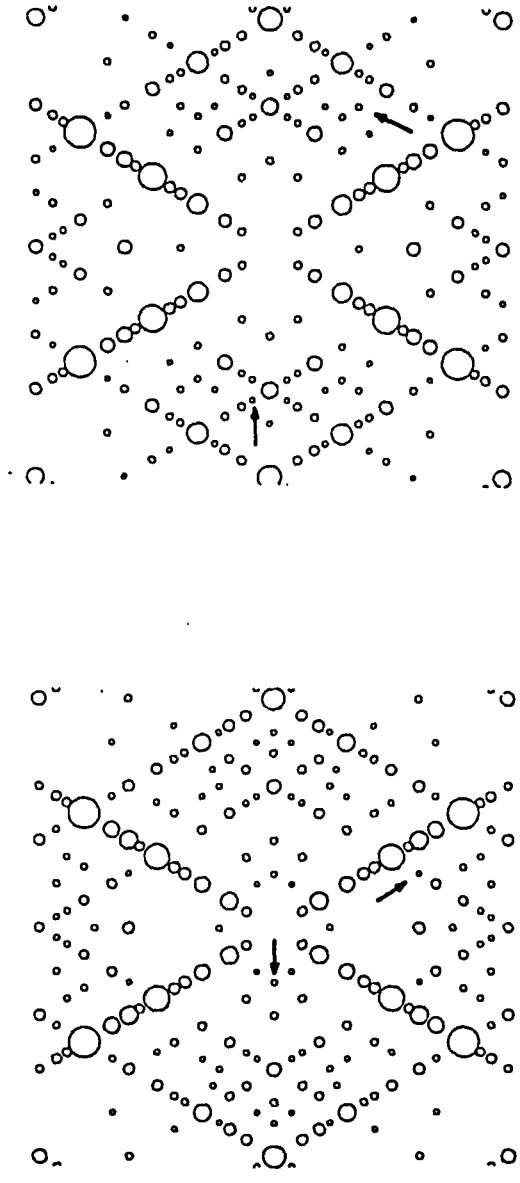

Fig.2.3b

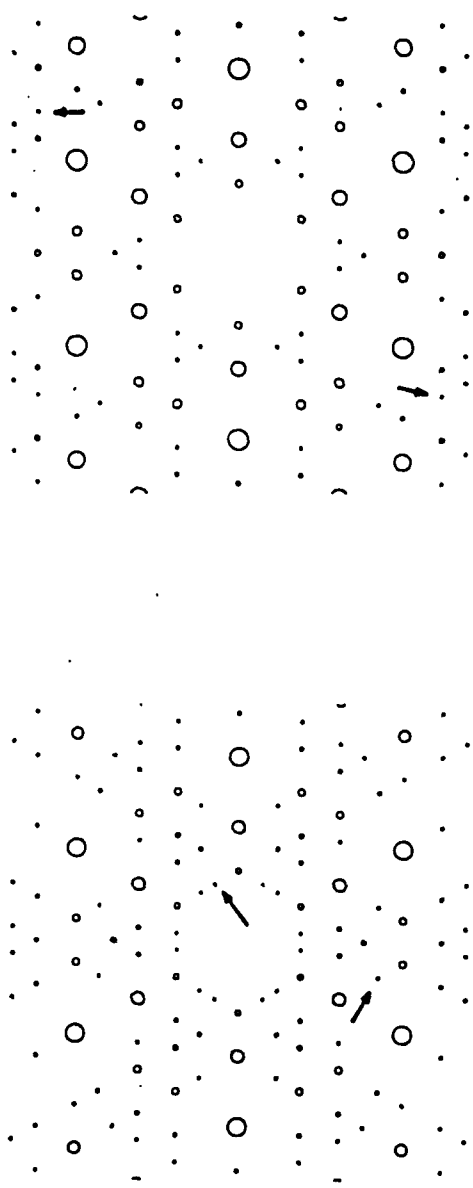

Fig.2.3c

CHAPTER 3

ENERGY SPECTRA AND THE QUASI-BLOCH THEOREM

3.1 VIBRATIONAL SPECTRUM

Consider a one dimensional chain of atoms connected by harmonic springs. If the system is periodic, Bloch's theorem tells us that the solution of the equation of motion is wave like, the phonon spectrum forms one or more bands, and the density of states is singular near the band edges. On the other hand if the lattice is totally disordered, the wave function exhibits localization behavior, and the spectrum is a discrete set. However as we pointed out in the last chapter, the quasiperiodic lattice is intermediate between periodic and disordered systems, so it would not be surprising if it showed spectral characteristics of both systems[39].

3.1.1 Numerical Analysis In One Dimension

Consider a chain of atoms connected by spring constants. Let $u_n e^{-i\omega t}$ be the displacement of the nth atom from its equilibrium position and $k_{n,n+1}$ the spring constant connecting the nth to n+1th atom and m_n the mass of the nth atom. The equation of motion is

$$-m_n\omega^2 u_n = k_{n\,n+1}(u_{n+1} - u_n) + k_{n-1\,n}(u_{n-1} - u_n); \quad n = 0, 1, \ldots, N \qquad 3.1.1$$

We are unable to solve a set of N of these equations analytically for quasiperiodic lattices. The difficulties come from the fact that the nearest neighbor configurations of the nth atom can not determine completely the nearest neighbors configuration of the n+1th atom even though the number of different near neighbor configuration is a finite small set. However by using the transfer matrix method[61] we have been able to obtain the spectrum numerically for N up to 8×10^3. Extensive calculations were carried out for the Fibonacci sequence and

some calculations were also done for the other examples given in section 2.1.

Introducing a displacement vector (u_{n-1}, u_n), one can write

$$\mathbf{u}_n = \begin{bmatrix} u_{n-1} \\ u_n \end{bmatrix} = \begin{bmatrix} a(n) & b(n) \\ 1 & 0 \end{bmatrix} \cdot \begin{bmatrix} u_n \\ u_{n+1} \end{bmatrix} = T_n \mathbf{u}_{n+1} \qquad 3.1.2$$

where

$$a(n) = 1 + \frac{k_{n\,n+1}}{k_{n-1\,n}} - m_n \frac{\omega^2}{k_{n-1\,n}}, \qquad b(n) = -\frac{k_{n\,n+1}}{k_{n-1\,n}} \qquad 3.1.3$$

For a finite chain of N+2 sites

$$\mathbf{u}_1 = T_1 T_2 \ldots T_{N-1} T_N \mathbf{u}_{N+1} = A u_{N+1} \qquad 3.1.4$$

To obtain the eigenfrequency we must impose a boundary condition. We will use the fixed ends boundary condition $u_0 = u_{N+1} = 0$* . Thus

$$\begin{bmatrix} 0 \\ u_1 \end{bmatrix} = \begin{bmatrix} A_{11} & A_{12} \\ A_{21} & A_{22} \end{bmatrix} \begin{bmatrix} u_N \\ 0 \end{bmatrix} \qquad 3.1.5$$

To have a non-trivial solution for u_N , ω must satisfy the eigenvalue equation

---

* The other boundary condition one can use is the periodic boundary condition $\mathbf{u}_{N+1} = \mathbf{u}_1$. Then one gets the eigenvalue equation det (A (ω) - I) = 0. The results are almost the same for both boundary conditions except for a small difference at very low frequency, and the difference vanishes as N --> ∞. The physical reason behind this is clear: at very low frequency the wavelength is long enough to be comparable with the length of the system numerical simulated. Since we are interested in N --> ∞ limit we will not further elaborate this point .

$$A_{11}(\omega) = 0 \qquad 3.1.6$$

From the eigenvalue equation the spectrum and density of states are obtained. For large N these spectra should approach the true spectra of a infinite system.

Consider the case that all atoms are identical, i.e. m_n =m for all n and there are only two different spring constants k_L or k_S (Fig.3.1), depend on whether the distance between two atoms is long or short as per the Fibonacci sequence. There are only three possible types of nearest neighbor configuration for the Fibonacci chain, namely LS,SL and LL . The corresponding transfer matrices T_j are

$$1)\quad SL;\quad T' = \begin{bmatrix} 1 + \frac{k_L}{k_S}\left(1 - \frac{m\omega^2}{k_L}\right) & -\frac{k_L}{k_S} \\ 1 & 0 \end{bmatrix} \qquad 3.1.7$$

$$2)\quad LS\ ;\quad T'' = \begin{bmatrix} 1 + \frac{k_S}{k_L}\left(1 - \frac{m\omega^2}{k_S}\right) & -\frac{k_S}{k_L} \\ 1 & 0 \end{bmatrix} \qquad 3.1.8$$

$$3)\quad LL;\quad T''' = \begin{bmatrix} 2 - \frac{m\omega^2}{k_L} & -1 \\ 1 & 0 \end{bmatrix} \qquad 3.1.9$$

The matrix A is the product of N of these matrices with the order determined by the quasiperiodic sequence. Numerical calculation was carried out for different $N(100 \le N \le 8000)$ with different values of $\lambda = k_L/k_S$.

The following conclusions are suggested from the results of numerical simulations:

1) In the low frequency region ($x = m\omega^2/k_S << 0.1$), the spectrum and wave function behave almost identically as for the ordinary periodic lattice. The integrated density

of states can be fitted by

$$D(\omega^2) \approx C\sqrt{\omega^2} \qquad 3.1.10$$

where C is a constant (Fig.3.2). The wave functions look essentially like a single harmonic periodic wave (Fig.3.4a), suggesting that a long wavelength wave propagates along the system with sound velocity proportional to the constant C. A simple estimation for C is given by taking the geometrical average of the parameters involved, namely the lattice spacing and spring constant, then treating the system as periodic with these averaged parameters. This gives $C = \tau / (2\pi\sqrt{1+\tau\lambda})$. The fitting is shown in Fig.3.2 and the agreement is good.

2) Careful examination of our results shows that the spectrum is selfsimilar. The selfsimilarity is more explicit in the high frequency region (Fig.3.3). From this we conjecture that the spectrum is "Cantor-like" for an infinite system. The spectra are band-like if one neglects small gaps which may not be distinguishable experimentally. Near the edges of these "bands" the density of states do exhibit van Hove singularities[62]. The general structure of the spectrum will be discussed in the next section.

3) In general the wave functions have three different types of behavior, a) extended; b) localized; c) between type a) and b) (Fig.3.4). Some workers[63] call type c) critical. Generally speaking the wave function is extended for very low frequencies and tends to be localized for high frequencies. However we do not find any region in which all wave functions are localized. In fact most wave functions are critical.

4) For different quasilattices the qualitative features are the same, although the detailed distribution of gaps are different.

Similar spectra and wave functions have been observed in the one dimensional

incommensurate system. In the work of Kohmoto et al[64] and Ostlund et al[65] the tight binding Hamiltonian obtained from a periodic potential was studied. By chosing a specific discontinuous periodic potential whose period is incommensurate with the lattice period they have reduced the problem to a product of transfer matrices which follow the Fibonacci sequence. However their transfer matrices are quasiperiodic only in the diagonal matrix element because it originated from the potential in the Schrodinger equation. And the system we studied has quasiperiodicity in both diagonal and off diagonal terms (Eq.3.1.7-3.1.9). Another difference is that they used a periodic boundary condition which permitted reduction to a one dimensional mapping. Obviously that system is qualitatively different from our system. Nonetheless the qualitative features of the spectra are the same.

3.1.2 The Structure Of The Spectrum

As we pointed out in the last section, in the limit N-->∞, there are an infinite number of gaps in the spectrum, the integrated density of states is selfsimilar, and the spectrum is Cantor-like. To further support this point, in this section we will develop a new technique, which combines the continued fraction expansion method and the real space renormalization method, to examine the spectra.

Introduce dimensionless parameters $x=m\omega^2/k_S$ and $\lambda=k_L/k_S$. We first carry out numerical calculations of the spectrum for different λ ranging from 0 to 1.0 (Fig.3.5a). For λ=0.0 namely k_L=0.0, the chain breaks into isolated atoms and islands of two atoms connected by k_S, hence the only possible eigenvalues are x=0 or 2. On the other hand for λ=1.0 the chain becomes a monatomic chain connected by the same spring constant. In this case no gap should appear. Define z_i by (see Eq.3.1.2, Eq.3.1.3)

$$\frac{u_{i-1}}{u_i} = a(i) + b(i)\frac{u_{i+1}}{u_i} = a(i)(1+z_i) \qquad 3.1.11$$

where (a_i, b_i) are functions of x and λ (Eq.3.1.3). Then z_i can be written as

$$z_i = \frac{b(i)a(i)^{-1}a(i+1)^{-1}}{1+z_{i+1}} = \frac{\rho_i}{1+z_{i+1}}; \qquad \rho_i = \frac{b(i)}{a(i)a(i+1)} \qquad 3.1.12$$

One can then write

$$z_1 = \cfrac{\rho_1}{1+\cfrac{\rho_2}{1+\cfrac{\rho_3}{1+\ldots}}} \quad \ldots \quad \ldots \quad 1+\frac{\rho_n}{z_{n+1}} \qquad 3.1.13$$

The boundary condition $u_0=u_{N+1}=0$ corresponds to $z_{N+1}=\infty$ and $z_1=-1$.

On the other hand Worpitzky's theorem[66,67] states that for ρ_j a function of any variable over a domain D:

If

$$\left|\rho_j \le \frac{1}{4}\right| \quad for\ all\ j \qquad 3.1.14$$

Then

a) the continued fraction z_1 (Eq.3.1.13) converges uniformly over the domain D;

b) $$|z_1| \le \frac{1}{2} \qquad 3.1.15$$

c) the constant 1/4 is the best constant that can be used in Eq.3.1.14 and Eq.3.1.15 is the best domain of values of z_1.

Let us apply this theorem to our problem: $z_1(x, \lambda)$ will not satisfy boundary conditions if Eq.3.1.14 holds. So, Eq.3.1.14 is a sufficient condition for x not to be part

of the allowed spectrum, i.e. x is in a gap.

As pointed out in the last section we can have three different types of transfer matrix, hence we have three different sets of (a_i, b_i). Because of the special geometrical properties of the sequence they can only give four different ρ_j (Fig.3.6)

$$\rho_1 = \frac{b_3}{a_3 a_2}; \quad \rho_2 = \frac{b_2}{a_2 a_1}; \quad \rho_3 = \frac{b_1}{a_1 a_3}; \quad \rho_4 = \frac{b_1}{a_1 a_2}; \qquad 3.1.16$$

If we consider the original sequence, then a and b take the following values, depending on the sequence

$$SL: \quad a_1 = 1 + \lambda - x; \qquad b_1 = -\lambda$$

$$LS: \quad a_2 = 1 + \frac{1}{\lambda} - \frac{x}{\lambda}; \quad b_2 = -\frac{1}{\lambda}$$

$$LL: \quad a_3 = 2 - \frac{x}{\lambda}; \qquad b_3 = -1 \qquad 3.1.17$$

For a given λ and x , if all the ρ_j satisfy Eq.3.1.14 then the point belongs to the gap region. Note the condition is sufficient but not necessary, therefore even if Eq.3.1.14 is not satisfied, the point may still belong to a gap. It is not surprising that by this method we only found a small portion of the gap regions obtained in the numerical study i.e., the triangle formed by three points:(0,2.0), (0,4.0), (1.0,4.0) in Fig.3.7.

As the sequence is selfsimilar, we have developed the decimation transformation on coefficients ρ_i. As an example, for the type of near neighbor shown in Fig.3.6b one can write

$$u_{i-1} = a_2 u_i + b_2 u_{i+1}; \qquad u_i = a_1 u_{i+1} + b_1 u_{i+2} \qquad 3.1.18$$

From these equations one immediately obtains

$$u_{i-1} = \left(a_2 + \frac{b_2}{a_1}\right)u_i - \frac{b_1 b_2}{a_1}u_{i+2} \qquad 3.1.19$$

After decimation the sequence LSL becomes S'L'. Comparing Eq.3.1.19 with Eq.3.1.18 one gets new coefficients (a'_1, b'_1). Similarly , the decimations change SLL and SLSL to L'S' and L'L' , respectively (Fig.3.6). The recurrence relations for (a,b) are the following

$$a'_1 = a_2 + \frac{b_2}{a_1}; \qquad b'_1 = -\frac{b_1 b_2}{a_1}$$

$$a'_2 = a_1 a_3 + b_1; \qquad b'_2 = a_1 b_3$$

$$a'_3 = a_1 a_2 + b_1 + b_2; \quad b'_3 = -b_1 b_2 \qquad 3.1.20$$

The sequence after decimation has the same geometrical properties as the original sequence and (a',b')s can form the same four different types of ρ_j. Hence we can again apply Worpitzky's theorem to the new set of ρ_j's. This procedure can be repeated. The result for decimations repeated 10-times is shown in Fig.3.5b: the agreement with Fig.3.5a is excellent. To confirm the conjecture we made before, namely that in the limit of an infinite system the spectrum is Cantor-like, we show in Fig.3.7 the result obtained by different numbers of decimations. One sees as n gets bigger the area of the gap region also gets bigger and eventually covers the whole figure. This is a clear indication that the spectrum (unshaded area in Fig.3.7) is a point spectrum.

The procedure just described is very efficient. As an example, the computer CPU time needed to get Fig.3.5b is two orders of magnitude less than that for Fig.3.5a, while the information is almost same.

The above result also favors the argument that the big gap region came from repeating a small unit cell. For example the segment LS appears an infinite number of times in the Fibonacci sequence with large frequency. In fact any segment of arbitrary length appears an infinite number of times in the infinite system, but with different frequency. In

section 3.3 I'll show that the apearing frequency, which corresponding to the Fourier amplitude, is the major factor that determines the gap width. We have also carried out successive approximations to the golden mean, that is the Fibonacci number. By treating the system as periodic with period F_n, one can see the splitting of the spectrum. Big gaps will be generated at the early stages of approximation and remain as gaps later on. The width of gap changes but convergence is rapid.

In the above calculations, the physical system implemented is that A=L, B=S (see Eq.2.1.2) and we associated the two different spring constants k_L and k_S with these distances respectively. This is not the only possible implementation; for example, one can take A=S, B=L instead. The geometrical and the scaling properties of the sequence will not change and the analysis carried out above is equally applicable. For example in Fig.3.8 we show a result with this later implementation. Note in this case there are combinations like SS but not LL in the sequence; hence taking $\lambda=k_L/k_S=0$ breaks the sequence into segments of either two or three atoms connected by the same spring k_S. Therefore the eigenvalues are $x=m\omega^2/k_S= 0, 1, 2, 3$. Mathematically this implementation is equivalent to the previous one if instead of λ changing from 0 to 1, λ changes from ∞ to 1.

3.2 ELECTRONIC SPECTRUM

Consider a tight binding Hamiltonian

$$H = \sum_i |i-1\rangle\, t_{i-1\,i}\langle i| + |i\rangle t_{i\,i+1}\langle i+1| \qquad 3.2.1$$

where |i> represents a Wannier state associated with site i and t_{ij} is the nearest neighbor hopping matrix. One can expand the electron wave function in terms of this orthogonal set

$$\Phi = \sum_i u_i |i\rangle \qquad 3.2.2$$

Schroldinger's equation then can be written as

$$Eu_i = t_{i-1\,i} u_{i-1} + t_{i\,i+1} u_{i+1} \qquad 3.2.3$$

or

$$u_i = \frac{E}{t_{i-1\,i}} u_i - \frac{t_{i\,i+1}}{t_{i-1\,i}} u_{i+1} = a_i u_i + b_i u_{i+1} \qquad 3.2.4$$

where E is the energy eigenvalue. Similar to Eq.3.1.18, one finds three different set of (a,b)

$$a_1 = x\,; \qquad b_1 = -\lambda$$

$$a_2 = \frac{x}{\lambda}; \qquad b_2 = -\frac{1}{\lambda}$$

$$a_3 = \frac{x}{\lambda}; \qquad b_3 = -1 \qquad 3.2.5$$

where $x=E/t_L$, $\lambda=t_L/t_S$ and t_L, t_S have meaning similar to k_L, k_S in last section. The analysis of the last section can be repeated but with new initial (a,b)s. The result is shown in Fig.3.9. The characteristics of the spectrum are the same as the vibrational spectrum, agreeing with a computer simulation[70]. And the conclusions drawn in last section are equally applicable.

The analysis and calculations in the above sections can be carried over to general one dimensional quasilattices in a straightforward way. The main conclusions should be the same. In summary, the quasiperiodic system reflects properties of both periodic and disordered system. The spectra (both phonon and electron) were shown to be Cantor-like

by decimation calculations and they possess characteristics of both periodic and disordered system. On the one hand it is a Cantor-like spectra, on the other hand it is band-like and exhibits van Hove singularities near the band edges if one neglects the small gaps. Similar spectral gaps and the van Hove singularity are also found in the Penrose tiling[62,68]. If the Penrose tiling model is a true basic structure for the new materials found, one needs a generalization of the present analysis to three dimensions in order to compare with experiments. However we expect the qualitative features of the spectra will carry over to two and three dimensional cases[68]. Our results also agree with some later studies[69,70,71,72].

In next section we will show that the characteristics of the energy spectrum can be understood in the general framework of a quasi-Bloch theorem, which plays a similar role as that of the Bloch theorem for periodic systems.

3.3 QUASI-BLOCH THOREM

In last section we demonstrated that the energy spectrum of a quasiperiodic system possesses a complex structure, especially the hierarchical gap structure. Several other numerical studies also reach similar conclusions. However the results remain to be put into a more general theoretical framework such as the Bloch theorem provides for periodic system.

In this section we show that a quasi-Bloch theorem can be developed based on the projection method. The theorem will enable one to draw qualitative conclusions about the wave function and energy spectrum of a quasiperiodic system in n dimensions.Using a boost technique we obtain a periodic "pseudo-Schroldinger" equation in (n+m)-Dimensions which, upon projection down to n dimensions produces the solutions for the quasiperiodic

system.

There have been many numerical simulations of the energy spectra of quasilattices[39,68,69,70,71,72].The results indicate that there is a complex structure consisting of many gaps and singularities in the energy spectrum. And wave functions exhibit extended, critical and localized behavior. The results of our present analysis are in agreement with those simulations and provided a basis for understanding those results and for further studies.

3.3.1 The Theorem

In this section we use the following notation: x -- an n dimensional vector designating the coordinate of the electron; $\{X_i\}$-- the lattice point of the quasiperiodic lattice in n dimensions; z -- an n+m dimensional vector, $z=x\oplus y$,where y is an m dimensional vector orthogonal to x; $\{Z_j\}$ -- the lattice point of a periodic lattice in n+m dimensions, $Z=X\oplus Y$ ($\{X\}$ or $\{Y\}$ by themselves do not form a periodic lattice); the reciprocal of (x,y,z,X,Y,Z) are denoted as (q,p,k,Q,P,K).

Consider the Schroldinger equation for an electron in a n dimensional quasicrystal described by a quasiperiodic potential V(x):

$$\left[-\frac{\partial^2}{\partial x^2}+V(x)\right]\phi(x)=\mu\phi(x) \qquad 3.3.1$$

here V(x) is a quasiperiodic function of x. Without loss of generality one can write

$$V(x)=\sum_i v(x-x_i) \qquad 3.3.2$$

where v(x) is the electronic potential due to a single ion. The summation is over all the quasilattice points $\{x_j\}$ at which the ions are located. Hence both V(x) and Eq.3.3.1 are

nonperiodic and the Bloch theorem is not applicable. The idea of our approach is to boost Eq.3.3.1 from n dimensions to higher (n+m) dimensions, such that one obtains a periodic pseudo-Schroldinger equation in n+m dimensions.

To construct the pseudo-Schroldinger equation let us consider the potential part first. The Fourier transform of V(x) is

$$\bar{V}(q) = \int V(x) e^{iqx} dx = \bar{v}(q) \sum_i e^{iqx_i}$$

$$= \bar{v}(q) F(q) \qquad 3.3.3$$

where $\bar{v}(q)$ is the Fourier transform of a simple ionic potential and F(q) is the structure factor of the quasicrystal.

There are many models for the structure of a quasicrystal. However the fundamental skeleton of the lattice in all of these structures are similar. For simplicity we will assume that the structure of a quasicrystal is a quasilattice in n dimensions obtained by a projection from a n+m dimensional periodic lattice. The structure factor of the quasilattice, namely the diffraction amplitude has been extensively studied (see last chapter), and we follow the general approach of Bak[19]. It is based on the fact that the diffraction pattern of a quasicrystal can be integer indexed. Therefore we define a quasilattice as a structure in n dimensions whose diffraction pattern can be integer indexed by n+m linear independent vectors. Mathematically this means that F(q) can be written as

$$F(q) = \sum_{K_i} f(K_i) \delta\left(q - K_i^{\parallel}\right) \qquad 3.3.4$$

where the summation is over a periodic lattice {K} in n+m dimensions and $K_i^{\parallel}$ is the projection of K on the n-dimensional sub-space spanned by q.

Define a pseudo-potential U(z) in n+m dimensions such that its Fourier transform is

$$\bar{U}(k) = \bar{v}(q)\sum_{K_i} f(K_i)\delta\left(q - K_i^{\parallel}\right)\delta\left(q - K_i^{\perp}\right)$$

$$= \sum_{K_i} \bar{U}(K_i)\delta(k - K_i) \qquad 3.3.5$$

where $K = K^{\parallel} \oplus K^{\perp}$ and $\bar{U}(K) = \bar{v}(K^{\parallel}) f(K)$. Therefore

$$U(z) = \int \bar{U}(k) e^{izk} dk = \sum_{K_i} \bar{U}(k_i) e^{izK_i}$$

$$= U(z + Z) \qquad 3.4.6$$

is a periodic function of z with fundamental period {Z} which is defined as the reciprocal lattice of {K} ($Z^*K = 2\pi \times integer$). From the definition of U(z) one can verify that

$$V(x) = \int U(z)\delta(y)dy \qquad 3.4.7$$

This is the simplest example of a Radon transform[73].

Next we consider how to boost the kinetic operator. An obvious choice is to leave the kinetic operator unchanged but re-expressed in the z coordinates. This turns out to be the critical step whose advantage will be seen shortly. Thus we obtain a boosted pseudo-Schroldinger equation in n+m dimensions:

$$\left(-\frac{\partial^2}{\partial x^2} + U(z)\right)\Psi(z) = E\Psi(z) \qquad 3.4.8$$

In terms of $z=\{z_i\}$ generally

$$\frac{\partial^2}{\partial x^2} = c_{ij}\frac{\partial^2}{\partial z_i \partial z_j} \qquad 3.4.9$$

with the c_{ij} defines the projecting plane. Then one has

$$\left(-c_{ij}\frac{\partial^2}{\partial z_i \partial z_j}+U(z)\right)\Psi(z)=E\Psi(z) \qquad 3.3.10$$

or symbolically $L(z)\Psi(z)=E\Psi(z)$. The operator L(z) is clearly translational invariant under lattice translation {Z} Therefore the solutions of Eq.3.3.10, according to Floquet theory will have Bloch form which can be indexed by wave vector k in n+m dimensional reciprocal space

$$\Psi_k(z)=e^{ikz}\Phi_k(z); \qquad E=E(k) \qquad 3.3.11$$

with $\Phi(z+Z)=\Phi(z)$. It is clear from Eq.3.3.10 that $E(k)=E(k^{\|})$ is a function of $k^{\|}$ only since $\Psi_{(q,p)}(z)$ satisfies the same equation as $\Psi_{(q,p+p')}(z)$, where $k=(k^{\|},k^{\perp})=(q,p)$ and p' is an arbitrary m dimensional vector. This is important as we will see that the eigenvalues of Eq.3.3.1 are exactly same as that of Eq.3.3.10 and from physical intuition certainly E(k) should not depend on p.

The important result is that the solutions of Eq.3.3.10 are directly related to those of Eq.3.3.1. This can be seen by applying the operator $\int\delta(y)dy$ to both sides of Eq.3.3.10. One gets

$$\left(-\frac{\partial^2}{\partial x^2}+V(z)\right)\Psi(z)\Big|_{y=0}=E\Psi(z)\Big|_{y=0} \qquad 3.3.12$$

since $V(x)=U(x,y)|_{y=0}$. Comparing with Eq.3.3.1 one immediately gets

$$\mu=\mu(k)=E(k)$$

$$\phi_k(x)=\Psi_k(z)\Big|_{y=0}=e^{ik^{\|}x}\Phi_k(x,y)\Big|_{y=0} \qquad 3.3.13$$

Therefore the nature of the electronic states in quasicrystals can be understood in terms of higher dimensional pseudo-Schroldinger equation. This offers one great advantage since now one can apply all the techniques which have been developed and extensively studied in the case of crystals to study the analytic properties of Eq.3.3.10 and therefore Eq.3.3.3.

3.3.2 Nearly Free Electron Approximation

The general approach just described can be used to analyze the analytical properties of the electronic spectrum in a quasicrystal. As an example we will show that in the weak potential limit the spectrum has a hierarchical structure of gaps. The number of gaps is infinite for the infinite system and the hierarchical structure can be indexed by a reciprocal lattice vector which is determined from the diffraction pattern of the quasilattice.

To solve Eq.3.3.10 one goes to Fourier space as is usually done for the case of the periodic crystal. Since Φ(z) and U(z) are periodic functions one can make the expansions

$$\Phi(z) = \sum_{K_i} c(K) e^{-iK_i z} \; ; \qquad U(z) = \sum_{K_i} \bar{U}(K) e^{-iK_i z} \tag{3.3.14}$$

Substituting Eq.3.3.14 and Eq.3.3.9 into Eq.3.3.10 one gets the basic equation

$$(\varepsilon(k - K) - E(k))c(K) + \sum_{K'} \bar{U}(K')c(K - K') = 0 \tag{3.3.15}$$

where $\varepsilon(k) = \dfrac{(hk^{\parallel})^2}{2M}$ is the free electron energy and the summation is over all reciprocal lattice points in n+m dimensions. In going to perturbation method one faces the problem of small denominators, namely the near degeneracy problem. This is because ε is a function of $k^{\parallel}$ only, and there are many different K which have their parallel components very close to each other, hence the near degeneracy of ε. However as we will show this actually does not

cause serious difficulty since the structure factor in the numerator goes to zero faster than the denominator.

In the weak coupling, nearly free electron approximation $\bar{v}(q)$ is a small, smooth quantity. Second order perturbation theory on energy eigenvalue leads to

$$E_K = \varepsilon_K + \sum_{K' \neq K} \frac{< K \mid U \mid K' >< K' \mid U \mid K >}{\varepsilon_K - \varepsilon_{K'}} \qquad 3.3.16$$

where we use the notation $E_K=E_K(k)$, $\varepsilon_K=\varepsilon(k-K)$. If the denominator in the summation is not small the correction to the energy is second order,therefore one only needs to restrict the summation to those K' which have eigenvalues close to that of state K. Denoting this set by K_j, one has

$$E_K = \varepsilon_K + \sum_{K' \neq K} \frac{\left|\bar{U}(K - K_j)\right|^2}{\varepsilon_K - \varepsilon_{K'}}$$

$$\approx \varepsilon_K + \sum_{K_j} \frac{\left|\bar{v}(0)\right|^2 \left|f(K_j - K)\right|^2}{2K^{\parallel} \cdot \left(K^{\parallel} - K_j^{\parallel}\right)} \qquad 3.3.17$$

Where we have approximated $\bar{v}\left(K_j^{\parallel} - K^{\parallel}\right)$ as constant since the argument is a small quantity and, only the leading term is kept in the denominator. For fixed $K^{\parallel}$, the set of K_j which has approximately the same parallel component as that of K in general can be written as (in the case m=n=1)

$$K_j = K + \left(\Delta K^{\parallel}, \Delta K^{\perp}\right) = K + (r_{n+1} - r_n\tau, r_{n+1}\tau + r_n) \qquad 3.3.18$$

where r_n are integers, and r_{n+1}/r_n is the successive approximation of the irrational number τ. For the case τ is the golden mean, r_n are Fibonacci numbers. From number theory one knows that the best approximation one can make as N->∞ is $r_{n+1} - r_n \approx \frac{1}{r_n}$. On the

other hand the diffraction amplitude is inversely proportional to $K^{\perp}$ which is the order of r_n. Therefore the term in the summation is the order of $\frac{|\bar{v}(0)|^2}{r_n} \approx \frac{|s(0)|^2}{r_n}$ which after summation over n is of the order $|v(0)|^2$ ($r_n \approx \tau^n$). Hence the correction is of the second order. So we conclude that for all practical purposes (and for the consistency of perturbation theory) the near degeneracy of large $K^{\perp}$, namely the small denominator problem can be exactly calculated and the correction is second order, therefore can be neglected[74].

However the degeneracy at the Bragg planes still exists. As in the case of a periodic crystal, this degeneracy will open up a gap at the Bragg plane with gap width proportional to the Fourier component of potential at the Bragg point[75],. Thus near the vicinity of K the eigenvalue can be written as

$$E_K(k) = \varepsilon(k^{\parallel}) \pm |\bar{v}(K^{\parallel})||f(K)| \qquad 3.3.19$$

One sees that there is an energy level splitting at every Bragg plane, and the amount of splitting is directly proportional to the structure factor or the diffraction amplitude at the Bragg point. From Eq.3.3.19 the splitting is meaningful only when the structure factor is not too small. In other words the effect is most important when k is on Bragg planes associated with dominant diffraction spots. Qualitatively when

$$|f(K)| \leq |\bar{v}(0)| \qquad 3.3.20$$

the gap width is of second order, namely it is the same order as the correction to the spectrum due to near degeneracy of $K^{\perp}$, therefore it is insignificant. This condition defines an effective reciprocal lattice which is not dense in the reciprocal space. For all practical calculations one needs only restrict oneself to this set of K vectors.

As the magnitude of the potential increases the simple perturbation theory just

presented will no longer be quantitatively valid. However one can expect the same qualitative effects will occur. The number of significant energy gaps will increase proportionally. In the strong coupling tight binding limit one expects that an infinite number of gaps will show up with the width of each energy gap having a similar hierarchical structure to that of the diffraction pattern.

The electronic spectrum of quasiperiodic systems in the tight binding approximation and in the Kronig-Penney potential, and the phonon spectrum have been extensively studied numerically by us and other groups (see section 3.1). The common basic conclusions are: 1) The spectrum is Cantor-like. There is a hierarchical structure of gaps which is dense in the limit of an infinite system. 2) The gap widths are different at different positions; if one only keeps those gaps which are larger than a certain amount then the spectrum can be divided into bands. 3) Wave functions are mostly critical and extended. There is some indication of localized state. These results now can be easily understood in terms of our present result. Especially the structure of the spectrum follows directly from this analysis. One finds that the hierarchical gap structure is intimately related to the diffraction pattern of the quasicrystal. All gaps can be indexed by wave vectors. And the gap width should be directly proportional to the diffraction amplitude at that wave vector.

3.3.3 An Example

In order to illustrate these results we calculated the integrated density of vibrational states schematically for a one dimensional quasilattice based on our qualitative predictions. In Fig.3.10 we plot the qualitative predictions of the spectrum, and comparing with previous numerical simulations Fig.3.3a one sees very good agreement. We started with the integrated density of states for the vibrational spectrum (the same equation holds for the tight binding model) in a periodic system. Using the dispersion relation

$E = \omega^2 = 4 \sin^2\left(\frac{q}{2}\right)$ (in dimensionless form) one obtains the integrated density of states $D(E) = \frac{2}{\pi} \sin^{-1}\left(\frac{\sqrt{E}}{2}\right)$. Since the structure factor of a one dimensional quasilattice (Fibonacci lattice) is analytically known, assuming a constant $\bar{V}(q)$ we calculated $\bar{U}(K)$ in Eq.3.3.19 for different K_i. A gap is opened at the energy corresponding to a K value using the dispersion relation above. Near every gap edge the square root singularity was fitted. The resulting density of states including the first 50 significant gaps are shown in Fig.3.10. Comparing with Fig.3.3a which is the result of numerical simulation of 2000 lattice sites, one sees that all the structural features of the spectrum are correctly reproduced. Considering the very crude schematic model we have used, the fitting is remarkable.

In the course of a study of incommensurate systems, a similar approach has been pursued by Romerio, Janssen and others[76,77,78]. However it was less systematic and was not pursued in depth. This was based on the judgement that though the results (such as energy spectrum) are rich in structure, they may not be experimentally observable, since the incommensurate term in the conventional incommensurate systems is weak and treated as perturbation. However in the case of quasicrystals the incommensurability is intrinsically built into the structure, so the incommensurate potential is not a weak perturbation at all. In fact the leading incommensurate terms are of the same order (1, τ^{-1}, τ^{-2}, ...) and there are an infinite number of terms. The effects of this intrinsic incommensurability on the electronic and other physical properties are not small. We believe systematic analysis could lead to some experimentally observable effect such as the negative differential conductivity in a strong electric field and oscillating of electric current due to Stark ladder and inter-band or Zener tunneling[79]. The theory can be tested as better and larger quasicrystals are made available for experiments.

In conclusion we have developed an analytical technique to study physical

properties of a quasiperiodic system. After suitably boosting the Schroldinger equation to a higher dimension we obtained a pseudo-Schroldinger equation which is periodic. Using the general Bloch-Floquet theory, the qualitative properties of eigenvalues and eigenfunctions can be analyzed. Then projecting the solutions down to the physical space we find the solution for a quasiperiodic system. The hierarchical gap structure in a quasiperiodic system found in numerical simulations is a natural result of this analysis. We predict that the gap positions can be determined by reciprocal wave vectors in the higher dimension and the gap width should be proportional to the scattering amplitude at that wave vector. The results are in full agreement with previous numerical simulations. This technique enables one to use the existing methods developed in the studies of crystal systems to study physical properties of quasiperiodic systems.

FIGURE CAPTIONS

Fig.3.1 A segment of a quasiperiodic harmonic chain. All atoms have the same mass and are connected by two different spring constants k_L and k_S. (page 65)

Fig.3.2 The integrated density of states in the low frequency region with $\lambda=1/\tau$.(see also Fig.3.3). The solid line is fitted by Eq.3.1.10 with C given in text. The system size is 6000 atoms. The horizontal axis is the scaled frequency $x=m\omega^2/k_S$, and the integrated density of states is normalized to 1. (page 66)

Fig.3.3 a) The integrated density of states for the Fibonacci chain of 2000 atoms with $\lambda=1/\tau$. The coordinates are same as in the Fig.3.2. b) The same as a), enlarged around x=3.10. c) The same as b), further enlarged around x= 3.0905. One see the selfsimilarity between a), b) and c). (page 67, 68, 69)

Fig.3.4 The wave function for $\lambda=1/\tau$ and 8000 atoms. The vertical axis is the square of wave the function (arbitrary unit), and the horizontal axis is the atomic coordinate (L=1.0, $S=1/\tau$. a) $x=m\omega^2/k_S=0.279\times10^{-5}$. It is a wave like extended state. b) x=0.627. There is a critical state. c) x=3.04, near the upper bound of spectrum. Obviously the state is localized at the right end. (page 70, 71, 72)

Fig.3.5 The phase diagram of the vibrational spectrum for the Fibonacci chain. The horizontal axis is $x=m\omega^2/k_S$ and the vertical axis is the relative strength of the spring constant $\lambda=k_L/k_S$. a) The numerical results. White blank areas belong to the gap. b) Gap regions (black area) predicted by Worpitzky's theorem with 10-fold decimation. One can see that this diagram is almost the exact complement of a). (page 73, 74)

Fig.3.6 The definition of (a,b) and the four possible combinations of ρ_j. a) LLS, b) LSL, c) SLL, d) SLSL. Those sites labeled by a cross are to be decimated. After decimation the segments b), c) and d) are shown in e), f) and g) respectively, which define the new coefficients (a',b'). (page 75)

Fig.3.7 Same as Fig.3.5b but with 40-fold decimation; the gaps cover almost all the region of the diagram. This is a clear indication that the spectra are point sets. The triangular part formed by three points A(3.0, 0.0),B(4.0, 0.0) and C(4.0, 1.0) is the gap region predicted by direct application of Worpitzky's theorem without a decimation transformation. (page 76)

Fig.3.8 The phase diagram of the vibrational spectrum for the Fibonacci lattice with second type of implementation. The coordinates are same as Fig.3.5, the result is obtained by 10-fold decimation. (page 77)

Fig.3.9 Electronic spectrum: the shaded area is the gap predicted by continued fraction expansion and renormalization. The horizontal axis is $x=E/t_L$ and the vertical axis is $\lambda=t_L/t_S$; a) 4-fold decimation. b) 10-fold decimation. (page 78, 79)

Fig.3.10 Vibrational integrated density of states for a one dimensional quasiperiodic system, as predicted by our theory using the simple model described in the text. Details on the construction of the cure are given in the text. This figure should be compared with Fig.3.3a which is the the numerical simulation results on a lattice of 2000 sites. One sees very good agreement. (page 80)

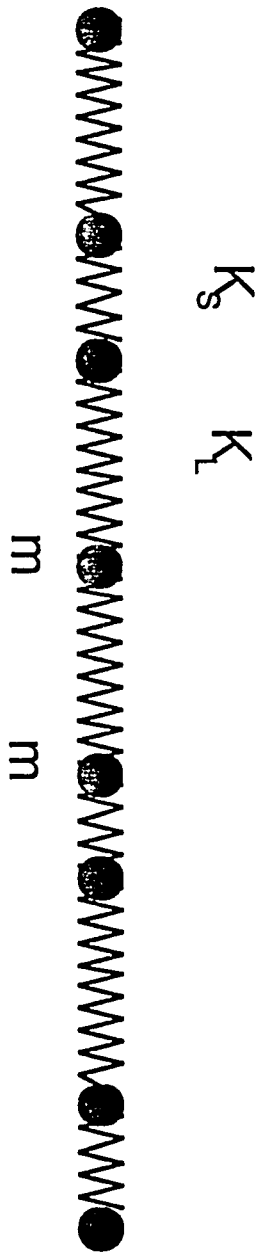

Fig.3.1

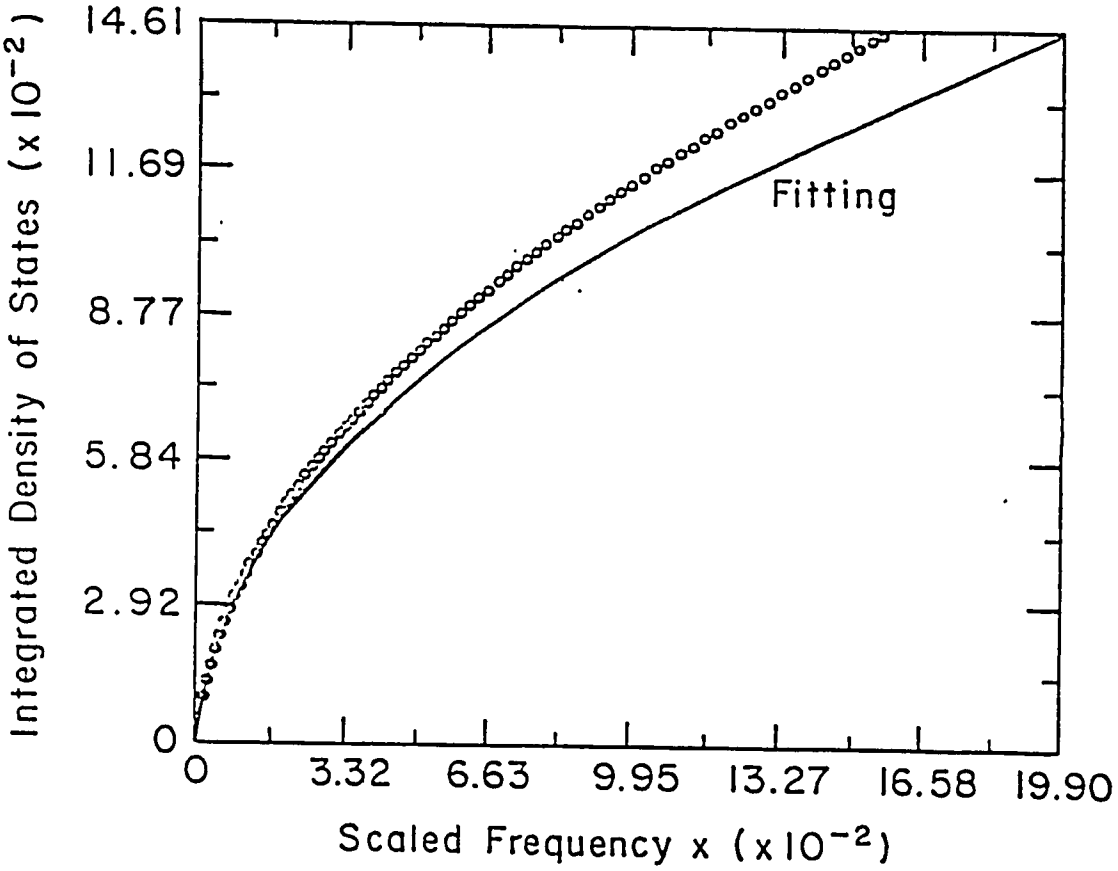
14.61
11.69
8.77
5.84
2.92
0
Integrated Density of States (x 10⁻²)
Fitting
0
3.32
6.63
9.95
13.27
16.58
19.90
Scaled Frequency x (x10⁻²)

Fig.3.2

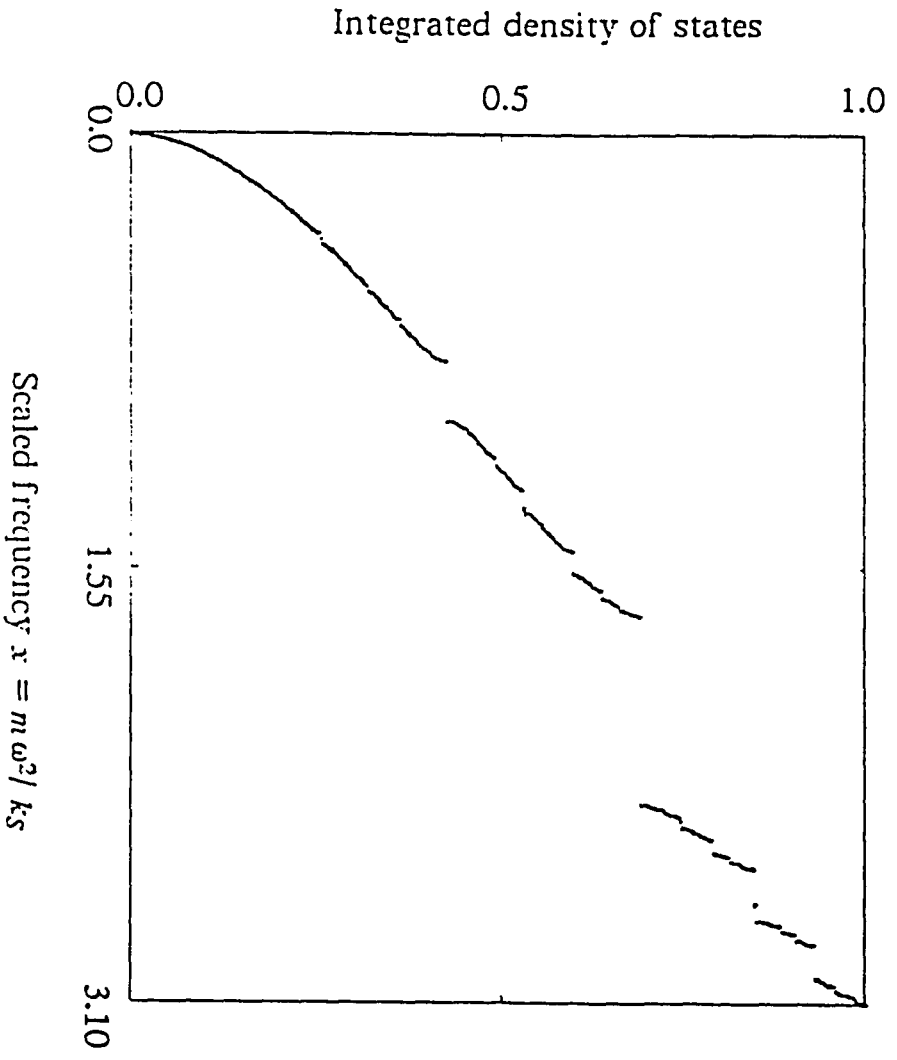
Integrated density of states
0.0
0.5
1.0
0.0
1.55
3.10
Scaled frequency $x = m\omega^2 / k_S$

Fig.3.3a

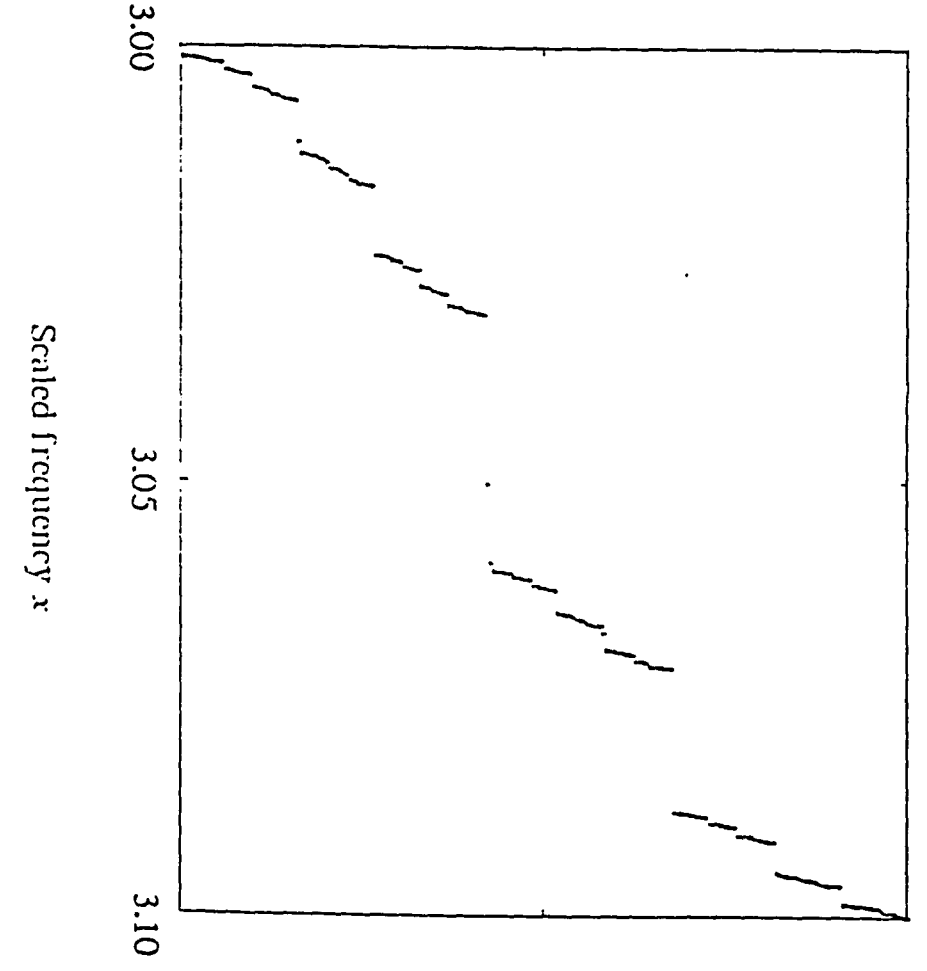

Fig.3.3b

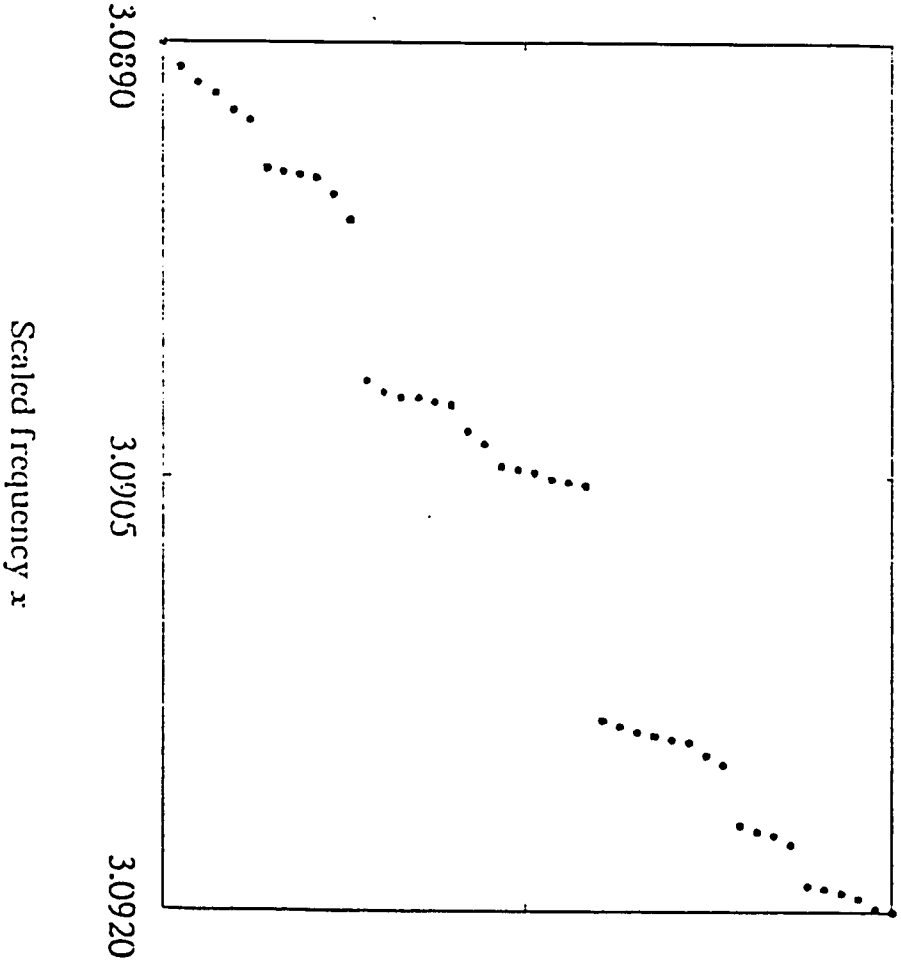

Fig.3.3c

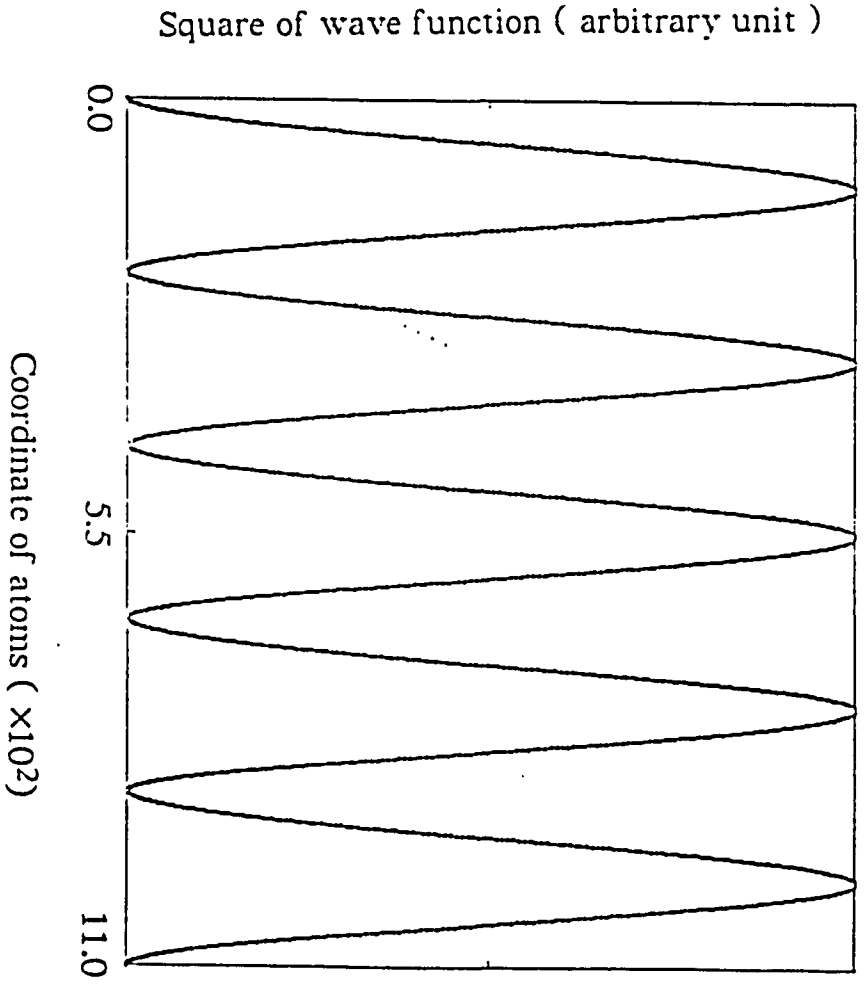
Square of wave function (arbitrary unit)
0.0
5.5
11.0
Coordinate of atoms (×10²)

Fig.3.4a

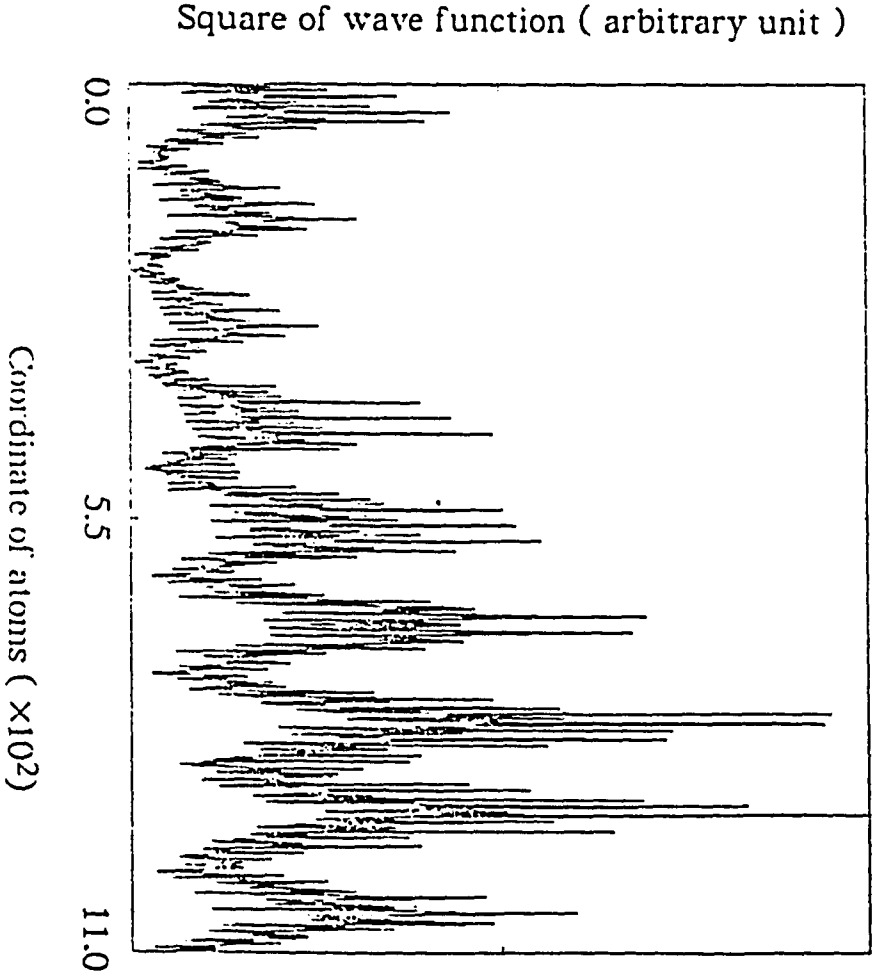
Square of wave function (arbitrary unit)
0.0
5.5
11.0
Coordinate of atoms (×10²)

Fig.3.4b

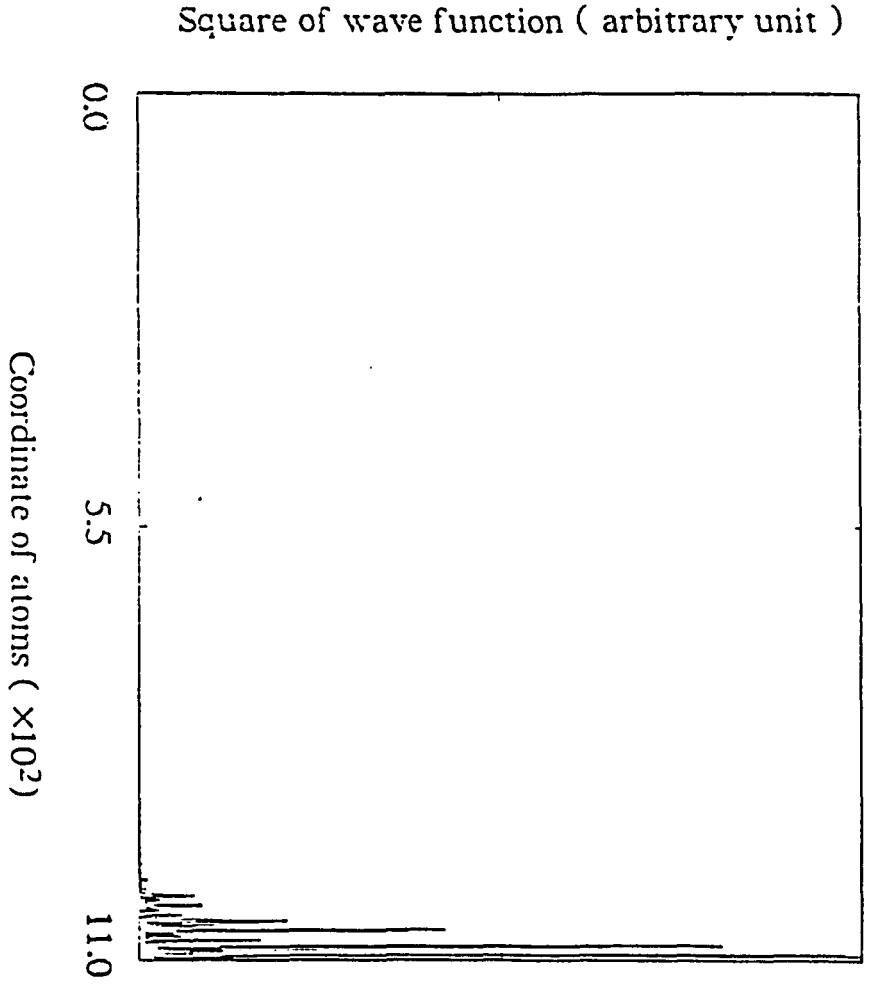
Square of wave function (arbitrary unit)
0.0
5.5
11.0
Coordinate of atoms (×10²)

Fig.3.4c

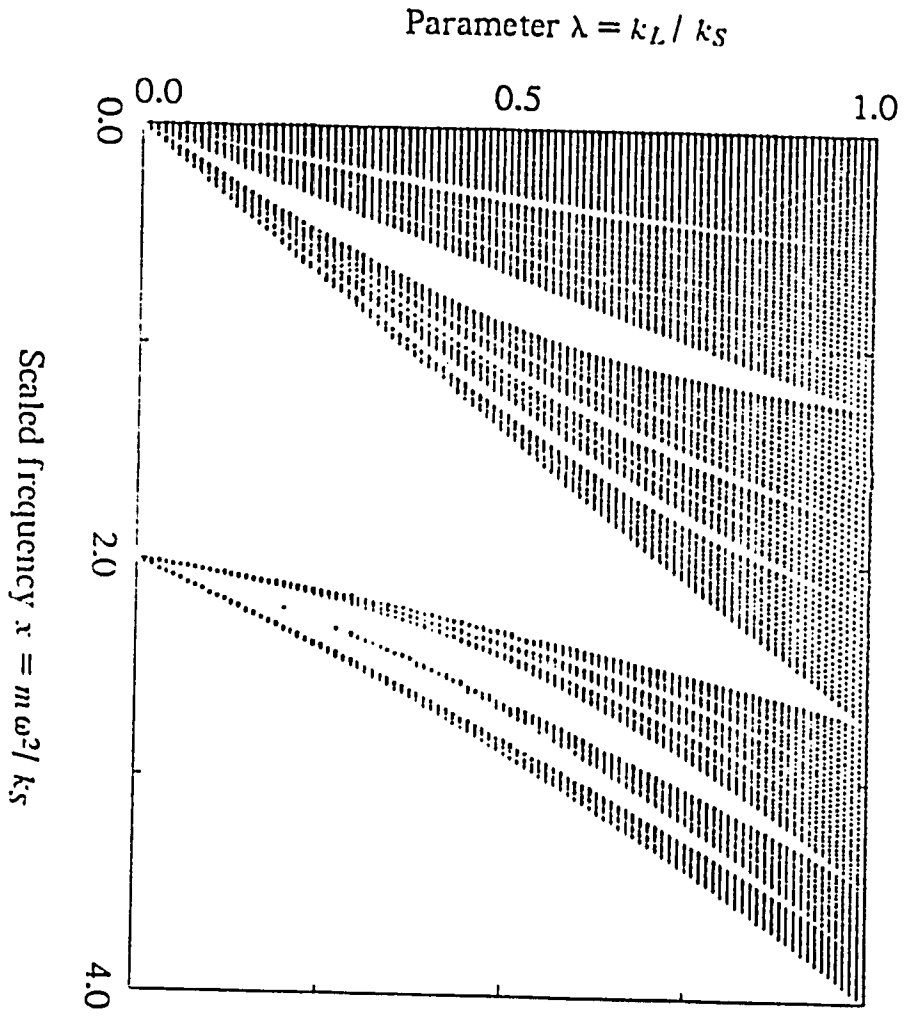
Parameter λ = k_L / k_S
0.0
0.5
1.0
0.0
2.0
4.0
Scaled frequency $x = m\omega^2 / k_S$

Fig.3.5a

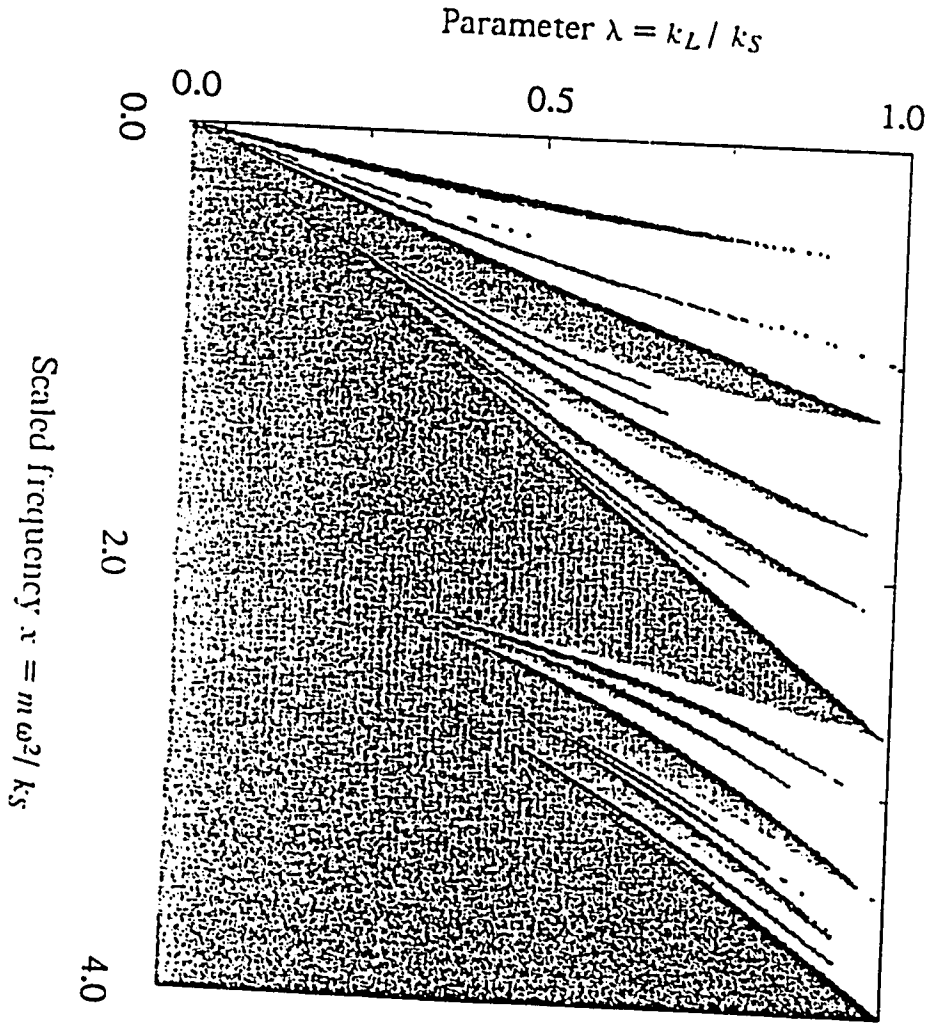

Fig.3.5b

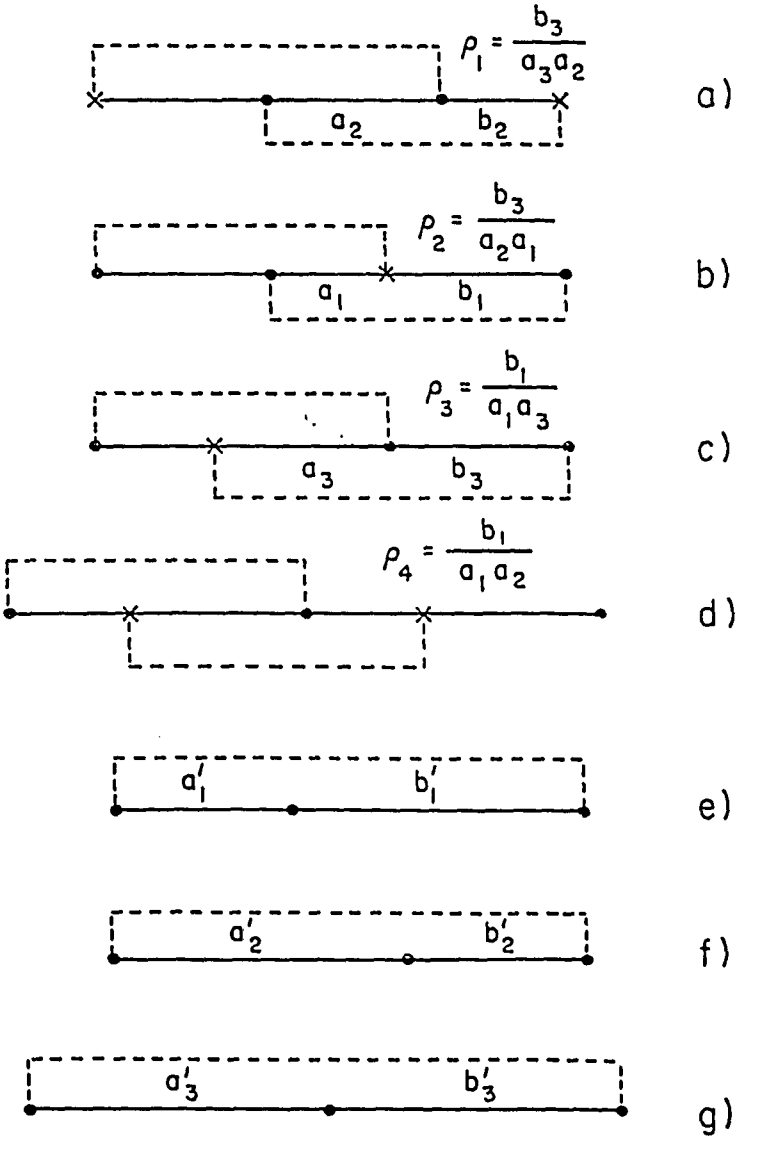
$\rho_1 = \frac{b_3}{a_3 a_2}$
a_2
b_2
a)
$\rho_2 = \frac{b_3}{a_2 a_1}$
a_1
b_1
b)
$\rho_3 = \frac{b_1}{a_1 a_3}$
a_3
b_3
c)
$\rho_4 = \frac{b_1}{a_1 a_2}$
d)
a_1'
b_1'
e)
a_2'
b_2'
f)
a_3'
b_3'
g)

Fig.3.6

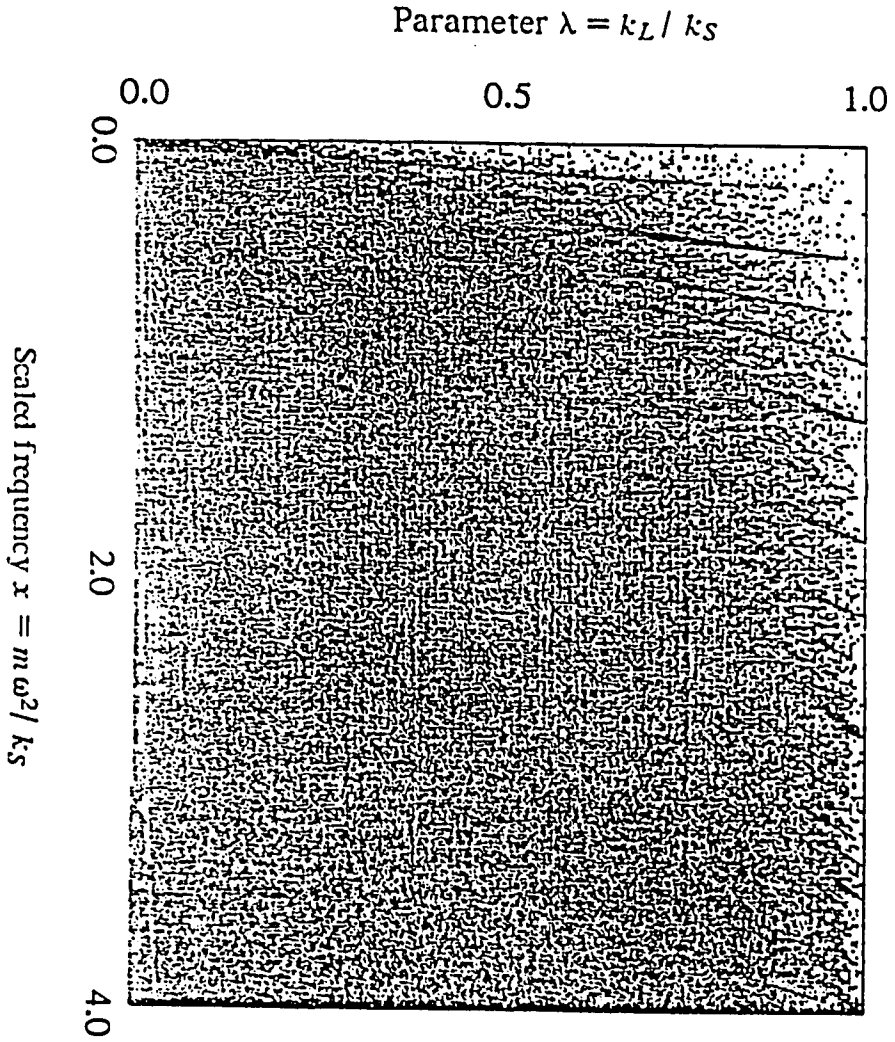
Parameter λ = k_L / k_S
0.0
0.5
1.0
0.0
2.0
4.0
Scaled frequency $x = m\omega^2 / k_S$

Fig.3.7

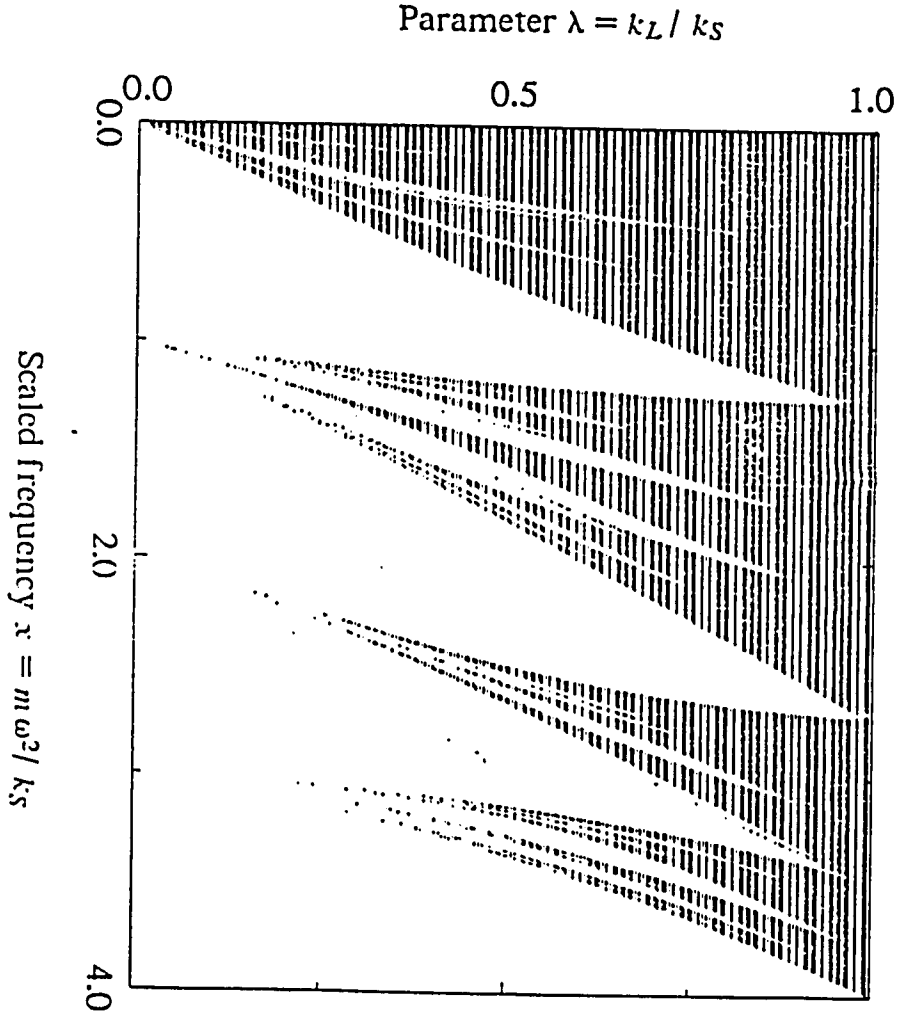
Parameter λ = k_L / k_S
0.0
0.5
1.0
0.0
2.0
4.0
Scaled frequency $x = m\omega^2 / k_S$

Fig.3.8

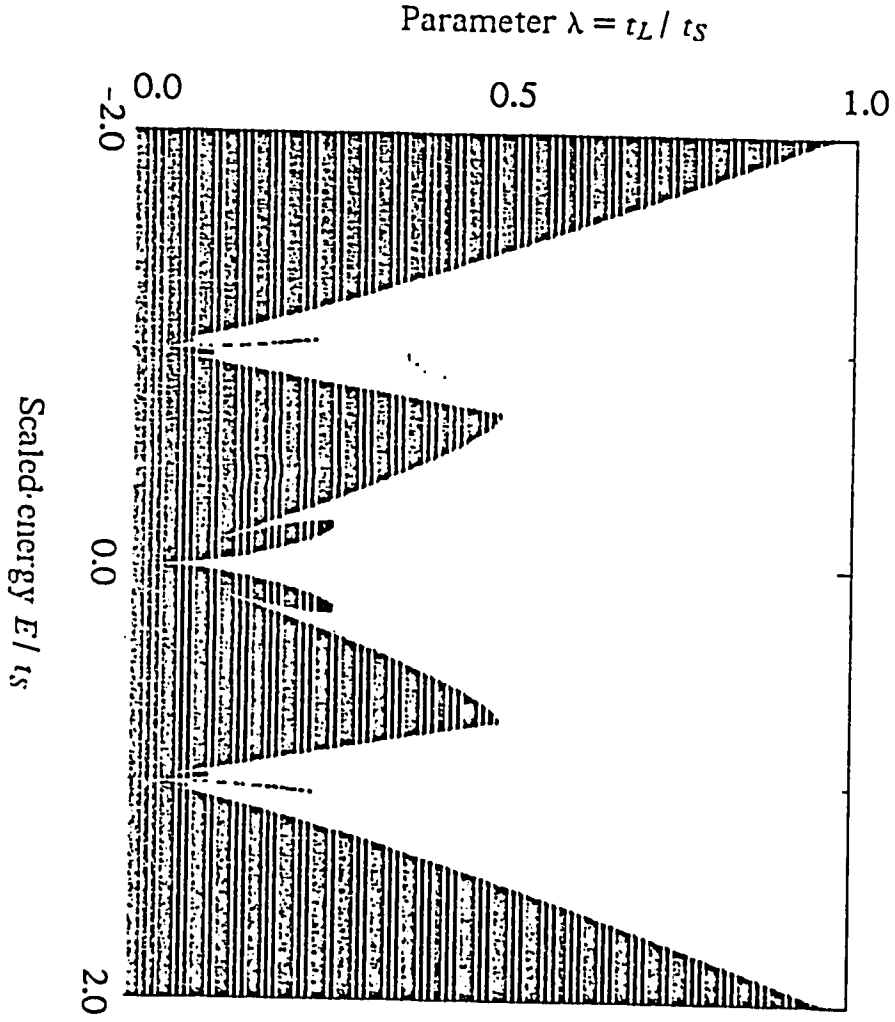

Fig.3.9a

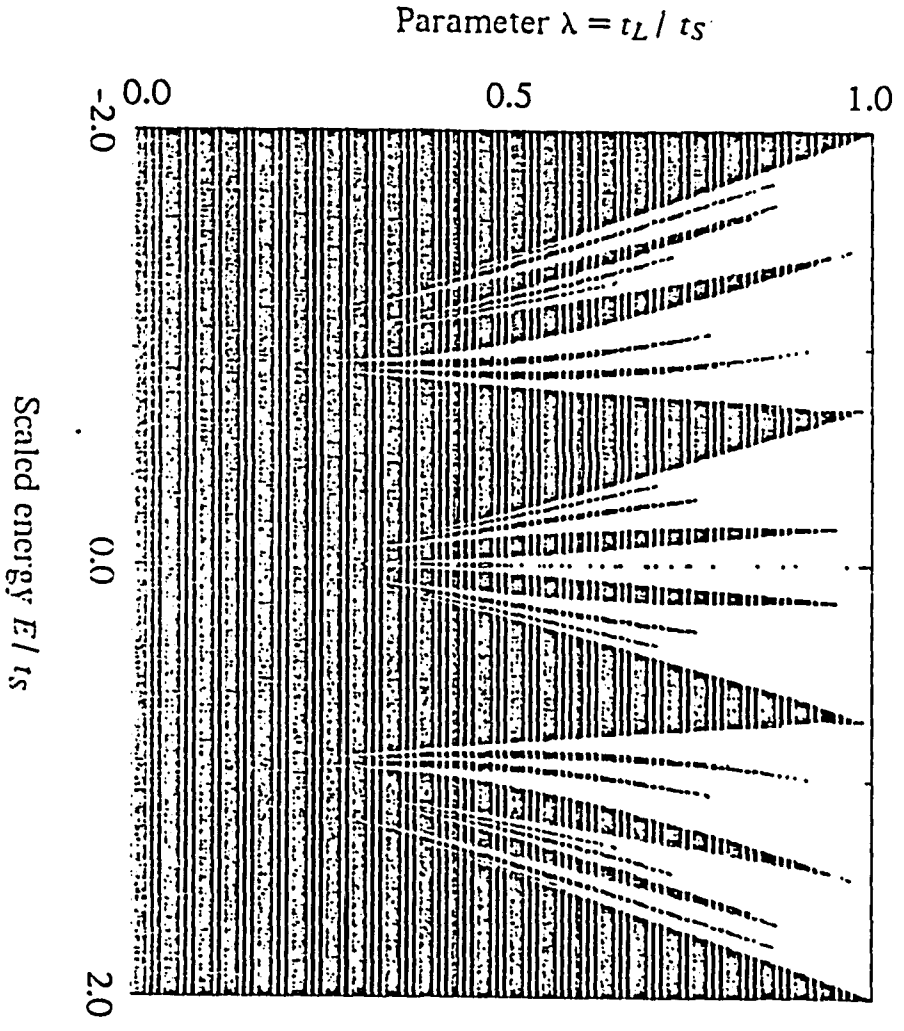

Fig.3.9b

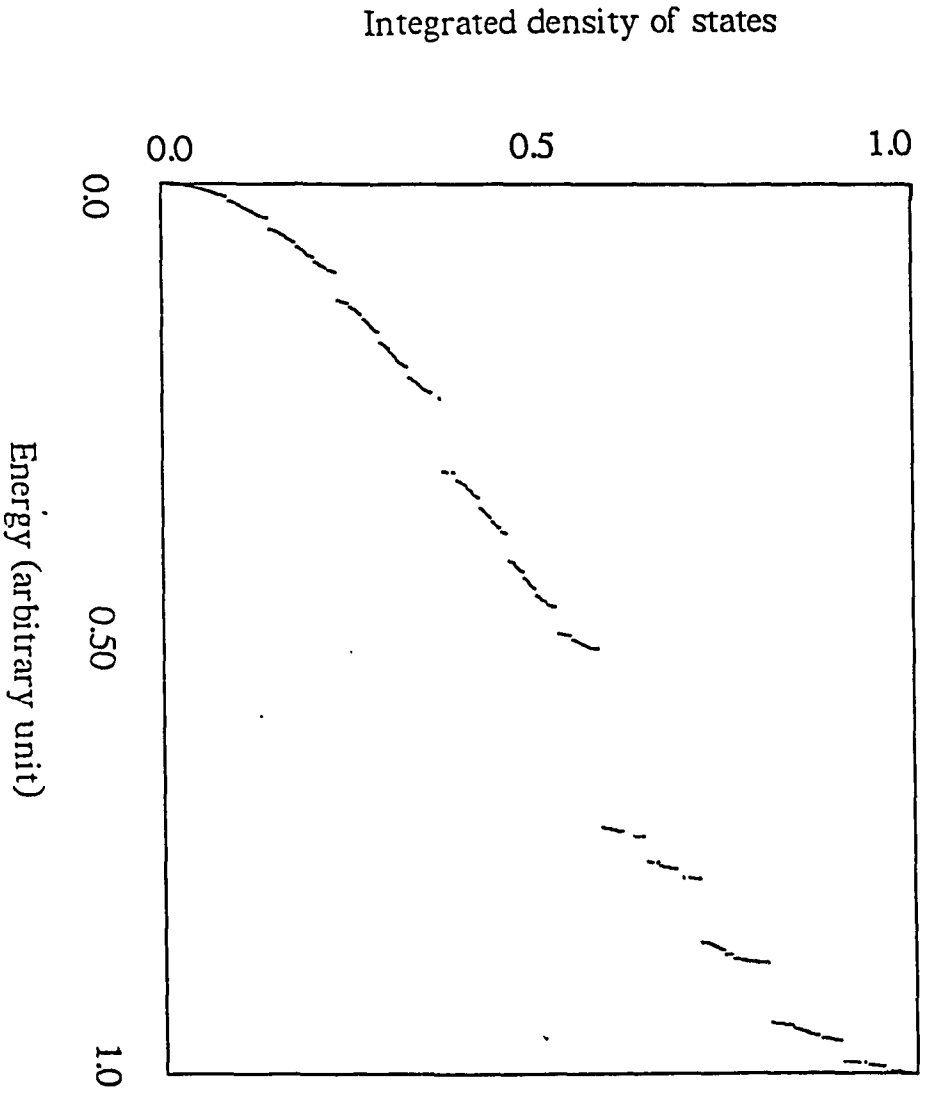
Integrated density of states
0.0
0.5
1.0
0.0
0.50
1.0
Energy (arbitrary unit)

Fig.3.10

CHAPTER 4

TIME DEPENDENT DYNAMICAL PROPERTIES

4.1 INTRODUCTION

In this chapter we study time dependent wave propagation in quasiperiodic and related systems[45]. Wave propagation in a modulated medium has been the subject of study for more than half a century since the early work of Brillouin. Two systems have been widely studied. The first is the optical wave propagation through a periodically modulated medium, pioneered by the studies of Brillouin on optical wave scattering from an acoustic column[80]. It is still a subject of practical interest. The second is wave propagation through a medium with random impurity modulation. It started with Anderson's theory of localization of an electron in a random medium, and recently became an active field of study of optical and acoustic localization[81].

The structure of a quasiperiodic system has been carefully analyzed in Chapter.2. The single distinguishing feature is that a quasiperiodic system is between a periodic and a random system. The electronic structure of quasiperiodic systems was studied in Chapter.3, where we also developed an analytical scheme -- a "quasi-Bloch" Theory -- which enables one to analyze the analytical properties of electronic eigenvalues and eigenfunctions of a quasiperiodic system. Experimentally however the situation is rather different. Because of the difficulty in obtaining good quasicrystal samples, there are few experiments on the measurement of electronic properties. Results of those experiments indicate that as far as transport properties are concerned, a quasicrystal is closer to an amorphous material than to a crystal[82,83], contrary to its structure.

In this chapter we will study time dependent wave packet propagation in a 1D quasiperiodic modulated system. We chose a 1D system and acoustic wave propagation because it is the simplest system which contains all essential ingredients of

quasiperiodicity. In the course of our studies we found it is necessary to compare our results with incommensurately modulated and random systems.

Consider a one dimensional chain of atoms of mass $\{m_i\}$ connected by spring constants $\{k_i\}$. The dynamical equation of motion for the ith atom is (cpmpare Eq.3.1.1)

$$m_i \frac{\partial^2 u(i,\,t)}{\partial t^2} = k_{i-1}[u(i-1,\,t) - u(i,\,t)] + k_i[u(i+1,\,t) - u(i,\,t)] \qquad 4.1.1$$

where u(i,t) is the displacement of the ith atom from its equilibrium position at t=0. Assume that at time zero a local disturbance u(i,t=0)=f(i) is injected at the center of the system. We examine how this disturbance propagates outwardly for different distributions of masses and spring constants. This problem is analogous to that of the motion of the profile of displacement after a chain has been plucked[84]. For mathematical simplicity and with no loss of generality we will take all the $\{k_i\}$ to be the same here. The systems to be examined are classified into the following categories:

a) Periodic, Mn=M;

b) Incommensurate, Mn=M0[1+hcos(2pn/l0)] with l0 irrational and h constant;

c) Quasiperiodic, Mn=ML or MS following the Fibonacci sequence;

d) Random, Mn=ML or MS randomly with the same concentration of that in c);

The initial condition is chosen to be $u(x,t)|_{t=0}=f(x)$; $\partial\, u(x,t)/\partial\, t\,|_{t=0}=0^+$. Depending on the form of f(x) different systems (types a, b, c, d) have qualitatively different response

---

+ We also have done some selective simulation with different initial condition, namely at time zero there is finite velocity injection at some local region but with no initial displacement. The qualitative conclusions are independent of initial conditions.

In section 2 we present the results of numerical simulation. We solved the problem analytically in the long wavelength limit in section 3. The quantitative predictions are compared with the results of section 2 and give good agreement between analytical and numerical solutions.

4.2 NUMERICAL RESULTS

4.2.1 Short Pulse

By a short pulse, we mean that the initial disturbence is a short pulse with width of a few lattice spacings. In the extreme case we take the pulse as a delta function located at the center of the chain. It is well known that in a one dimensional random system, such a wave is localized. Indeed our simulations show this. Fig.4.1 shows the displacement u(x,t) as function of x at time t=5000 (in time units of $\sqrt{m / k}$) after the injection of a delta pulse at x=0, t=0. The localization of energy around the origin is very clear in the case of a random system. On the other hand we know that for a periodic system (no modulation) the wave is extended, i.e. spreads uniformaly.

For a quasiperiodic modulated system, we found similar localization behavior as we did that of a random system (Fig.4.1b). This result shows that at the short wavelength limit a quasiperiodic system behaves essentially as a random system. This agrees well with the experimental finding that the transport properties of icosahedral crystals are closer to that of an amorphous material than to a crystal[82,83]. Another distinguishing feature is that despite the localization of wave energy, the wavefront velocity is well defined. In fact our simulation shows that the sound velocity is the same as that of a homogeneous system with the average mass. This agrees with our earlier finding on the phonon density of states (see Chapter.3).

To quantitatively measure the degree of localization, we calculated the "participation ratio" P for the wave as a function of time. Since the wavefront velocity is well defined, the time scale is equivalent to a space scale. The participation ratio of a wave packet covering a space region of N sites is defined as[70]

$$P(N(t)) = \frac{\sum_i |u(i,t)|^2}{N(t)\sum_i |u(i,t)|^4} \qquad 4.2.1$$

It is clear from this definition that P is much smaller than 1 for a localized wave (P=1/N for a wave localized at a single site). On the other hand if the wave is extended P will be of order 1 (P=1 for a constant function). It can be shown that for an pure exponentially localized wave PN=2l, where l is the localization length. Since in practice the wave is neither localized at a single site, nor it is a constant function, a more sophisticated measure is to examine P as a function of time (or N). For a localized wave the product P(N)N will asymptotically approach a constant and for an extended wave it is linear in N, in the limit of N--> ∞.

In Fig.4.2 we plotted ln(P(N)N) as function of N with delta initial condition for three different systems: with no modulation, with quasiperiodic modulation and with random modulation. It can be seen clearly from the figure that P(N)N asymptotically approaches a constant in the cases of random and quasiperiodic modulation, hence the pulse is clearly localized. But for a periodic system P(N)N is linear in N as N increases, which shows the wave is extended. One observes from Fig.4.2 that the participation ratios as a function of time are smooth in the case of a quasiperiodic modulated system and of a periodic system. But in the case of a random system it shows a large fluctuation even though the asymptotic behavior is well defined. This result can be understood if one

considers that as the wave front passes through the chain, it samples a variety of random configurations with both short and long range disorder, which will influence the over-all wave distribution pattern at a later time. Hence the wave pattern fluctuates in time, and this is reflected in the participation ratio. On the other hand for a quasiperiodic modulated system, although short range disorder exists everywhere (the single site distribution is same as that of random system we defined), there is no long range disorder. The number of possible configurations grows only linearly with the number of sites, which is a dramatically different result compared with the exponential behavior of a random system. Hence the fluctuation in quasiperiodic systems is much smaller. The result that the participation ratio of a quasiperiodic system has the characteristics of both periodic and random systems demonstrates once more that such a system is intermediate between the two different limiting systems. Therefore it is no surprise that icosahedral crystals have properties analogous to both crystal and glass.

4.2.2 Long Wavelength Limit

In the long wavelength limit the initial disturbance is taken to be a chopped monochromatic wave with wavelength much larger than the lattice spacing:

$$u(x,\ t)\big|_{t=0} = \begin{cases} a\cos\dfrac{2\pi x}{\lambda}; & |x| \le A \\ 0; & \textit{otherwise} \end{cases} \qquad 4.2.1$$

lattice spacing<<λ<<A. Again initial velocity is zero.

A) For the periodic case, namely when all m and k are identical respectively, the whole package of the initial wave will propagate outward along both directions (left and right) and without distortion. After some time, one sees two wave packets separated in

space propagating in opposite directions each with only half the amplitude of the initial wave. This is the well known solution of the simple wave equation. The decrease of amplitude is due to energy conservation and the virial theorem.

B) For an incommensurately modulated system with $m(n) = m_0(1 + \eta \cos(2\pi n / \lambda_0))$, a similar result is observed except when the wavelength λ is very close or equal to $2\lambda_0$, where λ_0 is the wavelength of modulation. At this special wavelength there is a resonance (beat) phenomenon: the wavefront is propagating along the chain but the total energy does not (see Fig.4.3, where a=1). Namely, after some time a standing-wave-like wave pattern is built up in the region between two wavefronts. There is no separation into two wave packets propagating along two directions even after a long time, instead the wave energy is spread over the entire region where the wavefronts passed. One can observe very nice "beat" patterns at the center portion of the string (Fig.4.3). However they are not true standing waves, since the amplitude of oscillation at a fixed point varies slowly with time. This indicates that there are two frequencies of oscillation.

To quantitatively analyze this phenomenon we analyzed the Fourier spectrum of u(x,t). For fixed time t, u(x,t) is a function of x. One finds that it consists of two components, one at wavelength λ_0 and another very close to λ_0. If one fixes x and observes u(x,t) as function of time t, one also finds there are two frequency components. However the splitting of these two frequencies depends on the amplitude of the modulation term (η). In the next section 4.3 we give a full analysis of this problem.

C) If the modulation is quasiperiodic with m(n)=m_L or m_S distributed according to the Fibonacci sequence, we found the behavior is very close to that of an incommensurately modulated system except that instead of only one resonant frequency one finds many. The value of these resonance wavevectors (wavelengths) are related to that of the main (high

intensity) diffraction peaks of the quasilattice. Again if the initial wavelength does not fall into those special values, the wavepacket will split into two and propagate along the chain without much distortion of the shape. In the next section we will show analytically how this peculiar phenomenon can be understood in terms of the structure of a quasiperiodic system and its relation to the incommensurately modulated system.

4.3 ANALYTICAL SOLUTIONS

In this section we will first present the two mode coupling theory to explain the resonance phenomenon observed for an incommensurately modulated system. Then we will use the result together with the structural properties of the quasiperiodic system to explain the phenomena observed in the quasiperiodic modulated system.

In the long wavelength approximation we can change the discrete index i to a continuous space coordinate x. Assuming that all spring constant k are the same and the modulation is only of the masses, one gets

$$\frac{\partial^2 u(i,\ t)}{\partial t^2} = \frac{k}{m(i)}\Delta^2 u(i,\ t) \quad \rightarrow \quad \frac{\partial^2 u(x,\ t)}{\partial t^2} = T(x)\frac{\partial^2 u(x,\ t)}{\partial x^2} \qquad 4.3.1$$

where Δ is the difference operator $\Delta u(i)=u(i+1)-u(i)$, and $T(x)=k/m(x)$.

4.3.1 Incommensurately modulated system

As we defined in the introductory section, in this case, $m(x)=m_0(1+\eta\cos(qx))$. However for mathematical simplicity we will use $m(x)=m_0/(1-\eta\cos(qx))$ instead, since η is a small number this does not make a qualitative difference. One gets $T(x)=\mu(1-\eta\cos(qx))=k(1-\eta\cos(qx))/m$, where $q=2\pi/\lambda_0$ defines the modulation wavelength. Two separate methods can be used to solve the equation. The conventional

method is to take the Fourier transform on the time domain, one gets

$$T(x)\frac{d^2u(x,\ \omega)}{dx^2} + \omega^2 u(x,\ \omega) = 0 \qquad 4.3.2$$

This equation is the standard form of Hill's equation with T(x) a periodic function of x. The solution of Hill's equation can be approximated by the solutions of the Mathieu equation which in general are given by Mathieu functions of non-integer order[85]. Though this procedure will lead to an approximate solution, the mathematics involves the stability problem of the Mathieu equation which is difficult to analyze, and the physical picture behind it is not transparent.

We will use a second method which is based on the observation from the numerical results that resonance occurs at the first Bragg peak: when the incident wavelength is twice the modulation wavelength. This indicates that one can express the solution in terms of a superposition of different Bragg modes. Since T(x) contains wave number q, if the initial displacement is a monochromatic wave with wave vector k_0 , from Eq.4.3.1 one sees that the mode k_0 will couple to mode k_0+q and k_0-q, and mode k_0+q will couple to mode k_0+2q and so on. So in general one can write the solution as a superposition of all these modes

$$u(x,\ t) = \sum_{n=-\infty}^{\infty}\phi_n(t)e^{ik_n x} \qquad 4.3.3$$

where $k_n=k_0+nq$, with n an integer. Substituting this equation into Eq.4.3.1 one gets a set of coupled linear differential equations

$$\frac{d^2\phi_n(t)}{dt^2} + \mu k_n^2\phi_n(t) + \frac{1}{2}\mu\eta\left[k_{n-1}^2\phi_{n-1}(t) + k_{n+1}^2\phi_{n+1}(t)\right] = 0 \qquad 4.3.4$$

Theoretically one should includes all modes in obtainning the solution. In practice the

amplitude of the modes decreases very fast as n increases, so one only needs to keep those few modes which are close to k_0. In our numerical simulation the most surprising feature is the resonance which occurs when k_0 is half that of q, namely at the first Bragg condition. Intuitively the resonance is due to the interference between the reflected waves of the two consecutive nodes of modulation. Since we found numerically that there is no other observable mode except k_0 and k_{-1}, we will keep only these two modes. Then Eq.4.3.4 reduces to

$$\frac{d^2\phi_0(t)}{dt^2} + \mu k_0^2\phi_0(t) + \frac{1}{2}\mu\eta k_{-1}^2\phi_{-1}(t) = 0$$

$$\frac{d^2\phi_{-1}(t)}{dt^2} + \mu k_{-1}^2\phi_{-1}(t) + \frac{1}{2}\mu\eta k_0^2\phi_0(t) = 0 \qquad 4.3.5$$

To decouple the equation, let us make the transformation

$$w_{1,2} = \phi_0 + \alpha_{1,2}\phi_{-1} \qquad 4.3.6$$

with properly chosen $\alpha_{1,2}$, one gets

$$\frac{d^2w_i}{dt^2} + \mu k_0^2\left[1 + \frac{1}{2}\eta\alpha_{1,2}\right]w_i = 0; \qquad i = 1, 2 \qquad 4.3.7$$

where

$$\alpha_{1,2} = \frac{k_{-1}^2 - k_0^2 \pm \sqrt{\left(k_{-1}^2 - k_0^2\right)^2 + \eta^2 k_0^2 k_{-1}^2}}{\eta k_0^2} \qquad 4.3.8$$

Eq.4.3.7 relate to two uncoupled simple harmonic oscillators. Fundamental solutions are of the form $e^{\pm i\omega_{1,2}t}$ with two frequencies of oscillation:

$$\omega_{1,2} = k_0\sqrt{\mu\left(1+\frac{1}{2}\eta\alpha_{1,2}\right)} \qquad 4.3.9$$

Inverting the transformation Eq.4.3.6 then substituting into Eq.4.3.3 one gets the solution

$$u(x,\ t) = \phi_0(t)e^{ik_0x} + \phi_{-1}(t)e^{ik_{-1}x}$$

$$\phi_0 = \frac{1}{\alpha_2 - \alpha_1}\left[\alpha_2\left(Ae^{i\omega_1 t} + Be^{-i\omega_1 t}\right) - \alpha_1\left(Ce^{i\omega_2 t} + De^{-i\omega_2 t}\right)\right]$$

$$\phi_0 = \frac{1}{\alpha_2 - \alpha_1}\left[\left(Ae^{i\omega_1 t} + Be^{-i\omega_1 t}\right) - \left(Ce^{i\omega_2 t} + De^{-i\omega_2 t}\right)\right] \qquad 4.3.10$$

Here A,B,C,D are constants to be determined by initial conditions at t=0. Assume the initial wave is a monochromatic wave with amplitude a, wavevector k_0, and no initial velocity

$$u(x,\ t)|_{t=0} = ae^{ik_0x}, \qquad \left.\frac{du(x,\ t)}{dt}\right|_{t=0} = 0 \qquad 4.3.11$$

One then gets

$$u(x,\ t) = \frac{a}{\alpha_2 - \alpha_1}\left[(\alpha_2\cos\ \omega_1 t - \alpha_1\cos\ \omega_2 t)e^{ik_0x} + (\cos\ \omega_1 t - \cos\ \omega_2 t)e^{ik_{-1}x}\right]$$

4.3.12

Notice α_1, α_2 are functions of initial wavevector and modulation wavevector and modulation strength. From the above solution one clearly observes that:

1) If we fix coordinate x, taking u(x,t) as function of time, the solution Eq.4.3.12 consists of two oscillating terms with distinct frequencies ω_1, ω_2. When η (amplitude of the modulation term) is small, from Eq.4.3.8 and 4.3.9, one finds for small modulation strength η the difference between these two frequencies is linearly proportional to η at the position where the first Bragg condition is exactly satisfied $k_{-1}=-k_0=-q/2$

$$\Delta\omega = \omega_1 - \omega_2 \approx \frac{\sqrt{\mu}}{2} k_0 \eta \qquad 4.3.13$$

In Fig.4.4 we have plotted this difference as a function of η obtained in numerical simulation for several η. The solid line is the prediction of Eq.4.3.13 with no adjustable parameters. One sees very good agreement. Also one observes from the above solution that the intensity of the two oscillatory terms depends on the space coordinate, and indeed this was found in our simulations.

2) Fixing the time t, u(x,t) is a function of coordinate x, then one finds that in general there are also two different oscillating modes k_0 and k_{-1}. However since this analysis is valid only near the Bragg condition, which implies $|k_{-1}| \approx k_0$, the two oscillating modes are very close. This leads to a long wavelength variation of oscillation amplitude as we found in the numerical simulation (Fig.4.3). However if the initial wave is exactly at the first Bragg peak one should not see any splitting in the spectrum. Again this is in agreement with our numerical simulations.

3) If the initial wave is not near the first Bragg condition but satisfies a higher order Bragg condition, the simple two model coupling solution is no longer valid. However one still expects that only very few modes will couple, and the response should be qualitatively similar. Namely it consists of a main vibration and both phase and amplitude modulation.

4) If there is no modulation, η=0. From Eq.4.3.8, 4.3.9 and 4.3.11, we have $\alpha_1 = \infty$, $\alpha_2 = 0$, $\omega_{1,2} = \sqrt{\mu}\ k_0$ and

$$u(x, t) = \frac{a}{2} e^{ik_0(x + \sqrt{\mu} t)} + \frac{a}{2} e^{ik_0(x - \sqrt{\mu} t)} \qquad 4.3.14$$

which represents the superposition of two waves propagating in opposite directions. This is the well known solution of the wave equation.

To summarize, we have shown analytically that there is a resonance when the wave

vector of the initial wave satisfies the first Bragg condition of the modulation. The resonance frequencies are found analytically and agree with numerical simulation. We predict that such a phenomena should be observable experimentally in acoustic wave propagation in an incommensurately modulated system.

4.3.2 Quasiperiodic Modulated System

Let us first define the 1D quasiperiodic system we studied. The basic equation is still Eq.4.3.1. We assume all spring constants K are the same. The masses vary in accord with a quasiperiodic sequence. We choose the well known example of a Fibonacci sequence, for the variation of masses

$$m(i) = m_0\left(1 + \frac{1}{\tau}\left[\frac{i+1}{\tau}\right] - \left[\frac{i}{\tau}\right]\right); \qquad i = 1, 2, 3, \ldots \tag{4.3.15}$$

again, here [x] represents the integer part of x, and τ is the golden number. Such a sequence m(i) can take only two possible values m_0 or $m_0\tau$. The Fourier spectrum of such a sequence is very similar to that of a Fibonacci lattice which has been analytically calculated in Chapter.2

Eq.4.3.15 can be rewritten as

$$m(i) = m_0 + \frac{m_0}{\tau}\left(\left[\frac{i+1}{\tau}\right] - \left[\frac{i}{\tau}\right]\right); \qquad i = 1, 2, 3, \ldots \tag{4.3.16}$$

The expression inside the bracket can take values either 0 or 1. The order of the sequence is exactly the Fibonacci sequence 1011011011..... The positions where it takes value 1 can be written as

$$x(l) = l + \left[\frac{l}{\tau}\right] = 1, 3, 4, 6, \ldots; \qquad l = 1, 2, 3, \ldots \tag{4.3.17}$$

Fourier transform of m(i) is

$$f(q) = \sum_l m_0 e^{iql} + \sum_l \frac{m_0}{\tau} e^{iqx(l)} \qquad 4.3.18$$

The first summation just gives the normal Bragg peaks

$$q_n^{(1)} = 2\pi n; \qquad n=integer \qquad 4.3.19$$

The second summation is a special case of the more general problem we solved in section 2.2.1. Taking $\rho=1$, $\sigma=\tau$ in Eq.2.2.7, one immediately get that f(q) consists of a dense set of Bragg peaks in reciprocal space located at

$$q_{m,n} = \frac{2\pi}{\tau}\left(n + \frac{m}{\tau}\right) \qquad 4.3.20$$

with diffraction amplitude

$$f(q_{m,n}) = \left| \frac{\sin \frac{\pi(m-n)}{\tau}}{\frac{\pi(m-n)}{\tau}} \right| \qquad 4.3.21$$

where n,m are integers. From the above equations one sees that the intensity of peaks decreases very fast as one deviates from the main peaks, even though the diffraction pattern consists of a dense set.

From the analysis of the last section, we expect that when the initial wave satisfies the first Bragg condition for any of those Bragg peaks given by Eq.4.3.20, one will observe a similar resonance as though the system is an incommensurately modulated with that Bragg wavevector. Indeed this is what we found numerically. Quantitatively however, the modulation strength η which appears in Eq.4.3.13 corresponds to the amplitude of the diffraction at the Bragg peak given by Eq.4.3.21. As one can see the diffraction amplitude decreases very fast when one moves away from the first few major diffraction peaks.

Hence when one is looking at the time domain Fourier spectrum the splitting of two peaks, according to Eq.4.3.13, will be very small and difficult to observe. However the particular resonances related to the most intense peaks should be observable. Fig.4.3b gives an example when the first Bragg condition is satisfied. If one deviates slightly from the major peaks, the resonance phenomenon disappears quickly, as the strength of the modulation decreases.

As we pointed out the relative intensities of individual peaks in Fig.4.4 corresponds to the amplitude of a particular harmonic with respect to the average background. From Eq.4.3.8 we know that the splitting between two different frequencies is directly proportional to this amplitude. Hence the splitting at any peak is directly proportional to the diffraction amplitude at that peak. In Table.4.1 we list the scaled splitting $\Delta\omega=(\omega_1-\omega_2)/(\omega_1+\omega_2)$ for several different peaks. The entry ω^{num} is the result of numerical simulation and the entry ω^{th} is calculated from Eq.4.3.13 using the diffraction amplitude f of Eq.4.3.21 as the modulation strength η. One sees good agreement between the two.

To summarize, wave propagation in a quasiperiodic system shows some unique features. If the wave is not monochromatic and the wavelength does not satisfy the Bragg condition, the propagation is qualitatively the same as that of an homogeneous system. But when the initial wave is monochromatic and satisfies the first Bragg condition, a new resonance phenomenon is present which behaves as if the system is incommensurately modulated with the wavelength of the Bragg peak and modulation strength equal to the diffraction amplitude of that peak.

4.4 CONCLUSION

In conclusion, we have studied time dependent wave packet propagation in homogeneous, incommensurately modulated and quasiperiodically modulated one

dimensional lattices. We found a "resonance" phenomenon in the incommensurate and quasiperiodic modulated system which is successfully explained in terms of two mode coupling theory. A quasiperiodic modulated system behaves very differently in the long and short wavelength limits. In the long wavelength ($\lambda >>$ lattice spacing) the system responses in the same way as that of a homogeneous system except when the initial wavelength satisfies the Bragg condition, then a quasiperiodic system behaves as if it is an incommensurately modulated system with strength of modulation proportional to the diffraction amplitude of that Bragg peak. This is in agreement with our earlier finding (Chap.3) that the electronic band structure of a quasiperiodic system is essentially determined by the diffraction pattern of the structure.

On the other hand, in the short wavelength limit the quasiperiodic system behaves the same as a random system. If the initial pulse is of the order of a few lattice spacings we find there is an indication of localization. This demonstrate that: not only is a quasiperiodic system structurally an intermediate state between crystal and amorphous material, but also the physical properties of quasiperiodic systems have the dual characteristics of both systems.

Table 4.1

Comparison of numerical simulation results with the two-mode-coupling theory and Eq.4.3.13 and Eq.4.3.21. λ is the wavelength of the initial disturbance. τ is the golden mean (1.618...), $\Delta\omega^{th}$ is the splitting of two frequencies predicted by theory, and $\Delta\omega^{num}$ is the simulation result.

$\lambda/2$	τ^2	τ^3	τ^4	τ^5	τ^6
$\Delta\omega^{num}$	0.56	0.12	0.04	0.01	0.005
$\Delta\omega^{th}$	0.560	0.125	0.034	0.008	0.002

Figure Captions

Fig.4.1 Shown are the displacement configurations of the whole chain u(x,t) as function of x at time t=5000 (in terms of unit $\sqrt{m / k}$). The initial pulse is a delta function: unit displacement at the center atom and zero elsewhere with no initial velocity. The localization of energy (proportional to displacement square) in the small vicinity around origin is clearly shown. a) Random modulation. b) Quasiperiodic modulation. (page 100, 101)

Fig.4.2 Participation ratio P as function of N. a) Homogeneous system, NP(N) is linear in N. This indicates that the wave is extended. b) Random system, the function quickly saturates at some finite value which defined the localization length. Note the large scale fluctuation in the participation ratio, this is associated with the intrinsic long range disorder of random system. c) Quasiperiodic modulation, similar behavior as that in the random system. However as one can see the localization length is smaller and there is no large scale fluctuation as there is in a random system. (page 102)

Fig.4.3 The "resonance" phenomenon. The initial wave is a finite monotonic wave of several wavelengthes with wavelength much larger than lattice spacing. Shown is the displacement configuration at time t=40,00 (in terms of unit $\sqrt{m / k}$. a) Incommensurate modulation. The modulation wavelength is $\lambda_0=21\tau+13$ and the initial wavelength is $\lambda'=2\lambda_0$ in order to satisfy the first Bragg condition. b) Same plot for quasiperiodic modulation with initial wavelength $\lambda'=2\tau^6=2(8\tau+5)\approx 35.89$ which corresponding to the first Bragg condition of wavenumber $q_{8,-5}=8\tau-5$. c) A

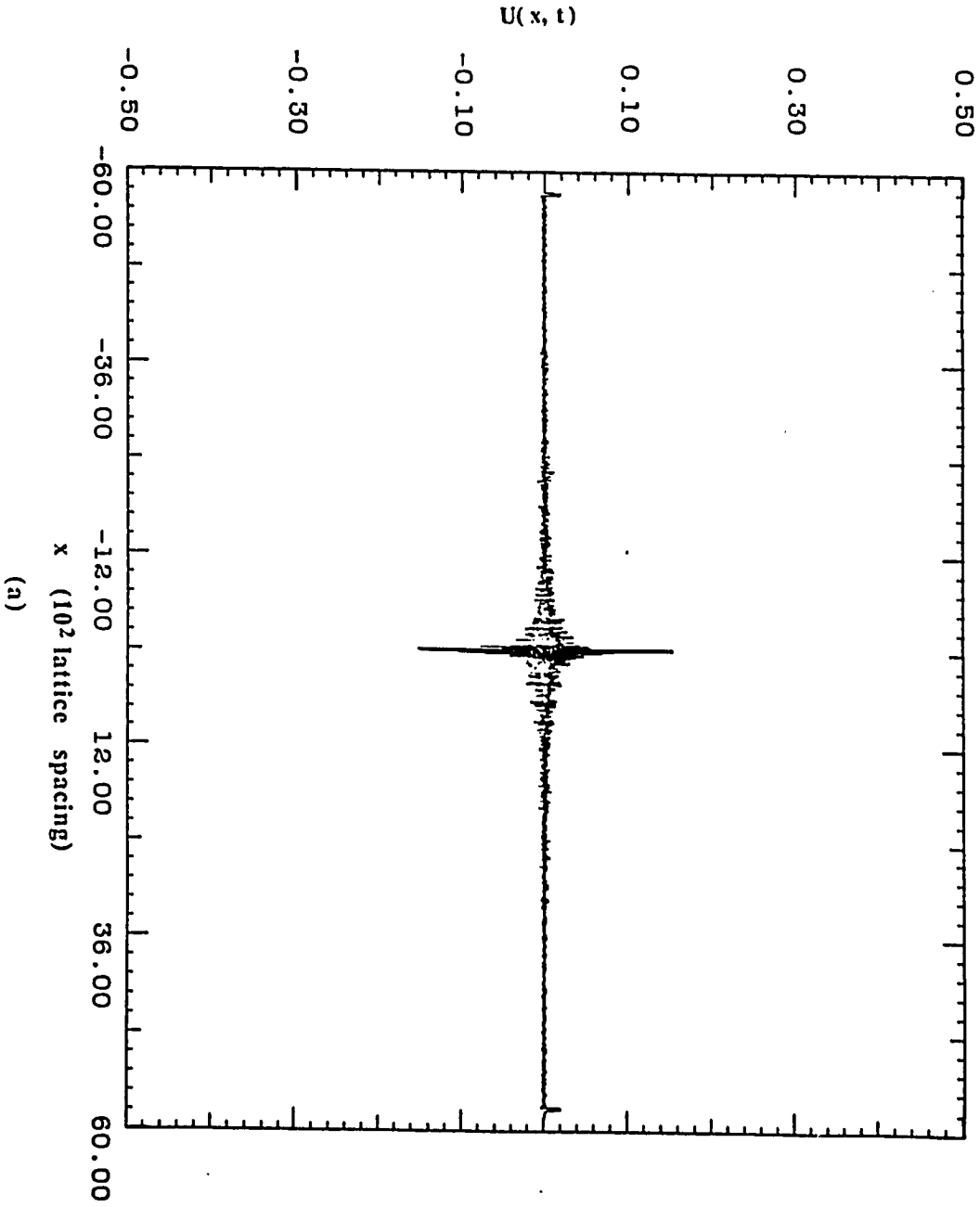
U(x, t)
-0.50
-0.30
-0.10
0.10
0.30
0.50
-60.00
-36.00
-12.00
12.00
36.00
60.00
x (10² lattice spacing)
(a)

Fig.4.1a

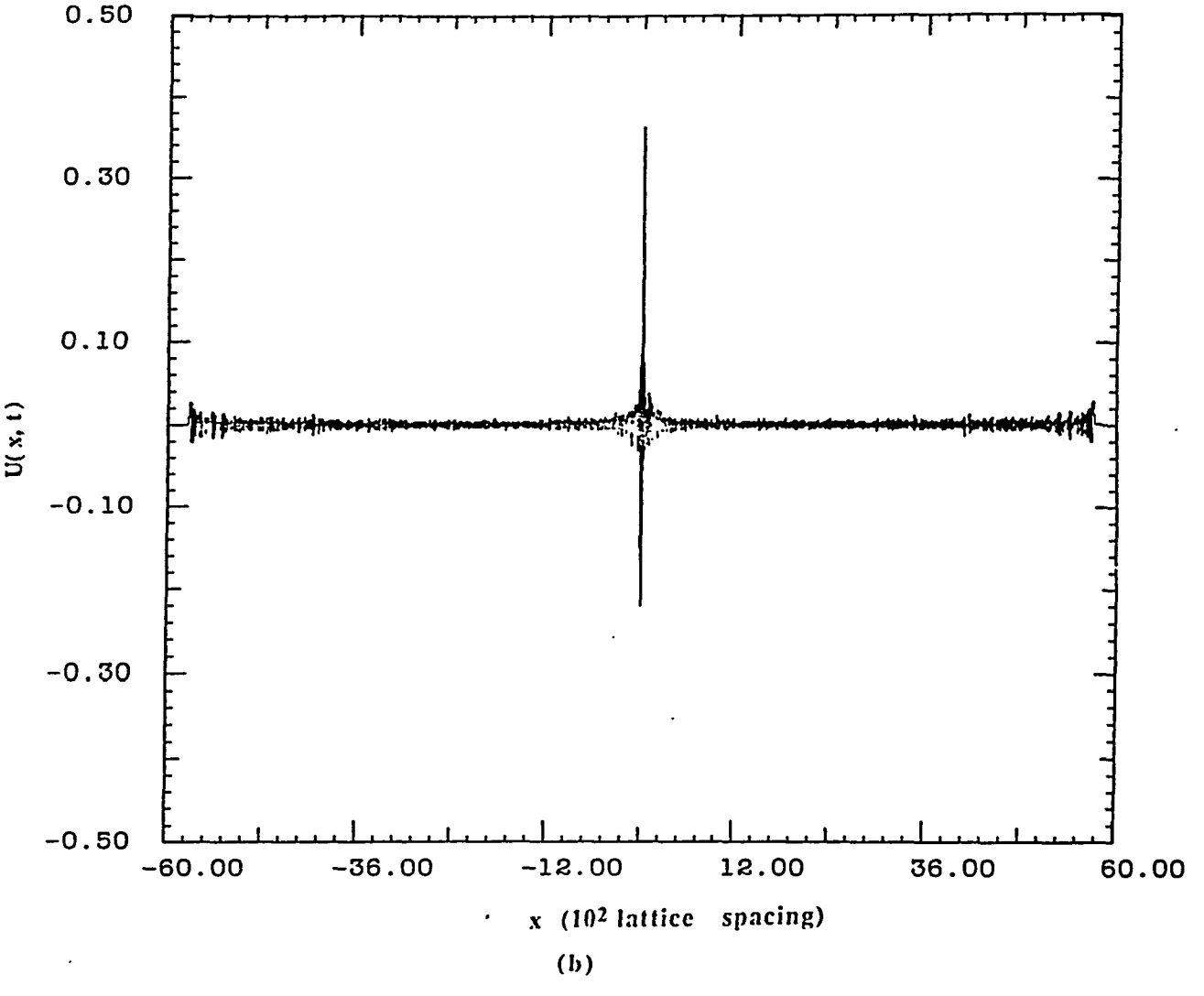
0.50
0.30
0.10
-0.10
-0.30
-0.50
U(x, t)
-60.00
-36.00
-12.00
12.00
36.00
60.00
x (10² lattice spacing)

(b)

Fig.4.1b

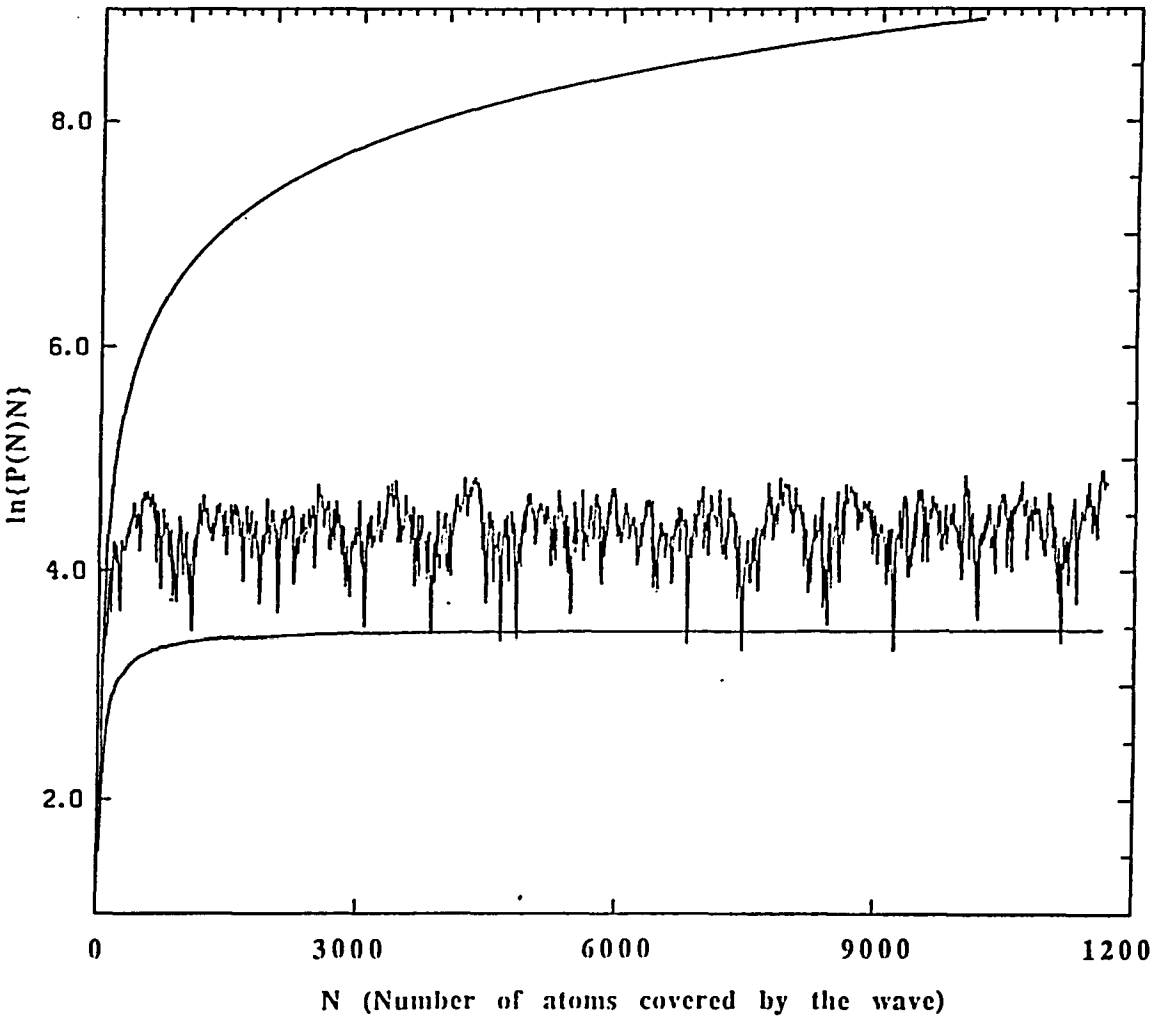
8.0
6.0
4.0
2.0
ln{P(N)N}
0
3000
6000
9000
1200
N (Number of atoms covered by the wave)

Fig.4.2

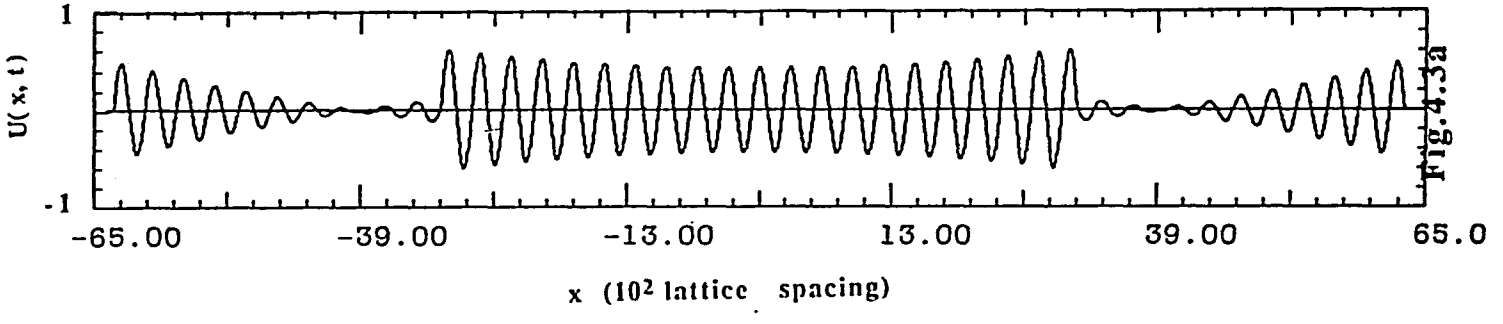

Fig.4.3a

(a)

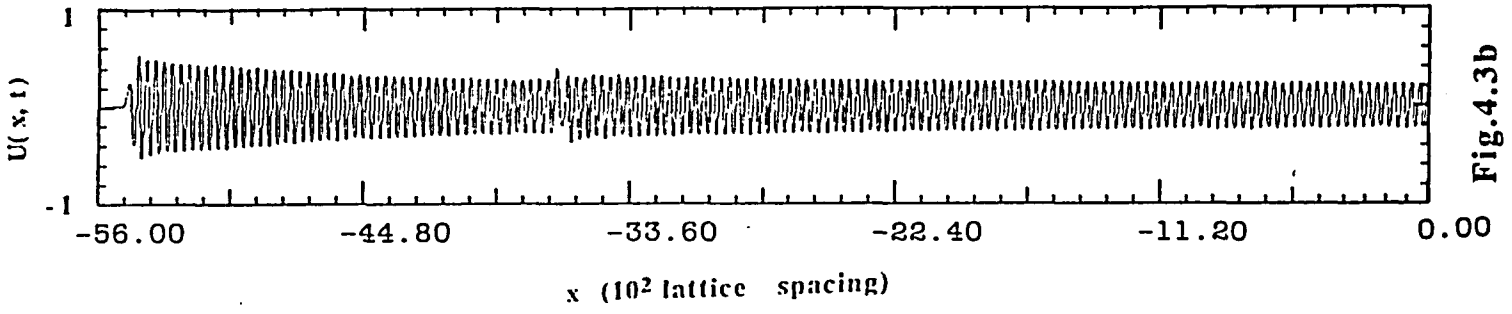

(b)

Fig.4.3b

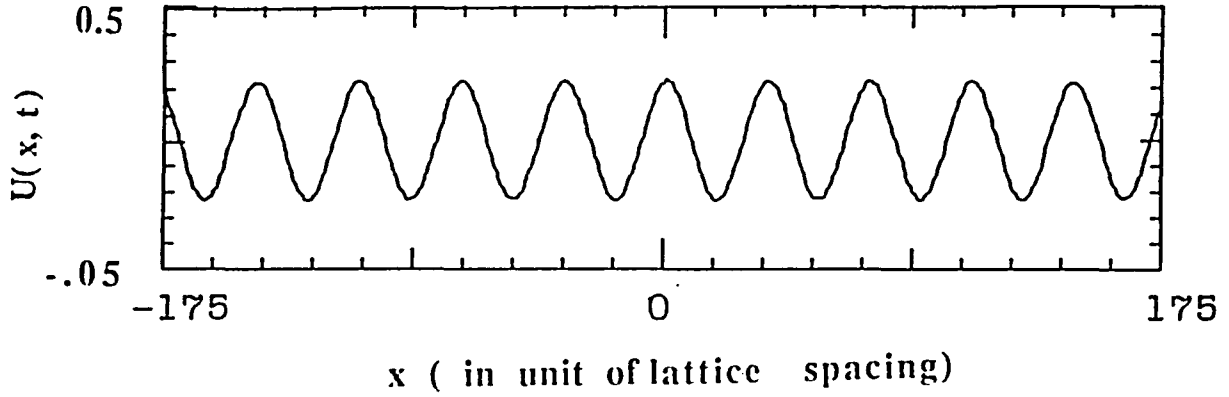

(c)

Fig.4.3c

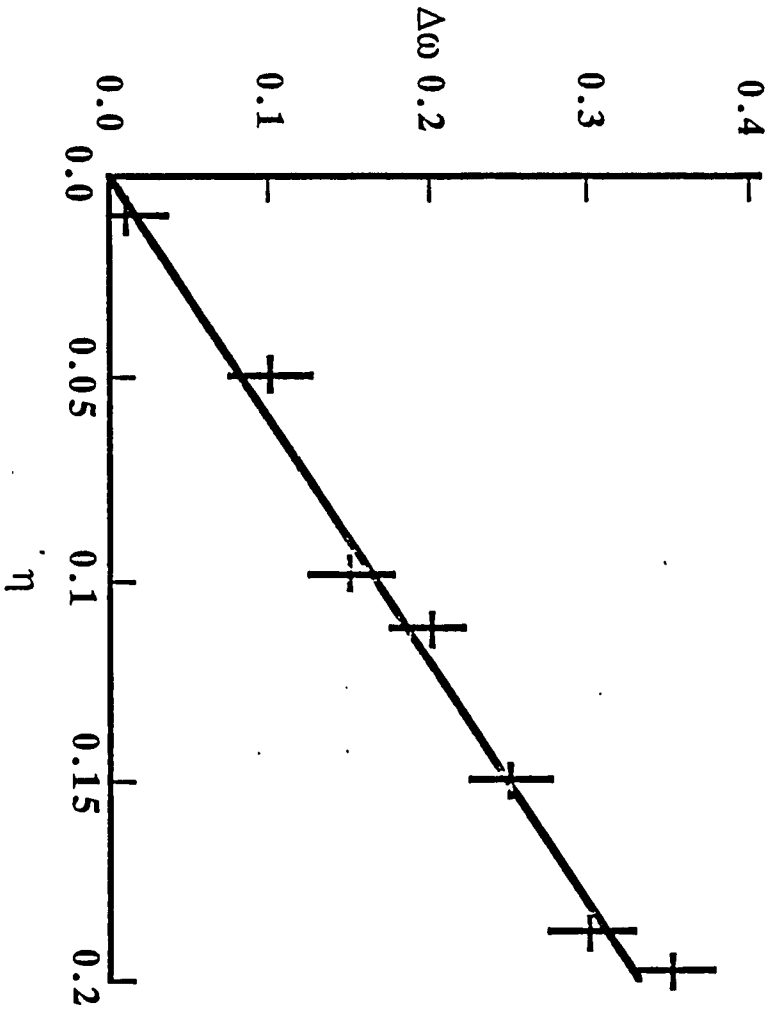

Fig.4.4

CHAPTER 5

CRITICAL PHENOMENA ON QUASILATTICES: "UNIVERSALITY"

Since quasilattices differ in many aspects from both periodic lattices and random structures, it is an important question whether or not critical phenomena on such systems are different from that of periodic lattices. Intuitively one expects it is not. Because near a 2nd order phase transition the correlation length diverges to infinity, fluctuations are long range, the detail short length scale structure does not play any role: a quasilattice from a long range point view is perfectly ordered just as a periodic system. So one expects that the same exponents in both periodic and quasiperiodic systems. In this chapter I study two different critical phenomena on quasilattices, namely the Ising model near T_c and the percolation problem. The results fully support the idea that "universality" is indeed valid for quasiperiodic systems.

5.1 ISING MODEL ON A QUASILATTICE

Consider a one dimensional Ising chain with separation d_{ij} of successive spins, where d_{ij} is given by either L or S which is determined by the sequence Eq.2.1.1 (L=τ, S=1); we take the nearest neighbor coupling either to be $-J_L$ or $-J_S$ (Fig.5.1). The Hamiltonian and partition function are

$$H = -\sum_{ij=nn} J_{ij}\sigma_i\sigma_j\ ; \qquad J_{ij} = \begin{cases} J_L; & if\ \ d_{ij} = L \\ J_S; & if\ \ d_{ij} = S \end{cases} \tag{5.1.1}$$

$$Z = \sum_{\{\sigma_i \pm 1\}} e^{-\beta H(\{\sigma_i\})} = \sum_{\{\sigma_i \pm 1\}} \exp\left(\sum_{ij=nn} K_{ij}\sigma_i\sigma_j\right); \qquad K_{ij} = \beta J_{ij} = \frac{J_{ij}}{kT} \tag{5.1.2}$$

Here nn stands for nearest neighbor. This model can be solved using an exact renormalization transform. Divide all spin variables into two sets: all spins inside the segment LS are designated as $\{\sigma_i^2\}$, the rest are designated as $\{\sigma_i^1\}$ (indicated by 2 and 1

in Fig.5.1). The real space renormalization transform is to transform all segment LS into L' and the rest L into S'. This is exactly the reversal of the recursive transformation which defined the Fibonacci lattice in section 2.1 (Eq.2.1.3).

Summing over all possible configurations of set 2, the partition function can be expressed in terms of new coupling constants K'_{ij} and spin variables of set 1. Apart from a constant factor the new partition function has the same form as the original. The renormalization transformation can be easily worked out to be

$$\begin{aligned} L' &= L + S\ ; & S' &= L \\ \tanh(K'_L) &= \tanh(K_L)\tanh(K_S)\ ; & K'_S &= K_L \end{aligned} \qquad 5.1.3$$

The renormalized system should have the same geometry as before for continuous application of the same renormalization transformation; this requires L'/S'=L/S, or L/S=τ, which gives L'=τL and S'=τS. The two fixed points are obvious. Denoting t=tanh(K), the fixed points are

$$\begin{aligned} t_L = t_S = t_c = 0; \quad & K_L = K_S = 0; \quad & T_c = \infty \\ t_L = t_S = t_c = 1; \quad & K_L = K_S = \infty; \quad & T_c = 0 \end{aligned} \qquad 5.1.4$$

Near the critical point T_c=0 Eq.5.1.3 can be linearized, one gets

$$\begin{pmatrix} \Delta t'_L \\ \Delta t'_S \end{pmatrix} = \begin{pmatrix} 1 & 1 \\ 1 & 0 \end{pmatrix} \begin{pmatrix} \Delta t_L \\ \Delta t_S \end{pmatrix} \qquad 5.1.5$$

The two eigenvalues of the transformation matrix are $\lambda_{max}=\tau$; $\lambda_2=-1/\tau$. The critical correlation length exponent ν is related to the largest eigenvalue

$$\nu = \frac{\ln \lambda_{max}}{\ln b} = \frac{\ln \tau}{\ln \tau} = 1 \qquad 5.1.6$$

where b is the geometrical scaling factor. We see that all the features are the same as in the

case of the ordinary one dimensional Ising model on a periodic lattice. The renormalization transformation carried out above does not depend on the particular lattice chosen (from the similar lattice defined by Eq.2.1.5). Rather it is to the intrinsic selfsimilarity, or the scaling invariance embedded in the definition of such quasiperiodic lattices by inflation (recursive) procedure such as those in Eq.2.1.5, that made it possible to carry out the renormalization transformation and determines the forms of recursion relations. Therefore the result (T_c=0, ν=1) should be valid for all one dimensional quasiperiodic lattices defined by inflation procedures. It is easy to show that the above renormalization transformation can be carried out, and same results are obtained for those 1D quasilattice defined by Eq.2.1.5 with two basic elements.

Similar studied have been carried out for two dimensional Penrose lattice, and the same conclusion were obtained[86].

5.2 PERCOLATION ON A QUASILATTICE

5.2.1 Introduction

In this section we report on an extensive numerical study designed to investigate percolation on a quasilattice. We test the scaling theory of percolation on a quasilattice lattice. According to the theory[87,88,89], which treats the percolation problem as general second order phase transition, critical behavior and critical exponents are independent of lattice structure. Our study is the first time to our knowledge that universality is numerically tested in a non-periodic lattice.

In section 5.2.2 we reexamine the geometrical structure of the Penrose lattice, and give the connection coefficients of vertices. The bond percolation threshold of the Penrose lattice is examined in section 5.2.3, and the result is interpreted in terms of the difference in

the global connectivity of lattices. Then in section 5.2.4, results of a detailed analysis of cluster statistics are presented which are in agreement with the two-exponent assumption of the scaling theory of percolation. Critical exponents are found to be the same as those on a periodic lattices. This confirms the universality prediction.

5.2.2 Lattice Structure in 2 D

We will restrict ourselves to the two dimensional quasilattice with pentagonal symmetry known as the Penrose Lattice. Fig.5.2 shows a portion of the Penrose lattice. It is a tiling of the plane by two different rhombii in a nonperiodic fashion. There are 8 different types of vertices in the Penrose lattice if one classifies them in terms of their nearest neighbor configurations# . We label them as 1 to 8 respectively as shown in Fig.5.2 (these vertices previously have been given names such as sun, star, etc). Each type of vertex has a different coordination number and appears in the Penrose lattice with a different frequency. The number of fat rhombuses is τ times larger than the number of thin ones. The orientation of these rhombuses are equally and uniformly distributed in the ten-fold symmetry directions. This implies isotropic distribution of vertices and bonds.

Let z(i) be the coordination number of the i'th type vertex, ρ(i) be its frequency (fraction of all vertices that belong to type i), and $\bar{z}$ be the average coordination number. Let p(i,j) be the frequency that an ith type of vertex is connected to a jth type vertex. Then the following relations hold:

Strictly speaking there are only 7 different types of vertices if one classifies according to branching pattern of the vertex. However for type 1 and 4 as shown in Fig.1 are generally treated as different in the literatures.

$$\sum_{i=1}^{8}\rho(i) = 1$$

$$p(i, j) = p(j, i) \qquad 5.2.1$$

$$\sum_{i,j=1}^{8} p(i, j) = \sum_{i=1}^{8} z(i)\rho(i) = \bar{z}$$

From de Brujin's algebraic description[30] of the Penrose lattice we derived the following exact expressions

$$\rho(1) = \frac{1}{\sqrt{5}\tau^5}; \quad \rho(2) = \frac{1}{\tau^6}; \quad \rho(3) = \frac{1}{\tau^7}; \quad \rho(4) = \frac{1}{\sqrt{5}\tau^7};$$

$$\rho(5) = \frac{1}{\tau^5}; \qquad \rho(6) = \frac{1}{\tau^4}; \quad \rho(7) = \frac{1}{\tau^2}; \quad \rho(8) = \frac{1}{\tau^3}; \qquad 5.2.2$$

$$p(i, j) = \frac{1}{\tau^7}\begin{Bmatrix} 0 & 0 & 0 & 0 & 0 & 0 & \sqrt{5}\tau^2 & 0 \\ 0 & 0 & 0 & 0 & 0 & 2\tau & 4\tau & \tau \\ 0 & 0 & 0 & 0 & 0 & 1 & 2 & 3 \\ 0 & 0 & 0 & 0 & 0 & 0 & 0 & \sqrt{5} \\ 0 & 0 & 0 & 0 & 0 & 0 & 2\tau^2 & 2\tau^2 \\ 0 & 2\tau & 1 & 0 & 0 & 0 & 0 & 2\tau^3 \\ \sqrt{5}\tau^2 & 4\tau & 2 & 0 & 2\tau^2 & 0 & 0 & 2\tau^4 \\ 0 & \tau & 3 & \sqrt{5} & 2\tau^2 & 2\tau^3 & 2\tau^4 & 0 \end{Bmatrix} \qquad 5.2.3$$

These results were confirmed numerically. A computer program has been developed to determine the interconnecting of lattices. Simulation on the Penrose lattice with lattice sizes up to 50,000 sites shows that the above equations are satisfied to order 1/N, where N is the total number of lattice sites in the system. This shows that the distribution of vertices in the Penrose lattice is uniform. In other words the long range fluctuation of the lattice structure is very small. On the other hand the short range

fluctuation is very large, for example the local coordination number and nearest neighbor configurations are very different for different vertices, as shown in Fig.5.2.

5.2.3 Percolation Threshold

For the past two decades, percolation problems have been extensively studied both analytically and numerically. On the analytical side the scaling theory which treats the percolation problem as a general second order phase transition has been very successful, and numerical simulation on periodic lattices gives results in good agreement with theory. The Penrose lattice is the first example of a nonperiodic lattice with a well defined global symmetry and structure. Due to the non-periodicity the local structure of the lattice is nonuniform and fluctuates, so it provides an ideal lattice structure to test the scaling theory (the critical behavior near the phase transition is a long range fluctuation phenomenon). We have simulated the bond percolation on the Penrose lattice extensively with lattice size up to 50,000 sites. In this section we discuss the percolation threshold. In the next section we will discuss universality and critical exponents.

Recall that bond percolation means that each bond in the lattice has probability p of being connected. The percolation threshold p_c is defined such that for $p \geq p_c$ there exists an infinite connected cluster, and below p_c all clusters are finite. (An example of infinite cluster is shown in Fig.5.3.) Quantitatively, one defines the percolation probability P(p) as the probability that a randomly chosen bond belongs to the unique infinite cluster. Then

$$P(p) = 0 \quad for \quad p < p_c; \qquad P(p) > 0 \quad for \quad p \geq p_c \tag{5.2.4}$$

Fig.5.4 shows results of simulations of P(p) on the Penrose lattice with 90,000 bonds. All data points are the result of averaging over 20 runs, except those close to p_c are the result of a 50 runs average (also see Fig.5.5). We also have analyzed the finite size

scaling effect, with lattice size 500, 1000, 10,000, 40,000 and 90,000 bonds, which shows very good convergence of p_c with lattice size larger than 10,000 bonds. From these studies and analysis of cluster distribution statistics around threshold (see next section), we conclude

$$p_c = 0.483 \pm 0.005 \qquad \textit{bond percolation} \tag{5.2.5}$$

As is well known, critical exponents are dimensional invariants, but the percolation threshold is different for different lattice structures. This is because it is the local lattice structure, namely the connectivity which determines p_c. An important quantity is the average coordination number of the lattice $\bar{z}$, which determines the average local connection. For the 2D bond percolation, it is known that $p_c \bar{z} \approx 2$ for triangular, square and honeycomb lattices. However for the Kagome lattice[90], which is periodic with coordination number 4 the same for all vertices, p_c=0.45. For the Penrose lattice, from Eq.5.2.1 and 5.2.2 one gets

$$\bar{z} = \sum_{i=1}^{8} z(i)\,\rho(i) = 4 \tag{5.2.6}$$

But p_c for the Penrose lattice (Eq.5.2.5) is smaller than that of the square lattice but larger than that of Kagome lattice, though they all have same average coordination number. Obviously $\bar{z}$ is insufficient to characterize the connection property of lattice structure.

An important factor which is missing is that we did not take the global structure of the lattice into account. Since p_c is determined by the existence of an infinite cluster which is a global structure, it is in general also dependent on the global connectivity of lattice. We now introduce a measure of this global connectivity. Quantitatively, let us define B(n) as the number of bonds to which a seed in the lattice can aggregate in n steps, with nearest neighbor hopping for each step. For a lattice which is homogeneous over a long range, one

expects that for large n

$$B(n) = gn^d \qquad 5.2.7$$

in d dimensions. The proportionality constant g is a measure of global connectivity. In general it will be different for lattices with same $\bar{z}$ but different lattice structure. For the case we are considering, namely $\bar{z}$ =4 in 2D, there are three lattices: Square (S), Kagome (K) and Penrose (P). It is not difficult to obtain g for these lattices

$$g(S) = \frac{\bar{z}^2}{4} = 4; \qquad g(P) = 5 - \frac{5}{2\tau^3} = 4.41; \qquad g(K) = \frac{9}{2} = 4.50 \qquad 5.2.8$$

Now compare with their percolation threshold

$$p_c(S) = 0.500; \quad p_c(S) = 0.483 \pm 0.005; \quad p_c(K) = 0.449 \pm 0.032 \qquad 5.2.9$$

we conclude that p_c is a decreasing function of g for fixed $\bar{z}$. For quantitative relation between these quantities, more work should be done.

5.2.4 Critical Exponents and Universality

The transition at percolation threshold is a second order continuous phase transition. According to the modern theory of phase transitions, the critical behavior near p_c is universal, in other words it is independent of the details of lattice structure. Quantitatively the scaling theory predicts that all critical exponents are the same for all lattices in the same dimension. Exponents are related by universality relations, and only two of them should be independent.

We have chosen to calculate cluster distribution exponents. The cluster-size distribution function $n_s(p)$ is defined as the number of clusters containing s occupied bonds each. Near the percolation threshold, the two exponents assumption[89] states

$$n_s(p) \propto s^{-\tau} f(z), \quad z \equiv (p - p_c) s^{\sigma}; \qquad s \to \infty, \quad p \to p_c \qquad 5.2.10$$

and has been very successfully tested for periodic lattices. The usual critical exponents of percolation theory are related to τ and σ by

$$\alpha = 2 - \frac{\tau - 1}{\sigma}, \quad \beta = \frac{\tau - 2}{\sigma}, \quad \gamma = \frac{3 - \tau}{\sigma}, \quad \delta = \frac{1}{\tau - 2} \qquad 5.2.11$$

The best values of τ and σ obtained for bond percolation on a triangular lattice are[89]

$$\tau = 2.05, \qquad \sigma = 0.39 \qquad 5.2.12$$

Percolation near p_c on a Penrose lattice with 45,000 sites were extensively simulated in our work. The primary restriction of the system size is the big memory required for indexing the non-periodic lattice. We calculated the cluster distribution function $n_s(p)$. In order to reduce statistical fluctuations we divide $n_s(p)$ into group[89] with size intervals from $s=2^2$ to $2^{i+1}-1$, i=0,1,2 ····. For each group we took s as the geometrical mean of the upper and lower end of the size interval. This approximation should be better the closer n_s is approximated by a s^{-2} decay law. Fig.5.5 shows the results of cluster statistics based on 50 runs on a lattice with 45,000 vertices (90,000 bonds). We also did several simulations on different lattices (different member of same local isomorphism class[46], or different part of the same infinite Penrose lattice) of the same size, and we found the same results. This is due to the small long range fluctuation we discussed in section 5.2.2, and the point is essential because for the infinite system all members of same local isomorphism class are degenerate[46,47].

In Fig.5.5a we plotted $\ln(n_s(p))$ against ln(s) at the percolation threshold p_c=0.483. The slopes of the straight line fit gives exponent $\tau=2.04 \pm 0.08$. Within the error bar it agrees very well with the known exponent (Eq.5.2.12). In Fig.5.5b we plotted

$\ln\ v(z) = \ln \frac{n_s(p)}{n_s(p_c)}$ against $z=(p-p_c)s^{\sigma}$ for different values of p. With $\sigma=0.39$ one sees that all points fall on a single curve. Therefore we conclude that percolation on a quasilattice belongs to the same universality class as percolation on a periodic lattice, and the critical behavior can be understood in the framework of scaling theory.

A side benefit of Fig.5.5b is that the plot is an effective way to determine p_c. As one can see from Eq.5.2.10 ln v(z) is 0 at z=0. Furthermore the deviation of $n_s(p)$ from $s^{-\tau}$ is different on two sides of z=0. For z>0 ($p>p_c$), $n_s(p)$ decays slower than $s^{-\tau}$, which makes ln v(z) increasing function of z. For z <0 ($p<p_c$), $n_s(p)$ decays faster than $s^{-\tau}$, lnv(z) is decreasing function of z. Therefore by examine the deviation of $n_s(p)$ from the explicit exponential decay law one can effectively determine the percolation threshold p_c. The value of p_c quoted in the last section is determined partially by this observation.

5.2.5 Conclusion

In summary we have analyzed the geometrical structure of the Penrose quasilattice. The connectivity structure of the lattice was analyzed and the connection coefficients were given. Bond percolation on the Penrose lattice was studied. We found the percolation threshold to be $p_c = 0.483 \pm 0.005$. This is smaller than that of square lattice and larger than that of Kagome lattice, though all of these lattices have the same average coordination number. We interpreted this in terms of difference of global connectivity in these lattices. Cluster statistics around p_c were measured, and the results agreed well with scaling theory. This is the first time that scaling theory has been explicitly tested on a nonperiodic lattice. We recently learned of another (more elaborate) study of the same problem by Yonazawa et. al.; their results agree with those reported here[91].

Figure Captions

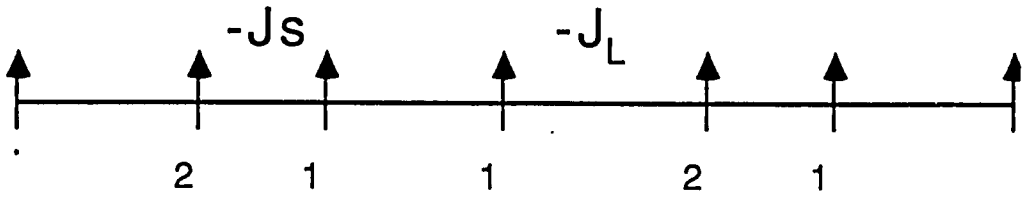

Fig.5.1

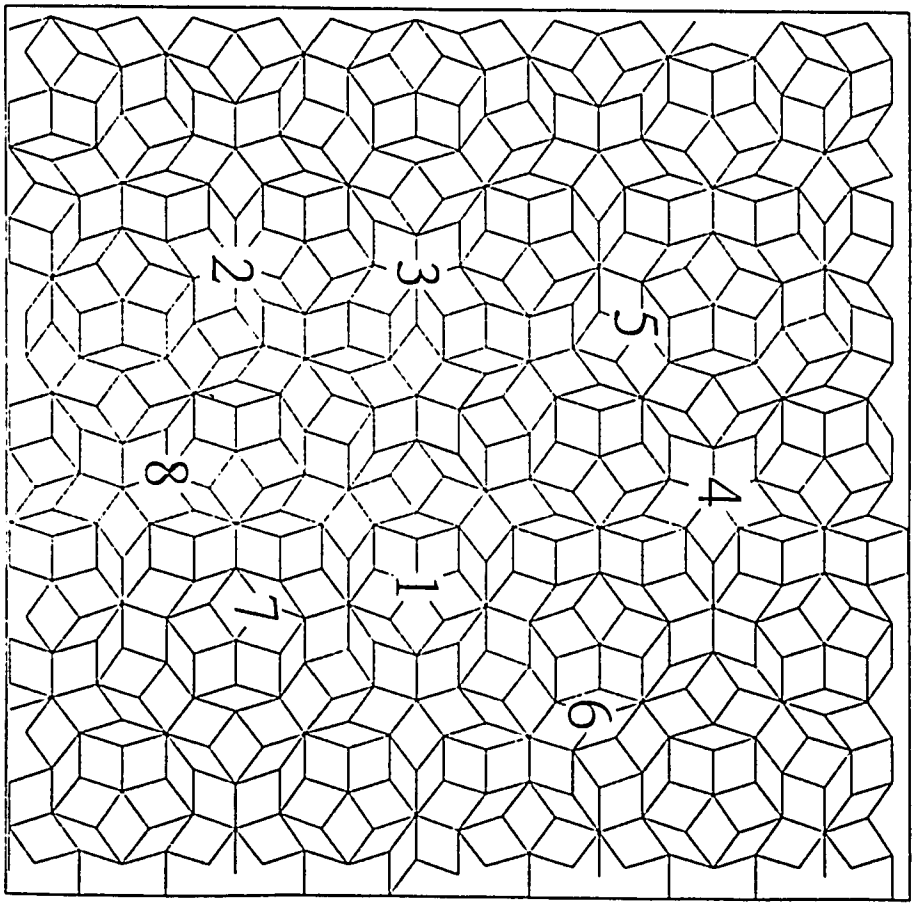

Fig.5.2

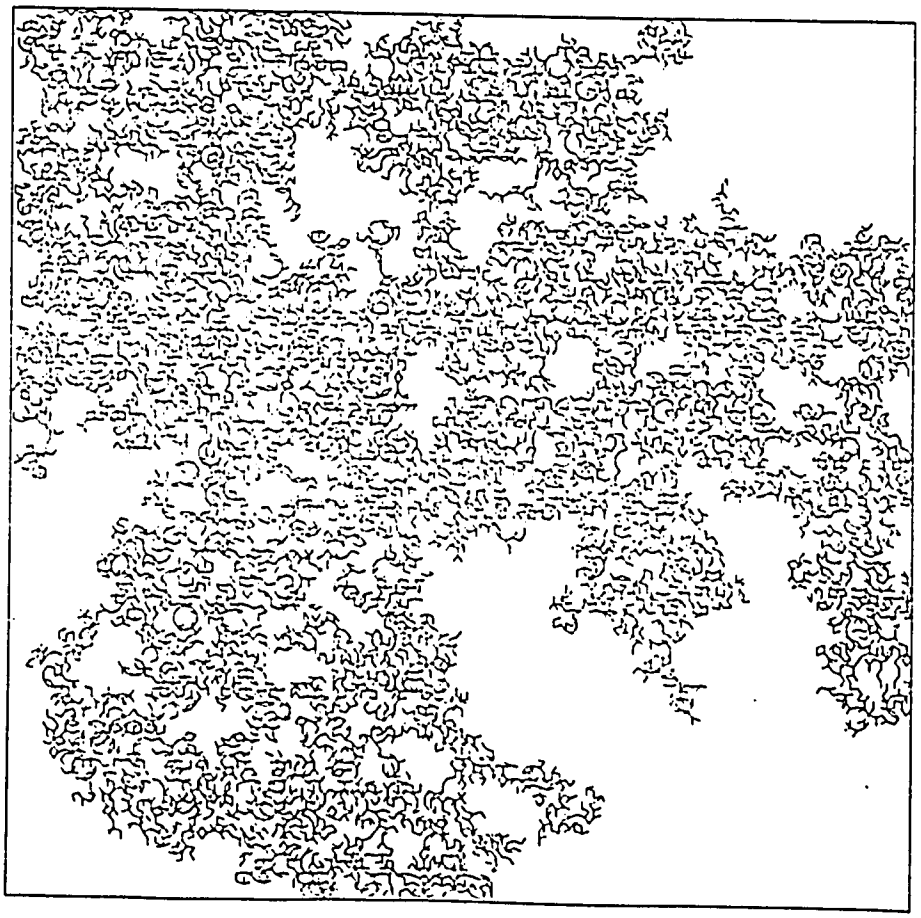

Fig.5.3

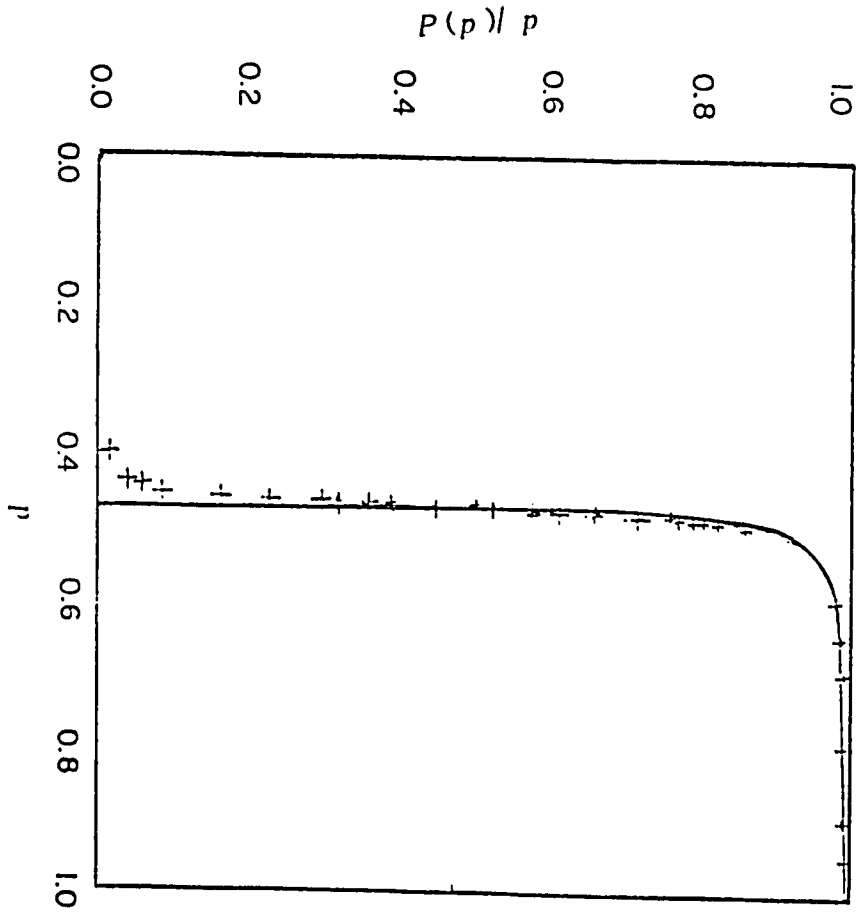

Fig.5.4

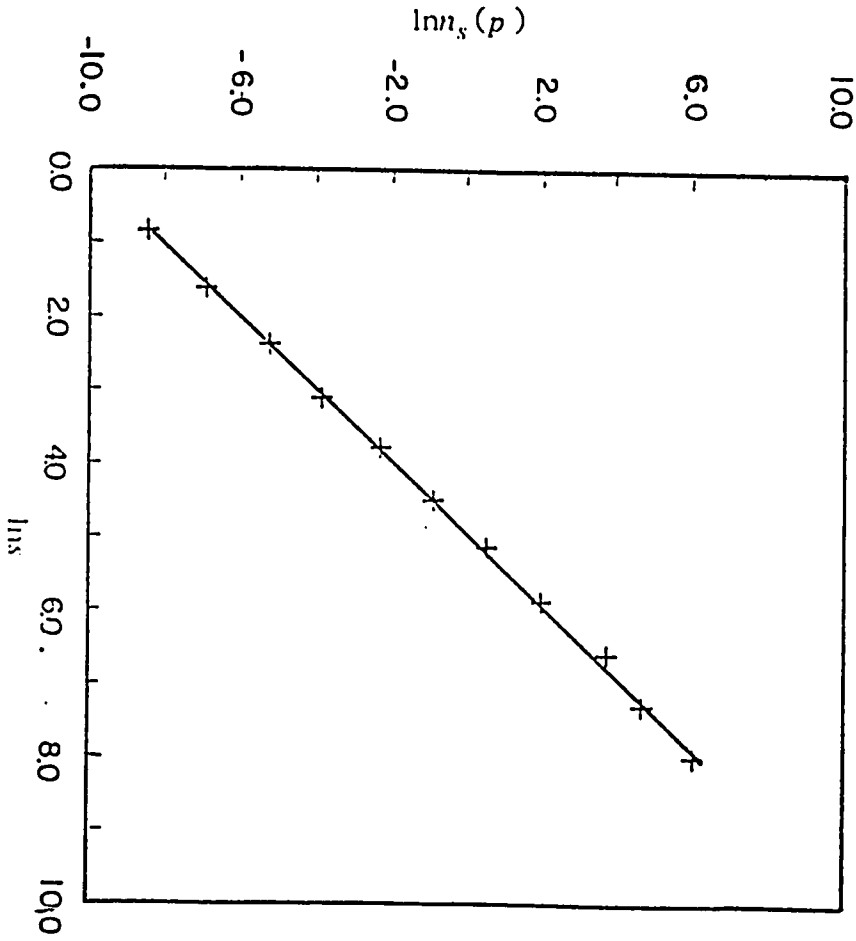

Fig.5.5a

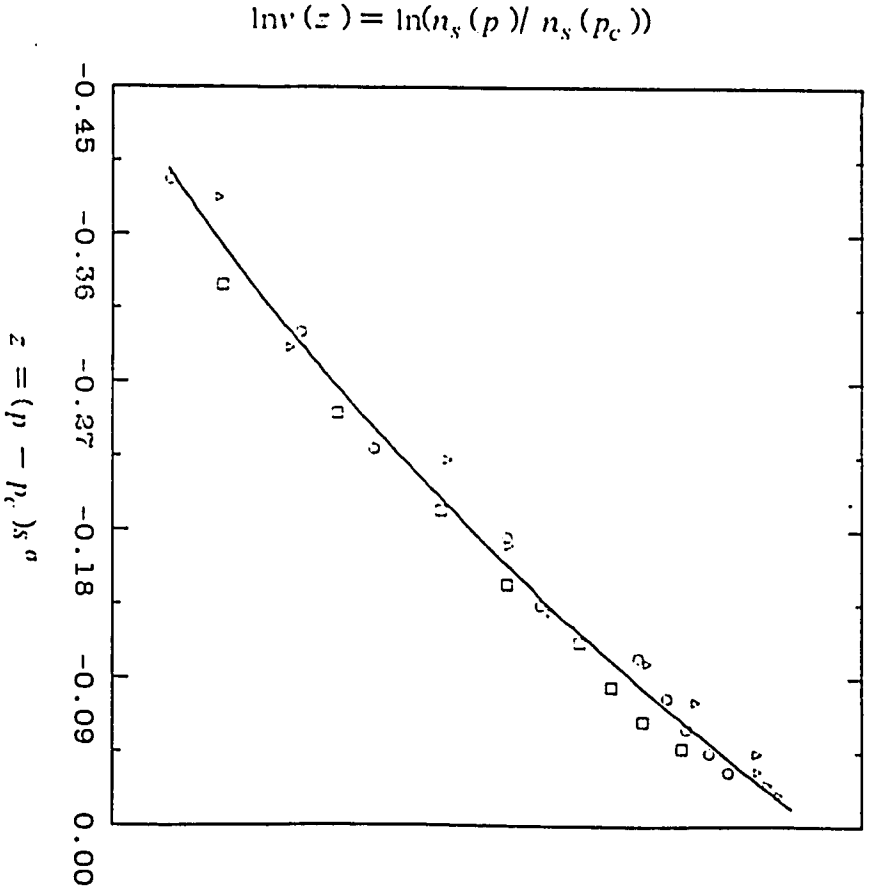

Fig.5.5b

CHAPTER 6

CONCLUSIONS

In conclusion, in this dissertation I have presented the results of studies on physical properties of quasiperiodic systems and other related aperiodic systems. Here I will comment on some possible future research directions.

I have analyzed the effects of mistakes on geometrical properties, such as diffraction pattern and correlation function. The effect of mistakes on electronic properties remain to be analyzed. In one dimension, one way to do this is to use the transfer matrix method we developed in Chapter 3.

Studies of energy spectra in two and three dimensions are necessary in order to compare theoretical results with experiments. The combination of numerical simulations and analytical analysis in the framework of the quasi-Bloch theory, similar to what I did in Chapter 3, can be used.

I have used quasi-Bloch theory successfully to predict the energy spectrum in one dimension. Similar studies in two and three dimensions should be investigated. More importantly is the analysis of wavefunctions in the framework of the quasi-Bloch theory. Studies on this line may answer some questions such as the occurrence of localized vs extended states.

In Chapter 4 I used the two-mode-coupling theory to analyze wave propagation in the long wavelength limit. However, as I pointed out, another approach is to utilize the solution of Mathieu's equation. Work along this line is in progress.

Simulations of wave propagation in 2D and 3D quasilattices are needed in order to understand the transport properties of quasiperiodic systems. This should be combined with studies of analytical properties of wavefunctions using the quasi-Bloch theory.

Recently it was shown that a 2D Penrose lattice can be grown by local matching rules. It remains to be shown that similar algorithms exist in 3D. If indeed 3D Penrose

lattice can be grown by local rules, then a combination of rigid growth and Mont Carlo simulation which permits defects, especially mistakes, to occur in the growing process will answer some questions concerning the quasicrystal growth.

Icosahedral packing models have been proposed to be possible structural models of quasicrystals. The problem with such models is that the correlation length is limited. As we learned from Chapter 2, simple type of mistakes do not break the long range correlation. One can ask what kind of mistake will break the correlation such that there is a finite correlation length. We would like to know whether this approach will lead to a structure similar to that of a random packing model with built in long correlation.

There are still many other problems remaining to be studied, especially the relation between quasiperiodic systems and other aperiodic systems, their similarities and differences. Studies of these subjects will no doubt bring us one step further in understanding the nature of quasicrystalline order and properties.

BIBLIOGRAPHY

[1] D. Shechtman, I. Blech, D. Gratias, and J. W. Cahn, Phys. Rev. Lett. 53, 1951 (1984).

[2] D. Shechtman and I. Blech, Met. Trans. 16A, 1005 (1985).

[3] A good general reference to both experiment and theory is: Workshop on Aperiodic Crystals (eds L. Michel and D. Gratias) J. de Phys. Paris, Coll. C3 Supp. 7 (1986).

[4] D. A. Lilienfeld, M. Nastasi, H. H. Johnson, D. G. Ast and J. W. Mayer, Phys. Rev. Lett. 55, 1587 (1985).

[5] J. A. Knapp and D. M. Follstaedt, Phys. Rev. Lett. 55, 1591 (1985).

[6] P. Sainfort, B. Dubost abd A. Dubus, C. R. Acad. Sci. Paris 301, 689 (1985).

[7] Z. Zhang, H. Q. Ye and K. H. Kuo, Phil. Mag. A52, L49 (1985).

[8] P. A. Bancel, P. A. Heiney, P. W. Stephens, A. I. Goldman and P. M. Horn Phys. Rev. Lett. 54, 2422 (1985).

[9] L. Bendersky, Phys. Rev. Lett. 55, 1461 (1985).

[10] S. J. Poon, A. J. Drehman and K. R. Lawless, Phys. Rev. Lett. 55, 2324 (1985).

[11] K. K. Fung, C. Y. Yang, Y. Q. Zhou, J. G. Zhao, W. S. Zhan and B. G. Shen, Phys. Rev. Lett. 56, 191 (1986).

[12] E. A. Stern, Y. Ma and C. E. Bouldin, Phys. Rev. Lett.55, 2172 (1986).

[13] G. V. S. Sastry and C. Suryanarayana, Scripta Met. 20, 1359 (1986).

[14] D. S. Zhou, H. Q. Ye, D. X. Li and K. H. Kuo, Phys. Rev. Lett. 60, 2180 (1988).

[15] D. Levine, P. Steinhardt, Phys. Rev. Lett. 53, 2477 (1984).

[16] M. Duneau and A. Katz, Phys. Rev. Lett. 54, 2688 (1985).

[17] V. Elser and C. Henley, Phys. Rev. Lett. 54, 1730 (1985).

[18] R. Zia and W. Dallas, Jnl. of Phys. A18, L314 (1985).

[19] P. Bak, Phys. Rev. Lett. 56, 861 (1986).

[20] P. Bak, Phys. Rev. Lett. 54, 1517 (1985), and ibid 56, 861 (1985).

[21] P. A. Kalugin, A. Kitaev, L. Levitov, JETP Lett. 41, 119 (1985).

[22] N. D. Mermin and S. M. Troian, Phys. Rev. Lett. 54, 1524 (1985)

[23] M. V. Jaric, Phys. Rev. Lett. 55, 607 (1985).

[24] O. Biham, D. Mukamel and S. Shtrikman, Phys. Rev. Lett. 56, 2191 (1986).

[25] P. W. Stevens and A. I. Goldman, Phys. Rev. Lett. 56, 1168 (1986), and 57, 2331 (1986).

[26] L. Pauling, Nature 317, 512 (1985).

[27] M. Widom, K. J. Strandburg and R. H. Swendsen, Phys. Rev. Lett. 58, 706 (1987).

[28] J. W. Cahn, D. Gratias and B. Mozer, *preprint* (July, 1988).

[29] R. Penrose, Bull. Inst. Math. Appl. 10, 266 (1974)

[30] N. de Brujin, Ned. Akad. Weten. Proc. Ser. A43, 39 (1981).

[31] M. Gardner, Sci. Am. 236, 110 (1977).

[32] A. L. Mackay, Physica 144A, 609 (1982).

[33] P. Kramer and R. Neri, Acta. Cryst. A40, 580 (1984).

[34] G. Onoda, P. Steinhardt, D. DiVincenzo and J. Socolar, Phys. Rev. Lett. 60, 2653 (1988).

[35] C. L. Henley, Comments Condens. Matter Phys. 13, 59 (1987)

[36] A. L. Makay, Rep. Prog. Phys. (1987).

[37] P. J. Steinhardt and S. Ostlund, *The Physics of Quasicrystals*, World Scientific, Singapore (1987).

[38] *Introduction to Quasicrystals*, ed. M. V. Jaric, Academic Press, Boston (1988).

[39] J. P. Lu, T. Odagaki and J. L. Birman, Phys. Rev. B 33, 4809 (1986).

[40] J. P. Lu and J. L. Birman, Phys. Rev. Lett. 56, 2706 (1986).

[41] J. P. Lu and J. L. Birman, J. de Physique Colloq. C3, Supp. 7, C3-251 (1986).

[42] J. P. Lu and J. L. Birman, in *Proc. Of XV International Colloquium Group Theoretical Methods In Physics* e.d. R. Gilmore and D. H. Feng, World Scientific Press (1987).

[43] J. P. Lu and Joseph L. Birman, Jnl. Stat. Phys. 46, 1057 (1987).

[44] J. P. Lu and Joseph L. Birman, Phys. Rev. B Rapid Comm. 36, 4471 (1987).

[45] J. P. Lu and Joseph L. Birman, Phys. Rev. B 38, October 1988.

[46] D. Levine and P. Steinhardt, Phys. Rev. B34, 596 (1986).

[47] J. Socolar and P. Steinhardt, Phys. Rev. B34, 617 (1986).

[48] A. Katz and M. Duneau, J. Physique 47, 181 (1986).

[49] T. Janssen, Acta. Cryst. A42, 261 (1986).

[50] E. Bombieri and J. E. Taylor, J. de Physique Colloque C3, Suppl. 7, C3-19 (1986).

[51] A. Wilson, X-Ray Optics 2nd Edn, London:Methuen (1962). T. Welberry, Rep. Prog. Phys. 48, 1543 (1985).

[52] S. Hendricks and E. Teller, J. Chem. Phys. 10, 147 (1942).

[53] J. R. Robertson, M. E. Misenheimer, S. C. Moss and L. A. Bendersky, Acta. Metall. 34, 2177 (1986).

[54] K. Hiraga, M. Hirabayashi, A. Inoue and T. Masumoto, J. Phys. Soc. Jpn. 54, 4077 (1985).

[55] T. Ishimasa, H. U. Nissen and Y. Fukano, Phys. Rev. Lett. 55, 511 (1985).

[56] J. L. Birman and H.-R. Trebin, Jnl. of Stat. Phys. 38, 371 (1985).

[57] N. D. Mermin, D. Roksar and D. C. Wright Phys. Rev. Lett., 2099 (1987). Also see D. Roksar, D. C. Wright and N. D. Mermin and Phys. Rev. B37, 8145(1988).

[58] P. Kramer, Jnl. de Physique Paris Colloque C3, Suppl. 7, C3-75 (1986).

[59] A. Janner, Jnl. de Physique Paris Colloque C3, Suppl. 7, C3-95 (1986).

[60] H. Brown, R. Bulow, J. Neubuser, H. Wondratschek and H. Zassenhaus, Crystallographic Groups of Four-Dimensional Space, John Wiley & Sons, New York (1978).

[61] H. Matsuda, Supp. of Prog. Theor. Phys. 23, 23 (1962).

[62] T. C. Choi, Phys. Rev. Lett. 55, 2915 (1985).

[63] S. Ostlund and R. Pandit, Phys. Rev. B 29, No. 3, 1394 (1984).

[64] M. Kohmoto, L. P. Kadanoff and C. Tang, Phys. Rev. Lett. 50, 1870 (1983).

[65] S. Ostlund, R. Pandit, D. Rand, H. J. Schellnhuber and E. D. Siggia, Phys. Rev. Lett. 50, 1879 (1983)

[66] H. Matsuda and K. Okada, Prog. Theo. Phys. 34, 539 (1965).

[67] H. S. Wall, Continued Fractions (Van Nostrand, New York).

[68] T. Odagaki and Dan Nguyen, Phys. Rev. B34, 5929 (1986).

[69] J. M. Luck and D. Patribis, Jnl. Stat. Phys. 42, 289 (1986).

[70] T. Odagaki and D. Nguyen, Phys. Rev. B 33, 2184 (1986).

[71] M. Kohmoto and B. Sutherland, Phys. Rev. Lett. 56, 2740 (1986), and Phys. Rev. B 34, 3849 (1986).

[72] B. Sutherland, Phys. Rev. B 34, 3904 (1986) and B34, 5208 (1986).

[73] *The Radon transform* , S. Helgason, Birkhauser Boston (1980).

[74] J. Sokoloff, Phys. Rev. Lett. 57, 2223 (1986).

[75] For example see A. H. Wilson Theory of Metals, Cambridge University Press (1965).

[76] M. V. Romerio, J. Math. Phys. 12, 552 (1971).

[77] C. deLanger and T. Janssen, Phys. Rev. B28, 195 (1983).

[78] E. I. Diaberg and Ya. G. Sinai, Func. Annal. Appl. 9, 279 (1976).

[79] J. B. Sokoloff Phys. Rep. 126, #4 (1985).

[80] L. Brillouin, Ann. Phys. (France). 9th Ser., 17, 88 (1922).

[81] P. W. Anderson, Phys. Rev. 109, 1492 (1986). S. He and J. D. Maynard, Phys. Rev. Lett. 57, 3171 (1986).

[82] H. S. Chen, C. H. Chen, A. Inoue and J. K. Krause, Phys. Rev. B 32, 1940 (1985).

[83] D. Pavuna, C. Berger, F. Cyrot-Lackmann, P. Germi and A. Pasturel, Solid State Comm. 59, 11 (1986).

[84] P. M. Morse and H. Feshbach, *Methods of Theoretical Physics* Vol.2, page 843, McGraw-Hill, NY 1953.

[85] N. W. McLachlan, *Theory and Application of Mathieu Functions* Dover (1947) and *Theory of Vibrations*, Dover (1951).

[86] V. E. Korepin, Phys. Lett. 118A, 285 (1986).

[87] D. Stauffer Phys. Reports 54 No 1, 1 (1979) and references therein.

[88] J. Hoshen, D. Stauffer, G. H. Bishop, R. J. Harrison and G. D. Quinn, Jnl. Phys. A Vol 12 No 8, 1285 (1979).

[89] P. Dean, Proc. Camb. Phil. Soc. 59, 297 (1963).

[90] R. Zallen *Physics of Amorphous Solids* , John Wiley & Sons New York (1983), page 168.

[91] F. Yonezawa, S. Sakamoto, K. Aoki, S. Nose and M. Hori, *preprint* (July 1988). I thank Prof. Yonazawa for the preprint and for discussions.

SUPPLEMENT: PUBLICATIONS

A. **Properties of One Dimensional Quasilattices,** Jian Ping Lu and Joseph L. Birman, Physical Review B Vol. 33, 4809 (1986).

B. **Mistakes in Quasilattices,** Jian Ping Lu and Joseph L. Birman, Physical Review Letters Vol. 56, 2706 (1986).

C. **Studies on Quasilattices: Mistakes And Long Range Correlation In One Dimension,** Jian Ping Lu and Joseph L. Birman, Journal de Physique Colloquium C3, Suppl. 7, C3-251 (1986).

D. **Symmetry Of Quasiperiodic Lattice And Decomposability Of Crystallographic Point Groups,** Jian Ping Lu and Joseph L. Birman, Proc. of XV International Colloquium Group Theoretical Methods In Physics, ed. R. Gilmore and D. H. Feng, World Scientific Press (1987).

E. **Percolation And Scaling On A Quasilattice,** Jian Ping Lu and Joseph L. Birman, Journal of Statistical Physics Vol. 46, 1057 (1987).

F. **Electronic Structure Of A Quasiperiodic System,** Jian Ping Lu and Joseph L. Birman, Physical Review B (Rapid Communication) Vol.36, 4471 (1987).

G. **Acoustic Wave Propagation In Quasiperiodic, Incommensurate And Random Systems,** Jian Ping Lu and Joseph L. Birman, to appeared in Physical Review B Vol.38, October 1988.

AUTOBIOGRAPHY

Jian Ping Lu (JP, Jason, Ah Jian), born January 10th, 1963 in Shatang, Fujian, China. Graduated from Wuzhi Elementary School in 1974, Shizhi Junior High in 1976, Shatang High School in 1978. Bachelor's degree in physics from the University of Science and Technology of China, 1982.